

Pressure Sensor Placement for Leak Diagnosis under Demand Uncertainty in Water
Distribution Systems

by

Mohammadamin Jahanpour

A thesis
presented to the University of Waterloo
in fulfillment of the
thesis requirement for the degree of
Doctor of Philosophy
in
Civil and Environmental Engineering

Waterloo, Ontario, Canada, 2018
© Mohammadamin Jahanpour 2018

Examining Committee Membership

The following served on the Examining Committee for this thesis. The decision of the Examining Committee is by majority vote.

External Examiner

Dr. Yves Fillion
Associate Professor

Supervisor(s)

Dr. Bryan Tolson
Associate Professor

Internal Member

Dr. Sriram Narasimhan
Professor

Internal Member

Dr. Tarek Hegazi
Professor

Internal-external Member

Dr. Kumaraswamy Ponnambalam
Professor

AUTHOR'S DECLARATION

I hereby declare that I am the sole author of this thesis. This is a true copy of the thesis, including any required final revisions, as accepted by my examiners.

I understand that my thesis may be made electronically available to the public.

Abstract

Leakages in concealed pipes in urban water distribution systems (WDS) can cause losses of up to 25% of potable water supply in municipalities. These losses are not only a tremendous waste of water but also the energy spent to treat and distribute it. Techniques for leak detection and localization in WDS have evolved considerably since the mid-1950s. Among these methods, model-based leak diagnosis methods (MFD) have been extensively studied in the literature, as they are more economical compared to others. MFD methods infer the existence and position of leaks based on continuously monitoring pressure levels in the WDS and comparing these to the expected values obtained from simulating a calibrated hydraulic model of the WDS. In the event of an anomaly (e.g., a leak), the sampled pressure levels (measured by the sensors) should significantly deviate from expected values which are obtained by simulation under an assumed no-leak condition. Although the methodology is efficient in terms of the number of required sensors and operational person-hours, it is at risk of failing to distinguish between the effect of leaks and water demand variations. This is because both leaks and demand fluctuations have a similar change on pressure levels along the network. This study aims to improve the robustness of the MFD method by explicitly considering the uncertainty in the nodal demands across the WDS. The influence of demand uncertainty on nodal pressure is analyzed by generating model-based system responses that are time-variable and conditional on known data (e.g., total demand across the WDS). Monte Carlo methods are used to generate conditional realizations of spatially variable sets of nodal demands such that simulated states match the available observed system states at the time any pressure observation is sampled. After characterizing the distributions of expected nodal pressures under the no-leak condition, a statistical detection test is defined that asserts the existence of a leak based on evidence from comparing the observations with their corresponding distributions. The performance of the proposed detection analysis is then evaluated in response to multiple synthetic leak and no-leak scenarios. To fine-tune the configuration of the detection test design parameters, its performance is evaluated by computing the false positive and false negative rates across the leak and no-leak scenarios. These two metrics are utilized to solve the sensor placement optimization problem as a multi-objective optimization problem. Results in two synthetic WDS case studies show that under the most influential source of uncertainty in WDS modelling (nodal demands), the proposed detection test functions well and multi-objective optimization can lead to robust sensor placement and other valuable insights.

Acknowledgements

I take this opportunity to express my special thankfulness to Dr. Bryan Tolson for his continuous guidance and support throughout my PhD studies and graduation. Bryan is a caring, patient, intelligent, and enthusiastic supervisor. It is my pleasure to thank my defence committee members Dr. Yves Filion from Queen's University, Dr. Sriram Narasimhan, Dr. Kumaraswamy Ponnambalam, and Dr. Tarek Hegazi from the University of Waterloo.

Table of Contents

Abstract.....	iv
Acknowledgements.....	v
Table of Contents.....	vi
List of Figures.....	x
List of Tables.....	xiii
Chapter 1 Introduction.....	1
1.1 Problem Statement.....	1
1.2 Research Contributions.....	2
1.3 Scope of Research.....	3
Chapter 2 Literature Review.....	5
2.1 Leak Diagnosis.....	5
2.1.1 Hydraulic Model-Based Fault Diagnosis (MFD).....	6
2.2 Hydraulic Modelling.....	9
2.2.1 Conservation of Mass.....	9
2.2.2 Conservation of Energy.....	9
2.2.3 Global Gradient Algorithm.....	11
2.2.4 Modelling a Leak in EPANET2.....	11
2.2.5 Demand Driven Versus Pressure Driven Simulation in the Context of Leak Modelling ...	12
2.2.6 Nodal Elements Terminology.....	13
2.3 Sensor Placement Optimization.....	13
2.4 Uncertainty Sources in Hydraulic Modelling.....	17
2.4.1 Structural Uncertainty.....	17
2.4.2 Parameter Uncertainty.....	18
2.4.3 Measurement/Data Uncertainty.....	18
Chapter 3 Quantitative Assessment of Existing MFD Method in Literature.....	19
3.1 Summary.....	19
3.2 Introduction.....	19
3.3 Deterministic MFD in Leak Detection.....	20
3.4 Quantitative Assessment of False Positive Rate under Deterministic MFD.....	22
3.4.1 No-Leak Scenarios.....	24
3.4.2 Leak Scenarios.....	26

3.4.3 False Positives	28
3.4.4 The Absence of State Variables in the Comparison	30
3.4.5 The Absence of Total Demand in the Comparison	30
3.5 Conclusion.....	31
Chapter 4 Exploratory Analysis on Pressure Signals Under Leak and Demand Noise.....	32
4.1 Summary	32
4.2 Introduction	32
4.3 Random Demand Realizations	34
4.4 System States.....	37
4.4.1 Consistency Criteria Between Simulated and Observed System States	38
4.5 Case Study Net3	39
4.6 Case Study C-Town.....	44
4.7 Conclusion.....	48
Chapter 5 Leak Detection Methodology	49
5.1 Summary	49
5.2 Introduction	49
5.3 Proposed Leak Detection Method	50
5.3.1 Observation Pairs Schedule.....	50
5.3.2 The Hypothesis Test for Leak Detection.....	52
5.3.3 Dependency of Random Variables	55
5.4 Leak Detection Method Performance Assessment.....	56
5.4.1 Leak and No-leak Scenarios and No-leak PDF Generation	56
5.4.2 False Positive Assessment.....	57
5.4.3 False Negative (i.e., Leak Detection Accuracy) Assessment	58
5.5 Detection Hypothesis Test Design	58
5.6 Step 1: Examining the Effect of ΔT and S	59
5.7 Case Study Net3	59
5.7.1 Observation Pairs Schedule.....	59
5.7.2 Experiment Definition	60
5.7.3 Examining the Effect of ΔT and S	61
5.7.4 Single Sensor and Single Leak Location.....	61
5.7.4.1 φ and ω Variation as a Function of S (fixed ΔT).....	63

5.7.4.2 φ and ω Variation by Leak Flow (fixed ΔT and S)	66
5.7.4.3 φ and ω Variation by Sensor Location (Fixed Leak Location and Size, ΔT and S)....	67
5.7.5 Single Sensor and All Leak Scenarios	70
5.7.6 Multiple Sensors and All Leak Scenarios	71
5.7.7 Alternative Method for Choosing ΔT and S	75
5.8 Case Study C-Town	75
5.8.1 Observation Pairs Schedule	75
5.8.2 Experiment Definition.....	76
5.8.3 Results.....	76
5.9 Conclusion	77
Chapter 6 PADDs Algorithm Assessment for Biobjective Water Distribution System Benchmark	
Design Problems	79
6.1 Summary	79
6.2 Introduction.....	80
6.3 Methodology	82
6.3.1 Benchmark Problems and Decision Variables.....	82
6.3.2 Objective and Constraint Evaluation	84
6.3.3 Computational Experiments.....	86
6.3.4 PADDs Result Post-Processing and Comparisons	88
6.3.5 Effective Archive Size of PADDs.....	89
6.4 Results.....	89
6.4.1 Best-Known Pareto Fronts	89
6.4.2 Contribution of Each MOEA	90
6.4.3 PADDs Selection Metrics Comparison.....	95
6.4.4 Effective Archive Size Comparison.....	101
6.5 Conclusion	104
Chapter 7 Sensor Placement	106
7.1 Summary	106
7.2 Introduction.....	106
7.3 Sensor Placement Optimization Problem	108
7.3.1 Practicality	108
7.3.2 Proximity.....	108

7.3.3 Justifiability	108
7.4 Case Study Net3	109
7.4.1 Practicality and Proximity	109
7.4.2 Justifiability	110
7.4.3 Optimization Results	111
7.5 Case Study C-Town.....	114
7.5.1 Practicality and Proximity	115
7.5.2 Justifiability	115
7.5.3 Optimization Results	115
7.6 Conclusion.....	122
Chapter 8 Summary, Conclusions, and Recommendation for Future Work	123
8.1 Summary and Conclusion.....	123
8.2 Future Research.....	126
Chapter 9 References.....	128
Appendix A	139

List of Figures

Figure 3-1. Net3 water distribution system layout.....	23
Figure 3-2. One random demand realization along with the nominal demand pattern	24
Figure 3-3. Histogram of pressure residuals at node #1 for time-step 12:00 to 1:00 AM	25
Figure 3-4. Pressure residuals variation per node for a) time-step 12 to 1 AM and b) time-step 1 to 2 AM (τa , and τt are explained in the following)	27
Figure 3-5. False positive ratios for different threshold scenarios at a) time-step 1 and b) time-step 2	29
Figure 4-1. Location of the selected nodes for pressure analysis in Net3.....	40
Figure 4-2. Histograms of nodal pressure responses with and without a leak at various sensor locations and leak magnitudes (the leak is located at the sensor locations).....	42
Figure 4-3. Variation of pressure drop by the leak flow	44
Figure 4-4. C-Town WDS layout.....	45
Figure 4-5. Histograms of nodal pressures with and without a leak at various sensor locations and leak magnitudes (C-Town)	47
Figure 5-1. Timing structure for one night of pressure observations to include in proposed leak detection analysis	51
Figure 5-2. Total hourly demand of Net3	60
Figure 5-3. Scatter plots of false positive and false negative ratios under example single sensor locations and single location leak conditions (Net3)	63
Figure 5-4. False negative variation by S for node 14 (Net3).....	64
Figure 5-5. False negative variation by S for node 61 (Net3).....	64
Figure 5-6. False positive variation by S for node 14 (Net3).....	65
Figure 5-7. False positive variation by S for node 61 (Net3).....	65
Figure 5-8. Scatter plots of false positive and false negative ratios under example single sensor location and single location leak condition for different leak flows (Net3).....	66
Figure 5-9. False negative variation with S (number of days of observation pairs), for different leak flows, for node 14 (Net3).....	67
Figure 5-10. Sensor performance as a function of distance from a leak on node 61 (Net3).....	68
Figure 5-11. False negative scatter heat map for four leak sizes on node 14 (Net3)	69
Figure 5-12. Scatter plots of false positive and false negative ratios under example single sensor location and all leak scenarios (Net3)	71

Figure 5-13. System level performance for an example sensor fleet in Net3 network. Scatter plot of false positive and false negative ratios (panel a) under two example sensors and all leak scenarios and the subset of detection method configurations that are non-dominated (panel b).....	72
Figure 5-14. System level performance for an exhaustive sensor fleet (sensors on every node) in Net3 network. Scatter plot (panel a) under all sensors and all leak scenarios and the subset of detection method configurations that are non-dominated (panel b).....	72
Figure 5-15. System level false negative variation with days of sampling (S) for the all sensor condition for Net3 network	74
Figure 5-16. System-level false positive variation with days of sampling (S) for the all sensor condition for Net3 network	74
Figure 5-17. System level performance for an exhaustive sensor fleet (sensors on every node) in C-town network. Scatter plot (panel a) under all sensors and all leak scenarios and the subset of detection method configurations that are non-dominated (panel b).	76
Figure 6-1. Pseudocode for Calculation of Objective Functions for Network Design.....	86
Figure 6-2 Select approximate Pareto fronts generated by PADDs algorithms and multiobjective evolutionary algorithms used by Wang et al. (2015).....	92
Figure 6-3 Approximate Pareto fronts (PFs) obtained by PADDs algorithms the aggregated results from 30 optimization trials with the full NSE budgets listed in Table 6-1 (left column) and partial budgets (right column) using 1/100 th of the full NSE budgets.	95
Figure 6-4 Empirical cumulative distribution functions (CDFs) of normalized hypervolume (NHV) metric applied to full budget (see Table 6-1) and partial budget (1/100th the number of solution evaluations as the corresponding full budget). A value of 1-NHV=0 is best.	100
Figure 6-5 Selection probabilities, effective archive size, and relative effective archive size comparison for CHC (left column) and HVC (right column), obtained from partial budget optimization results for BIN network problem.....	102
Figure 7-1. Average false positive and false negative ratios for all the nodes (Net3).....	110
Figure 7-2. Best-found Pareto fronts for sensor placement optimization problem of Net3	112
Figure 7-3. False negative variation with the number of sensors in Net3	114
Figure 7-4. Best-found Pareto fronts in objective space for sensor placement optimization problem of C-Town with $\Delta T = 1, S = 9, \alpha = 0.01$	116
Figure 7-5. False negative variation with the number of sensors in C-Town with $\Delta T = 1, S = 9, \alpha = 0.01$	117

Figure 7-6. Best-found Pareto fronts for sensor placement optimization problem of C-Town with $\Delta T = 3, S = 5, \alpha = 0.01$ and $\Delta T = 3, S = 9, \alpha = 0.01$	119
Figure 7-7. False negative variation with the number of sensors in C-Town with $\Delta T = 3, S = 5, \alpha = 0.01$ and $\Delta T = 3, S = 9, \alpha = 0.01$	120
Figure 7-8. False negative variation with the number of sensors in C-Town with $\Delta T = 3, S = 5, \alpha = 0.005$	121

List of Tables

Table 2-1. Matrix-based versus scenario-based approaches to the sensor placement problem in WDSs	15
Table 3-1. Net3 specifications.....	24
Table 4-1. Required data for two consecutive time-steps	33
Table 4-2. Results of the simulations under the leak and no-leak conditions for Net3 network.....	41
Table 4-3. C-Town specifications	44
Table 4-4. Results of the nodal pressure simulations under the leak and no-leak conditions (C-Town)	46
Table 5-1. Illustration of evidence accumulated over time in one night from the <i>ith</i> sensor, in the proposed leak detection approach	52
Table 5-2. Number of nodes (from a total of 91 nodes) showing non-randomness	56
Table 5-3. Demonstration of ΔT , and $N1$ variations for Net3.....	60
Table 5-4. False positive (φ) and false negative (φ) ratios under the single sensor and single leak condition (Net3)	62
Table 5-5. System level false positive (φ) and false negative (φ) ratios given sensors at all nodes and all leak scenarios condition for Net3 network.....	73
Table 6-1 Specifications for benchmark design problems. All specifications based on or taken from (Q. Wang et al. 2015).	87
Table 6-2 Percentage of Solutions Contributed to the Best-Known PF via each MOO algorithm. Highest percentage for each benchmark network are bolded.....	91
Table 6-3 Average of the maximum Effective Archive Size (EAS) throughout each of the 30 PADDs- CHC and PADDs-HVC optimization trials.	103
Table 7-1. Best-found Pareto front for sensor placement optimization problem of Net3 with $\alpha = 0.01$ (Net3).....	111
Table 7-2. Best-found Pareto front for sensor placement optimization problem of Net3 with $\alpha = 0.1$ (Net3).....	112
Table 7-3. Best-found Pareto front solutions for sensor placement optimization problem of C-Town network based on $\Delta T = 1, S = 9, \alpha = 0.01$	116
Table 7-4. Best-found Pareto front for sensor placement optimization problem of C-Town network based on.....	118

Table 7-5. Best-found Pareto front for sensor placement optimization problem of C-Town network based on $\Delta T = 3, S = 9, \alpha = 0.01$	119
Table 7-6. Best-found Pareto front for sensor placement optimization problem of C-Town network based on $\Delta T = 3, S = 5, \alpha = 0.005$	121

Chapter 1

Introduction

1.1 Problem Statement

Aside from water main repair costs, as high as \$1 billion worth of drinking water in Ontario, Canada is reported to leak out of the municipal pipes every year (Zechner 2007). It is further assessed that in Ontario, 20–40%, and in some cases close to half, of all the water pumped through municipal water systems never reaches consumer taps (Zechner 2007).

Ageing pipe infrastructure, abrupt pressure fluctuations, freezing and thawing, or even ground settlement are among the many causes which make the occurrence of leaks and bursts an inevitable fact (Gheisi et al. 2016; LeChevallier et al. 2003; S. J. Lee et al. 2015; Mainali et al. 2015). Leaks cause loss of drinkable water in water distribution systems (WDS). The loss includes waste of energy used to obtain and transfer water from resources, expensive chemicals applied to treat it, and energy to distribute it within the urban area. Leaks also cause pressure loss at demand locations, heightened energy usage, extra pump capacity expansions, and even environmental harm (Abraham et al. 2017; Buchberger and Nadimpalli 2004; Mahmoud et al. 2017; Puust et al. 2010). This problem is much more serious in arid and semi-arid regions with limited availability of water resources and a growing population.

Techniques for leak detection (i.e., deducing the presence of a leak in the WDS) and localization (i.e., finding the location of the leak) in WDS have evolved considerably since the mid-1950s (Abdulshaheed et al. 2017; Li et al. 2015). The water audit structure for drinking water utilities suggested by AWWA and IWA (Alegre et al. 2006) allows water utilities to make a meaningful assessment of their water loss. A water audit uses water balance calculations over network assets and could be assumed as the simplest method for detection of leaks and more generally the non-revenue water. A water audit makes it possible to detect a leak but not to localize it in the network. Furthermore, it is not viable to obtain a high spatial resolution of flow measurements in a WDS due to the large number of pipes, yet it can be worked out for moderate-sized subareas in most networks. In fact, the concept of the district metering area (DMA) formalizes this strategy where networks are designed or upgraded to allow for subareas to have their total water usage monitored by installing flow meters on all pipes crossing the DMA boundary.

Leak detection and localization methods relying on pressure sensors have been extensively studied in the literature as these methods are significantly more economical compared to other methodologies. Many

studies used model-based fault diagnosis (MFD) theory to detect and localize leaks in a pressure sensor equipped WDS. This method relies on investigating the influence of a leak incident on the pressure in the WDS junction nodes. The basic idea in this method is to compare the current status of the system (i.e., measured pressure at certain locations in the network) with previously simulated leak-free status and generate residuals. The residuals are ideally zero in a leak-free case and different from zero when leaks exist.

Many publications have based their leak diagnosis methods on a deterministic application of the MFD logic and report success in picking up leaks often in a very highly precise manner. However, any other change in water demand (e.g., a sudden increase in water use in a specific house) could also cause similar changes in nodal pressure compared to what a leak would generate. In fact, water demand pattern in a WDS has a significant role in pressure changes in the network and water demands are subject to substantial temporal and spatial uncertainties. These uncertainties pose a remarkable disadvantage to the deterministic application of MFD theory as they lead to errors in detection.

Deterministic MFD methods are used in leak localization in many studies. The idea in these methods is looking for the leak (location and size) whose effect would best match the pressure variations sampled from the field. This produces the base for formulation of an optimization problem for pressure sensor placement with the objective of maximizing the capability of localizing leaks in the network by these studies. However, the same concern about the limitation of the deterministic MFD in detection of a leak remains about leak localization and sensor placement because, as some of these studies have pointed out, results of leak localization and sensor placement change significantly with the variation in nodal demand values.

In this work, the application of MFD theory to leak detection is re-established based on paying extreme attention to both the uncertainty of nodal demands and the known WDS states at the time of pressure measurements. This new leak detection approach is then utilized within a new approach to the sensor placement optimization problem. More specifically, this thesis sets out to address two major challenges: 1) Detection of leakages using the MFD method while considering extensive uncertainty in nodal demands, and 2) Solving the large-scale optimization problem of sensor placement while considering the uncertainty in nodal demands.

1.2 Research Contributions

Specifically, this work makes the following contributions:

- 1- Conducts a quantitative assessment of the rate of false positives (believing there is a leak when there is actually no leak) caused by the deterministic application of MFD. This amounts to investigating the magnitude of pressure drops in the absence of a leak due to the presence of demand noise (uncertainty in nodal demand).
- 2- Establishes a novel stochastic comparison framework under nodal demand uncertainty within which, through an exploratory analysis, it becomes feasible to distinguish between the pressure responses in the presence of a leak and those coming from the no-leak condition.
- 3- Introduces a novel leak detection technique that is able to infer the existence of leaks based on a statistical hypothesis test that contrasts observations (nodal pressures) against their plausible probability distributions under the no-leak condition. The methodology, which is based on a nightly sampling of nodal pressures, goes beyond only improving the robustness of the currently utilized deterministic MFD approaches in leak detection and localization using pressure sensors by presenting a new variation of MFD focused on properly accounting for nodal demand uncertainty and the known states of the WDS at the time of each pressure observation.
- 4- Conducts a thorough multi-objective optimization algorithm comparison study for WDSs in order to identify the most appropriate and efficient algorithm to select for solving the computationally intensive sensor placement optimization problem.
- 5- Introduces a novel two-step stochastic multi-objective optimization framework to optimally place a fleet of pressure sensors in the network to minimize both system-level false positives and system-level false negatives simultaneously.

1.3 Scope of Research

This work assumes application of EPANET2 (Rossman 2000) for modelling and solving hydraulic models of a WDS. Other hydraulic solvers could also be considered for this purpose. However, EPANET2 is the most common hydraulic analysis tool for WDS simulation in the literature and it is often the case that the computational methods embedded in EPANET2 are emulated in other hydraulic modelling software packages. The scope of this thesis is as follows:

- 1- EPANET2 simulates the network system in steady-state condition under the demand-driven boundary conditions. The simulation of the system over time is achieved with the extended period simulation (EPS) which is a series of steady-state simulations (Boulos et al. 2006).

- 2- Water demand (and leaks) must be assumed to occur at network junction nodes in EPANET2 models, while actual demands (and leaks) occur along pipes and thus between modelled junction locations. Pérez et al. (2011) believe that this incorrect specification of leak location introduces only a minor inaccuracy compared with those due to other uncertainties in the modelling process.
- 3- The proposed leak detection methodologies is only applicable where total hourly demand, and some system states such as tank levels, pump statuses, and valve states are known at the designated sampling times.
- 4- Among all sources of uncertainty in modelling WDS, this study focuses only on uncertainty in nodal demand. This is because demand fluctuations, is a key source of uncertainty with that significantly impacts nodal pressures. Generally, uncertainties in nodal demands and pipe roughness coefficient are among the most commonly studied uncertainty sources in the context of design and leak diagnosis of WDS (2005; 1998)).

Chapter 2

Literature Review

2.1 Leak Diagnosis

Methods of leak diagnosis all depend on some sort of WDS monitoring data and such data are collected by different types of hardware or devices. This hardware can include for example pressure gauges, flow meters or acoustic devices. All methods of leak diagnosis also require some sort of processing of the monitoring data to determine if it is anomalous and thus indicates the presence of a leak. Such processing includes for example, an inspection of the data by a technician, a simple or complex statistical analysis/comparison against past monitoring data or a comparison against expected monitoring data derived from some sort of model of the system (e.g., a hydraulics model). Puust et al. (2010) provide a review of methods for leakage management.

A useful classification of leak diagnosis methods by Gong et al. (2013) groups methods with hardware devices and begins by distinguishing acoustic and non-acoustic devices. Depending on the characteristics of the device in use, different diagnosis methods have variable detection ranges and operation costs. Methods based on acoustic/vibration signals, often used for detecting relatively small leaks (Ayala–Cabrera et al. 2013; Mutikanga et al. 2012; Stoianov et al. 2007), have become very widely used since the 1990s (Prodon et al. 2010). In these methods, hydrophones or vibration sensors are used to record ambient noise in pipes. Once the signal deviates from the normal recordings a potential leak is detected. These methods require numerous sensors spread over the entire network. Non-acoustic methods such as ground penetrating radar provide cross-sectional profiles of the soil around pipes in order to detect water leakage (M. Farley 2007). These methods are time-consuming and generally inefficient for large networks.

Processing methods for the monitoring data typically rely on software to leverage the data generated by the hardware with the application of various algorithms and network hydraulic models to diagnose leaks. A variety of data (e.g., nodal pressure and flow in pipes) are fed to a software tool which is designed to detect anomalies. Depending on the analysis structure, the software-based processing methods are also subdivided into the following categories:

- 1) hydraulic model-based fault diagnosis methods (either steady-state or transient conditions hydraulic models are used)

- 2) data-driven approaches, which instead of a hydraulic model, rely on data-mining and artificial intelligence algorithms to identify possible leakage areas based on certain rules (Millán-Roures et al. 2018; Mounce et al. 2009; Romano et al. 2017; Y. Wu et al. 2017).

Note that the above discussion avoids adopting the broad division of methods for leak diagnosis proposed in Li et al. (2015) which group methods into either hardware-based or software-based methods.

2.1.1 Hydraulic Model-Based Fault Diagnosis (MFD)

The standard theory of model-based fault diagnosis (MFD), described in Gertler (1998), has been used repeatedly in the context of software-based processing for leak detection in WDS (Pérez et al. 2011). Methods developed based on MFD essentially operate based on the analysis of differences between the measured and simulated values (under no-leak condition) of pressures where a threshold is defined and used in the hope to determine if differences are due to a leak and not random demand variations.

Based on the type of hydraulic model used to generate simulations, these methods are categorized into steady-state MFD and transient MFD. EPANET2 (Rossman 2000) is often used as the hydraulic model solver for steady-state MFD in the literature. As for the transient MFD, to the best of my knowledge, there was no verified comprehensive modelling software package that could serve as the modelling module of an MFD framework. However, the principals of both steady-state and transient analysis are explained below.

2.1.1.1 Steady-State MFD

Application of steady-state MFD in leak detection and localization have been studied since the work of Pudar and Liggett (1992), which evaluates the effect of a leak on the pressures across a distribution network and presents its overall effect using leak signatures under the steady state condition. The signatures are then used to perform leak detection and localization. Detection process in MFD theory works by matching the observed nodal pressure by their expected values under the no-leak condition. If the magnitude of the discrepancy between the two is larger than the threshold, it is believed that there is a leak in the network. In the localization phase, which is triggered after a positive result from the detection step, efforts are made to localize and isolate the component that is in fault by matching the observed signatures with simulated ones under leak conditions (Pérez et al. 2011).

For a small network, Pudar and Liggett (1992) solved the leak localization problem by analytically solving the inverse problem of finding the equivalent orifice areas of possible leaks using measurements

of pressure and/or flow. Obtaining the leak signatures by analytically solving the system of equations is intractable to do in large networks due to the complex nature of a large scale WDS model which is governed by a multivariable, non-linear, and non-explicit system of equations. As an alternative solution, Pérez et al. (2009) replaced the analytical method with computer simulation runs using EPANET2 which computes the numerical derivatives to obtain the leak signatures.

Later on, steady-state MFD was applied by many studies (Campisano and Modica 2015; Casillas, Garza-Castañón, PuigVargas-Martinez 2015; Hagos et al. 2016; Nasirian et al. 2013) for leak diagnosis. Ponce et al. (2014) worked on this methodology by carrying out an extended time-horizon analysis of pressure sensitivities, which was an improvement granting more flexibility to the method. Unfortunately, the aforementioned studies demonstrate a deterministic adaptation of MFD in WDS and thus do not appropriately consider the multiple sources of uncertainty found in these complex systems. Ponce et al. (2014) report that uncertainties may be significant. A comprehensive discussion and analysis of this concern, which constitutes the motive of this study, is presented in Chapter 3.

Goulet et al. (2013) roughly account for uncertainties by proposing a leak-scenario falsification method. This work is among very few studies in the field that discusses the network uncertainties in the context of leak detection; however, there are some areas in which their study can be challenged. Network uncertainties were simplified in their work by using analytical solutions. They represented the uncertainty with extended uniform distributions which range over a bound of $\pm 20\%$ of the predicted value. A disadvantage of the study, which is shared with all the other studies in the field is the fact that the false positives are not considered in the diagnoses methodology. That is almost certainly the reason very small leaks (i.e., 13 GPM) are claimed to be distinguishable in their work. Qi et al. (2018) point out this problem and explain that many studies that focus on the application of pressure data for leak detection include smaller leaks into their range of successful detectability (Bicik et al. 2011; Jung and Lansey 2014). Qi et al. (2018) also highlight the limitations of this methodology by suggesting descriptive metrics to define the detection coverage of the sensor fleet.

A final potential drawback of the study of Goulet et al. (2013) is the application of velocity sensors to measure flow instead of pressure in their work. Typically, such flowmeters are installed over the WDS for water auditing purposes such as mass balance. Optimum locations of such instruments for leak diagnosis under the leak-scenario falsification method can conflict with their true auditing purpose based on which they need to be located in the network.

2.1.1.2 Transient MFD

Governing equations in steady state hydraulic models are the conservation of mass and energy. Extended period simulation (EPS), also known as quasi-steady-state analysis, is a series of steady-state simulations with time steps often in the order of hours. EPS is considered acceptable for most normally operated networks. However, rapid demand changes and dynamic conditions such as water hammer and backflow are likely. Accurate simulation of pressures across a network under such dynamic conditions requires a transient model. Transient simulation modelling, also known as water hammer analysis, solves the full momentum equation at time steps in order of seconds or less. The full transient analysis considers an elastic-water-column in which water density may be variable (Boulos et al. 2006).

Leakage detection and localization using analysis of fluid transients is a well-studied area (Beck et al. 2005; Covas et al. 2003; Covas et al. 2005; Z. Kapelan et al. 2004; Taghvaei et al. 2006; X. Wang et al. 2002; Z. Y. Wu et al. 2009) and it requires large amounts of data to be obtained in a very short time (seconds or less) when the fluid is under a transient state. Moreover, transient simulation is less sensitive to the pipes' roughness coefficients than in a steady-state simulation (Boulos et al. 2006).

Based on analysis of fluid transients, inverse transient analysis (ITA) has been one of the most active research areas in leak diagnosis in the field. Liggett and Chen (1994) first proposed this technique for leakage detection and calibration. ITA generally involves researching and modelling the behaviour of water supply systems under transient events. The technique is based on the deliberate generation of transient waves or impulses at one location and the measurement of the propagated transients with highly sensitive pressure transducers at other locations in the system. The observed transient pressures are used to identify model parameters including leakage and pipe roughness.

Using ITA, Kapelan et al. (2003) described the leakage detection problem as an optimization problem. They compared actual pressure monitoring data with the simulation pressure data obtained from the transient model and minimized the summation of mean square error between them to locate a leak. The range of validity of the ITA is carefully studied by Nixon et al. (2006). They concluded that its applicability is limited to only the instantaneous small amplitude disturbances within simple in-lab serial configurations (e.g., reservoir-pipe-valve type or reservoir-pipe-reservoir systems).

ITA initially appears to be an attractive alternative to steady-state inverse analysis for leakage detection. However, to date, there are no reports in the literature about the successful application of ITA-based methods to water mains distribution systems. As these networks are often highly looped and contain many pumps, tanks, and valves, any induced transients will become greatly damped. This will probably prevent

the success of transient induction as a general method for leakage location predictions. Moreover, ITA requires accurate transient model and pipe network boundary conditions, the model error is the main limiting factor applied to the actual pipe network. Also, the method often requires a large number of high-sensitivity sensors for high-frequency sampling. No effective method has yet been found to accurately distinguish a signal response caused by leakage or by other similar noises such as reflections caused by pipeline fittings and those arising from demand changes (Boulos et al. 2006).

2.2 Hydraulic Modelling

In this thesis, the steady state hydraulic approach is used to solve the network hydraulics. WDS hydraulics can generally be analyzed and solved using the three conservation laws: mass, energy, and momentum. The basic analysis (i.e., steady-state method) can generally be accomplished with mass and energy conservation principles which are explained in this section often citing to (Boulos et al. 2006; Rossman 2000; White 1999). EPANET2 (Rossman 2000) is the hydraulic modelling software package utilized in this thesis.

2.2.1 Conservation of Mass

The principle of conservation of mass states that the mass in a closed system must remain constant over time. Therefore, the mass flow rate into the system must equal the mass flow rate out of the system and no internal storage occurs since water is assumed to be incompressible. The mass balance equation for junction node i is as follows:

$$\sum_{j=1}^J q_{ij} = D_i \quad (2-1)$$

where q_{ij} is unknown flow in the pipe connecting node i and j ; J is the number of pipes connected to the i^{th} network junction node; D_i is the known demand at i^{th} junction node.

2.2.2 Conservation of Energy

The energy associated with a moving fluid can be categorized into three forms: 1) potential energy, 2) pressure energy, and 3) kinetic energy. Expressed on a per unit weight basis, energy components are known as elevation head (z), pressure head ($\frac{P}{\gamma}$), and velocity head ($\frac{V^2}{2g}$). The algebraic sum of these three components accounts for nearly all the energy contained in a unit weight of water flowing through a particular section of a pipe, H^T , Eq. (2-2).

$$H^T = z + \frac{P}{\gamma} + \frac{V^2}{2g} \quad (2-2)$$

The principle of conservation of energy states that the total energy at the upstream junction node of pipe i , ($H_{i,u}^T$) equals the energy at the downstream junction node of the pipe ($H_{i,d}^T$) plus the energy change in pipe i , (ΔH_i), due to losses (H_L) or gains (H_G) as shown below.

$$H_{i,u}^T = H_{i,d}^T + \Delta H_i \quad (2-3)$$

A certain amount of energy loss (H_L) due to friction occurs when the water mass flows in the pipe from one section to another. Pumps can be used to introduce an amount of energy (H_G) to the flow. The energy loss between two points is defined as total head loss (H_L).

$$\Delta H_i = H_L - H_G \quad (2-4)$$

Total head loss is the sum of frictional head loss (H_{Lf}) and minor head losses (H_{LM}) as shown in Eq. (2-5) and defined more precisely in the subsequent two sections.

$$H_L = H_{Lf} + H_{LM} \quad (2-5)$$

2.2.2.1 Frictional Head Losses

Frictional losses are due to the fluid's contact with the pipe wall as follows:

$$H_{Lf} = r q_i^n \quad (2-6)$$

where q_i is flow rate, r is resistance coefficient, and n is flow exponent. Different definitions for r and n exist. Some more commonly used formulas are 1) Hazen-Williams, 2) Darcy-Weisbach, and 3) Chezy-Manning. The Hazen-Williams formula can only be used for water and is the most commonly used headloss formula in the US WDS applications and is the headloss formula used in all modelling of this thesis. Resistance coefficient and flow exponents for the Hazen-Williams formula is presented in Eq. (2-8) (Rossman 2000).

$$\begin{aligned} r &= 4.727 C^{-1.852} d^{-4.871} L \\ n &= 1.852 \end{aligned} \quad (2-7)$$

where C is Hazen-Williams roughness coefficient, d is pipe diameter (ft), L is pipe length (ft). Eq. (2-6) calculates the headloss in feet.

2.2.2.2 Minor Head Losses

Minor losses (H_{LM}), also known as local losses, are caused by the added turbulence that occurs at various pipe network components/forms (i.e. valves, bends, fittings, etc.). The importance of including such losses depends on the layout of the network and the degree of accuracy required. In most systems, frictional head loss accounts for the vast majority of energy losses. Minor losses are often assumed to have a negligible effect on the system. However, the minor headloss becomes the product of the minor loss coefficient (K) and the velocity head of the pipe as follows:

$$H_{LM} = K \frac{V^2}{2g} \quad (2-8)$$

where K = minor loss coefficient (determined empirically), V = flow velocity, and g = acceleration of gravity.

2.2.3 Global Gradient Algorithm

Equations developed in the previous section when applied to the network form a set of non-linear equations, which can then be solved using a number of different methods. The set of nonlinear equations include the mass balance equations (Eq. (2-1)) for each node and the energy equations (Eq. (2-3)) for each pipe. The unknowns to be solved for are the nodal pressures, pipe flow rates, and tank levels. To solve the system of nonlinear equations, the time series of nodal demands, constant water levels of each reservoir, and initial tank levels are required. In addition, the initial status of time-controlled pumps and valves must be specified.

A number of solution approaches are available to solve the system of equations. EPANET2 uses a method called the global gradient algorithm (GGA) by Todini and Pilati (1988). This is also called the Gradient Method or the Simultaneous Network Method, which is a variant of the Newton-Raphson method.

2.2.4 Modelling a Leak in EPANET2

In EPANET2 (Rossman 2000), emitters are used to simulate leakage in a junction node. Emitters are essentially devices associated with junctions that model the flow through a nozzle or orifice that discharges to the atmosphere. The flow rate through the emitter varies as a function of the pressure available at the junction node.

$$q_j(t) = EDC \times \hat{p}_j(t)^\gamma \quad (2-9)$$

where $q_j(t)$ and $\hat{p}_j(t)$ are leak flow rate and simulated pressure at the junction node j at time t , respectively; EDC is emitter discharge coefficient, and γ is emitter pressure exponent. For nozzles and sprinkler heads γ equals 0.5 and the manufacturer usually provides the value of the discharge coefficient. As for leaks, the discharge coefficient and pressure exponent for the leaking crack or joint have to be estimated. Emitter pressure exponent can vary from 0.5 to 2.5 depending on pipe materials (Lambert 2002).

EPANET2 models an emitter at a junction as a fictitious pipe between the junction and a fictitious reservoir. Resistance coefficient and flow exponent of the fictitious pipe are $\frac{1}{\gamma}$ and $\sqrt[\gamma]{1/EDC}$, respectively. Zero minor loss is assumed for the fictitious pipe. The head at the fictitious reservoir is the elevation of the junction. The computed flow through the fictitious pipe becomes the flow associated with the emitter.

In reality, a leak could possibly appear at any point in a network pipe. For this reason, the exact modelling of any possible leak is not possible in EPANET2. To mitigate this issue, it is usually assumed that leaks only appear at existing junction nodes although additional junction nodes along a pipe could theoretically be added to a model.

2.2.5 Demand Driven Versus Pressure Driven Simulation in the Context of Leak Modelling

Demand-driven analysis (DDA) assumes the existence of enough pressure at the network nodes to provide the demanded volume of water at all times in the network. In absence of the sufficient nodal pressure, the demand cannot be fully supplied and only a partial delivery occurs at the node. This situation is the focus of another method of WDS analysis known as the pressure-driven analysis (PDA). Application of PDA has gained in momentum in the recent WDS leak modelling literature. Based on the considerations listed below, the hydraulic models in this thesis are solved using a DDA solver.

1- This study assumes the availability of water volume and pressure to satisfy nodal demands. Under this assumption, performing a demand-driven analysis can be justified. However, leaks are modelled as pressure-dependent outflows of the system (Eq. (2-9)) and increase with an increase in pressure in the node (Gupta et al. 2016).

2- This study focuses on relatively small leak flows which constitute a rather small portion of the network demand. Therefore, it is assumed that the flow rate through the leak follows Eq. (2-9). For example, Qi et al. (2018) use pressure-driven leak simulations for leak sizes ranging from 50 LPS to 3,500 LPS which are effectively bursts and thus create conditions such that nodal demands can't be satisfied. In this work, leak sizes are restricted to be of magnitude 50 LPS or less.

3- There are multiple previous studies simulating leaks with a demand-driven hydraulic model (Blesa et al. 2016; Casillas et al. 2013a; Casillas, Garza-Castañón, PuigVargas-Martinez 2015; Casillas et al. 2015; Pérez et al. 2009; Pérez et al. 2011; Pérez et al. 2015; Ponce et al. 2014; Sarrate et al. 2014).

4- A tool that facilitates a straightforward implementation of PDA (without modification of source code of EPANET2) was not available until the work of Paez et al. in (2018). They explained different methodologies in the literature to model the partial flow as a function of nodal pressure. They introduced a method to perform extended period simulations with pressure driven demands using EPANET2. Their method is based on adding artificial network elements such as valves and reservoirs to the demand nodes.

Generally speaking, the methods proposed in this thesis are hydraulic model-based leak diagnosis methods and do not critically depend on the type of hydraulic model (e.g., pressure-driven versus demand driven).

2.2.6 Nodal Elements Terminology

In this thesis, the terminology below is used to refer to different nodal elements in a WDS.

1. Nodes (may or may not have base demand)
 - Demand node: nodes with positive base demand value (points where water exits the network).
 - Zero-demand nodes: nodes without base demand. They are simply nodes in the network where link elements join together.
2. Tanks: nodes with storage capacity, where the volume of stored water can vary with time.
3. Reservoirs: nodes that provide constant head value thus can act as infinite external sources or sinks of water in the network.

2.3 Sensor Placement Optimization

The problem of optimal sensor placement in WDS has been studied for a few different monitoring contexts. For example water quality (Tolson et al. 2012) and for hydraulic monitoring. The generic problem solved involves obtaining maximum information about acoustic, pressure, or flow for monitoring the network with a minimum number of sensors and thus the least cost. The concept of information theory has been implemented in Christodoulou et al. (2013) where they suggest placing the sensors in a way that the total entropy in the network is maximized (an entropy metric was defined for pipe segments).

MFD-based pressure sensor placement involves relying on the MFD theory or approaches, described in Section 2.1.1 above, to optimally locate a sensor fleet. There are two approaches utilizing MFD concepts: matrix-based and scenario-based.

The first group of matrix-based studies (Meseguer et al. 2015; Pérez et al. 2011) focus on the sensitivity matrix itself and try to come up with a candidate sensor placement setting that maximizes the potential of the sensor fleet in locating any leak in the network. The general idea in this approach is that those locations where sampled pressure data under the influence of a leak are more distinguishable from expected pressures with no leak are more desirable. For example, Meseguer et al. (2015) used a weighted sum of three metrics (i.e., the number of unique leak signatures, the sum of the size of the largest groups of undetectable leaks, the sum of the biggest geographical areas of the groups of non-isolable leaks) in sensitivity matrix. Numerous studies come with a variety of distinguishability metrics which are reviewed in Bonada et al. (2014). Bonada et al. (2014) also further evaluate the metrics by means of a cross-correlation analysis to understand their behaviour and find out which metrics are independent and which are redundant.

The second approach of scenario-based studies of optimum sensor placement based on the MFD is trying to find the best candidate sensor placement setting that is most successful in localizing a set of predefined leak scenarios in the network. These approaches are referred to as the scenario-based approach, henceforth. For example, Casillas et al. (2013b) used MFD to optimally place sensors minimizing the number of leaks that cannot be isolated (while considering leaks on every network junction node). They formulated the sensor placement problem as a non-linear integer optimization problem and used both a genetic algorithm and semi-exhaustive search method to solve it. In their study, the optimum configuration of sensors would change with different leak sizes assumed. In a subsequent study, Casillas et al. (2015) improved the methodology by trying to minimize the effect of the leak magnitude. In contrast to the matrix-based approach, a candidate sensor placement is evaluated against a set of leak experiments which could be manually defined based on historical records of water main breaks.

The challenge with scenario-based approaches is that the optimized sensor placement design would be the best one only in localizing a pre-defined set of leak scenarios and not necessarily other ones. The matrix-based methods can be solved significantly faster compared to the scenario-based ones because the matrix-based methods only focus on the sensitivity matrix itself and look for a sub-matrix that provides the maximum distinguishability. Whereas scenario-based methods would need to evaluate each candidate solution by checking its performance in the localization of each leak scenario which requires numerous

hydraulic simulations of the distribution system (or DMA). The matrix-based sensor placement formulation is much more common than the scenario-based one from the perspective of occurrence in the literature (Bonada et al. 2014).

However, scenario-based methodologies have the benefit of favouring sensor system layouts that have actually (rather than potentially) been able to successfully localize leaks. Furthermore, the sensor placement optimization would be solved only once to decide where to install the sensors, therefore, it is acceptable that the use of scenario-based methodologies in the objective function formulation makes the one-time sensor placement optimization procedure slower. Scenario-based approaches allow flexibility in the definition of custom leak scenarios; scenarios could be constructed to concentrate on more vulnerable or sensitive pipes of the WDS. Furthermore, by expanding the scenarios in both number and variety, the reliability of the obtained sensor configuration in detection and localization of leaks should potentially improve. Features of the two sensor placement approaches are summarized briefly in Table 2-1.

Table 2-1. Matrix-based versus scenario-based approaches to the sensor placement problem in WDSs

	Matrix-based	Scenario-based
Presence in the literature	Many	rare
Targeting	any possible leak	specific leak scenarios
Optimization pace	Fast	slow
Provide flexibility for DMA specific situation	No	yes

Building on Casillas et al. (2013b), the work of Steffelbauer et al. (2014) considered demand uncertainty to solve a sensor placement optimization problem using the MFD approach. The gap they addressed was the fact that previous works generally tend to place sensors in locations in WDS that are more sensitive regarding pressure changes due to leakages; however, it should be noted, they pointed out, that the same locations are also probably more sensitive to stochastic changes in demands. To incorporate demand uncertainty they modified the objective function of Casillas et al. (2013b) to penalize candidate locations that are more sensitive to demand fluctuations and favour less sensitive ones. The results in Steffelbauer et al. (2014) show that considering demand uncertainty will completely change optimal sensor positions in the same case study, which implies the important role of uncertainty sources.

Kang and Lansey (2012) presented a hydraulic model-based burst detection approach. They employed Monte Carlo method to quantify variations in nodal pressure and pipe flow because of uncertainties (i.e., demand and pipe roughness) and quantified and presented the variations in flow and pressure in terms of the control limits. For their case study, they evaluated 10,000 Monte Carlo samples and calculated the control limits of system hydraulics (pressure and flow) as the 95% confidence level. They assumed the control limits are intended to include normal system variations because of uncertainties in system demand and pipe roughness and any events causing system responses to be out of the limits, such as sudden industry water usage, firefighting, or a pipe burst, are considered abnormal events. Their work by far is the most comprehensive one from the perspective of including demand uncertainty in MFD methods. However, similar to previous works, their sensitivity matrix, which is the baseline to compare pressure observations with, is static and constant over the time.

Although this thesis does not cover WDS water quality, there is a large body of work in the field of sensor placement for contamination warning systems that warrant a brief note. In these studies, reviewed by Hart and Murray (2010), the sensor placement problem is often presented in the format of an optimization problem. Optimization objectives in these studies include minimization of the expected time of pollution detection, the expected population of people affected prior to detection, the expected demand of contaminated water prior to detection, and maximizing the detection likelihood of the pollution (Hart and Murray 2010). These optimization studies typically rely on hydraulic models and a corresponding WDS water quality simulation model.

Both single (Krause and Guestrin 2009; Watson et al. 2008), and multi-objective (Aral et al. 2008; Dorini et al. 2008; Ostfeld et al. 2008) optimization algorithms have been applied to optimally place an array of sensors in the network to achieve more efficient online contaminant monitoring systems. Some studies (Carr et al. 2004; Chastain Jr 2006) included model uncertainties (e.g. nodal demand uncertainties). The Battle of the Water Sensor Networks (BWSN) summarized by Ostfeld et al. (2011) present various methods for optimally design and contaminant monitoring system which serves as protection against biological or chemical contaminant introduction into WDS. The BWSN problem of the battle falls into the category of scenario-based optimization methods where solutions are evaluated based on their performance regarding a definite set of scenarios. Uncertainty in time, location, quantity, and consequences of the injected contamination is considered in the definition of BWSN problem based on which the false positive and false negatives are evaluated for each participant's solution.

2.4 Uncertainty Sources in Hydraulic Modelling

In this section, an overview of different uncertainty sources in hydraulic modelling is provided. WDS hydraulic models are rife with many sources of uncertainty. Hall (2003) divides uncertainty sources in the modelling process into two categories: aleatory and epistemic. Aleatory uncertainty, also known as statistical or irreducible uncertainty, represents unknowns that differ in each time the experiment is run. In the context of WDS models, change of nodal water demand is an aleatory uncertainty. Even better knowledge (i.e., currently available measurement and modelling technology) of urban water usage cannot be determined sufficiently to eliminate the resulting chaotic demand changes during time. Epistemic uncertainty, also known as systematic or reducible uncertainty, refer to uncertainty sources that are known in principle but not in practice. They result from incomplete system knowledge but could be reduced by incorporating additional knowledge and features into the model. For example, the location of nodal demands in a WDS hydraulic model can be improved in accuracy using available GIS information.

Hutton et al. (2012) suggested three main categories of uncertainty sources to be dealt with in modelling WDS. Each of those categories, as explained below, include aleatory and/or epistemic uncertainty sources.

2.4.1 Structural Uncertainty

Those errors in modelling which cause generate an unrealistic mathematical representation of WDS classify as model structural uncertainty sources, and these errors include skeletonization and definition of demand locations.

1. Skeletonization

Hydraulic Models become increasingly complicated and become computationally impractical if they include all pipes of the WDS. Therefore, modellers often remove pipes not considered essential for system analysis. Outputs of highly skeletonized models adversely affect our understating from network behaviour in many aspects such as demand satisfaction prediction as explained by Walski et al. (2003). Problems associated with highly skeletonized hydraulic models are listed in Hutton et al. (2012). This source of uncertainty, however, is becoming less important with the rise of computational power that enables modellers to solve large, complex all-pipes models of WDSs.

2. Demand Locations

In a hydraulic model, water demands are aggregated at junction nodes. In reality, consumers extract water from along pipes within the network (Abraham et al. 2017; Lansey 2011).

Both model structural uncertainty sources mentioned above classify as epistemic, since incorporating more information could reduce them to any desired level.

2.4.2 Parameter Uncertainty

WDS model input parameters (e.g., roughness, emitter coefficient) are uncertain. For example, pipe roughness value can vary over both the pipe length and the time (Kleiner and Rajani 2001). Roughness values can neither be controlled in currently available physical experiments nor exactly inferred by statistical methods (they can empirically estimate using expensive fire-flow tests, however). Uncertainty in pipe roughness values could be assumed both aleatory and epistemic. Monte-Carlo methods could be applied to significantly improve the estimations (epistemic part); however, methodologies to model the parameter precisely enough are not available (aleatory part).

2.4.3 Measurement/Data Uncertainty

Data uncertainty refers to uncertainty in data used to define initial conditions (e.g., tank levels), model inputs (e.g., demands), and model state observations utilized in the evaluation of model predictions (e.g., pressure). Uncertainty in nodal demands, which is the focused source of uncertainty in this study, is an example of data uncertainty with both aleatory and epistemic characteristics. Note that in this study total demand for a network or a part of the network is assumed to be measured without uncertainty but the spatial distributions of that demand among the nodes is uncertain.

Measurement errors affect the accuracy with which system states may be quantified, both through direct measurement, and indirectly when such measurements are employed to calibrate WDS models. Quantification of these uncertainty sources is required such that they may be propagated into calibrated states and parameters, and finally model forecasts (E. Blokker et al. 2009; E. Blokker et al. 2011).

Chapter 3

Quantitative Assessment of Existing MFD Method in Literature

3.1 Summary

This chapter is a very detailed literature review and corresponding quantitative reproduction of model-based fault diagnosis (MFD) methods in the context of leak diagnosis in water distribution system (WDS). It follows from the concern raised in Chapter 2 about gaps in consideration of uncertainty in MFD methods. In this chapter, the procedure often practiced in the literature to apply MFD is first delineated. Next, an uncertainty analysis is implemented on a small case study taken from the literature with the aim of performing a quantitative assessment of the deterministic MFD exposed to uncertainty in nodal demands. It is shown that the magnitude of pressure drops in absence of a leak due to the presence of demand noise (uncertainty in demand) can well exceed the size of pressure drops only because of a leak, which results in high values of false positive leak detection rates. The experimental leak size is taken to yield around the same leak flow that is published in the literature where successful detection is reported. Resulting significant false positives confirm the concerns raised in Chapter 2 about ignoring the effect of uncertainty in nodal demands and furthermore, uncover a substantial disadvantage to the dominant deterministic application of MFD reported by many publications in the field.

3.2 Introduction

The MFD-based leak detection process is based on computing the difference (residual) between the pressure measurements, $p_i(t)$, which are sampled from sensors in the field, against their corresponding hydraulic model simulated value (expectation) under the no-leak condition, $\hat{p}_i(t)$, according to Eq. (3-1):

$$r_i(t) = \hat{p}_i(t) - p_i(t) \quad i = 1, \dots, N \quad (3-1)$$

where $r_i(t)$ is the residual obtained from sensor i at time-step t , and N is the number of pressure sensors available in the network.

In the practical application of the methodology, p would be the sampled from sensors installed in the field. Values of \hat{p} are obtained by hydraulic analysis of the network model under the nominal nodal demand condition and in absence of a leak. Conventionally, the nominal nodal demand values are available from the calibrated model of the network.

In a deterministic adaptation of MFD, the expected nodal pressure values under no-leak condition are obtained by simulating the network model under constant, nominal network conditions. This implies that the same condition (i.e., nodal demand) is assumed to exist at the time of sampling the nodal pressure. A leak anomaly is deduced to exist somewhere in the network if and only if any observed pressure residual exceeds its threshold value (τ_i) (Eq. (3-2)).

$$|r_i(t)| \geq \tau_i \quad (3-2)$$

Some studies (Casillas et al. 2013b; Casillas, Garza-Castañón, PuigVargas-Martinez 2015; Casillas et al. 2015; Pérez et al. 2009; Pérez et al. 2011; Ponce et al. 2014) utilize the threshold value as an indirect way of addressing demand uncertainty in the network. This is done by increasing the threshold magnitude so that residuals caused by only the demand noises can be ignored. Unfortunately, this also functions to filter out pressure variations caused by relatively small leaks which cannot be properly distinguished from the effect of regular demand variations on pressure. This approach effectively ignores the smaller leaks and focuses on bigger ones (bursts) and functions to reduce the false-positive rate at the expense of increasing the rate of non-detection (false negative).

This trade-off (between false positives and false negatives) has not been paid attention to in these studies where detection is simplified to the deterministic approach explained above based on which success in localization and instructions for sensor placement are frequently reported. The localization strategy is, for example, explained in the work of Ponce et al. (2014). This concern is thoroughly discussed in the following sections of this chapter.

3.3 Deterministic MFD in Leak Detection

After reviewing past MFD studies, Blesa et al. (2016) admit a reoccurring absence of consideration of model uncertainties, notably nodal demands, in MFD-based leak detection research. The problem with the deterministic adaptation of MFD is the assumption that the nodal demands employed to simulate nodal pressure responses will remain the same when sensors are sampling pressures in the field. In reality, nodal demands in WDS are well-known to randomly vary (from their nominal values) over time and this fact challenges the deterministic MFD methods as shown in the rest of this chapter. Demand fluctuations influence nodal pressures analogous to how a leak would; therefore, deterministic MFD will generate false positives when applied in real WDS with demand noise and the question is how significant will this impact be.

The detection part of the deterministic MFD, as presented in studies of (Blesa et al. 2016; Casillas et al. 2013b; Casillas, Garza-Castañón, PuigVargas-Martinez 2015; Pérez et al. 2009; Pérez et al. 2011; Ponce et al. 2014), is simply based on the inequality of Eq. (3-2). Here, a few relevant statements from those works with regard to detection are given. Pérez et al. (2011) mention that the existence of a fault is determined in the network when any residual becomes bigger than the threshold; otherwise, they assume that the system is working properly. Ponce et al. (2014) imply that the exceedance of residuals is enough evidence for the existence of an anomaly. Blesa et al. (2016) mention “A threshold-based test is usually implemented in order to cope with noise and model uncertainty effects. At the absence of faults, all residuals remain below their given thresholds. Otherwise, when a fault is present, the model is no longer consistent with the observations. Thus, some residuals will exceed their corresponding thresholds, signalling the occurrence of a fault.” (p. 137).

Pérez et al. (2011) explain that the choice of the threshold has to be done with input noise and modelling errors in mind: “The robustness of a fault detection system means that it must be only sensitive to faults, even in the presence of model-reality differences (Chen and Patton 2012)” (p. 1159). They illustrate how low values of threshold improve the performance of the MFD method in revealing the existence of an anomaly somewhere in the system (detection) while high threshold values facilitate isolation of the anomaly (localization). However, what is missing in Pérez et al. (2011) suggested methodology which is exercised by many successive studies is an actual quantitative assessment of the extent to which input noise (e.g. nodal demand fluctuation) in a WDS model could generate false positives at the stage of leak detection. There is a consensus, in all previous MFD studies, over the detection method suggested by Pérez et al. (2011) but the influence of the system noise was never contrasted against the effect of leaks, objectively.

The issue of false positives at the stage of detection is of prime importance because they trigger the localization search process during which machine/human resources are engaged to look for a non-existing anomaly. Pérez et al. (2011) explain that in a real application of the method, robust residuals need to be used. It is necessary to point out that although they have mentioned the problem, they did not address it properly. In the work of Blesa et al. (2016) and research-chain of (Casillas et al. 2013a; Casillas, Garza-Castañón, PuigVargas-Martinez 2015; Casillas et al. 2015; Ponce et al. 2014) the threshold value, or how it was obtained/assumed, is not discussed. Ponce et al. (2014) mention, as a conclusion, that the unaccounted variation of nodal demands could induce the methodology to indicate a leak when in fact there is none. Furthermore, regarding one of their localization methods which requires an evaluation of the residuals against threshold values, Ponce et al. (2014) state: “Looking at the tables presented above,

we are able to conclude that binarization and Euclidean distance methods are not efficient enough at locating leaks. In the case of the binarization method, this may be due to the fact that we have to establish a threshold in order to binarize the vectors and in several cases it is not possible to know the correct value.” (p. 659).

Motivated by the incomplete assessment of this issue in literature, the remainder of this chapter presents a quantitative assessment of the influence of nodal demand uncertainty on the performance of the deterministic adaptation of MFD. The aim is to evaluate the validity of the assumptions accepted for long-time in the deterministic MFD based leak detection method for which an example is the Blesa et al. (2016) statement: “At the absence of faults, all residuals remain below their given thresholds.” (p. 137).

It needs to be pointed out, however, that the uncertainty of demand has been paid attention to at the stages after the detection (i.e., leak isolation and sensor placement). For instance, Blesa et al. (2016), although confirm that in general the residuals change depending on the leak magnitude and the nodal demands, yet do not address the concern at the detection phase. Instead, they proceed to create an optimization framework for sensor placement while more than one nodal demand setups are examined. They fail to put forward a method for solving the problem of leak effects being lost in the demand fluctuations at the very first step of the diagnosis which is the detection step. They instead resolve the optimization problem with different demand distributions to obtain a sensor configuration that is best for few scenarios. Another example is the work of Casillas et al. (2015) where they too point out the idea of robustness and uncertainty but by that, they only mean the variability of considered leak size in their localization framework (not detection).

3.4 Quantitative Assessment of False Positive Rate under Deterministic MFD

To investigate the concern with the reliability of the deterministic adaptation of MFD, the probability of residuals exceeding the threshold as a result of nodal demand fluctuation only (in absence of a leak) is estimated for a medium-sized literature network (Net3). The aim is to examine and compare the residuals in presence of a leak against a synthetic observation coming from random noise in nodal demands when there is no leak present. A similar leak to the one of Pérez et al. (2011) is taken, and it is shown that the effect of such a leak could be masked significantly by the influence of demand uncertainty which in turn results into large false positive ratios.

Net3, displayed in Figure 3-1, is the hydraulic model of a medium-size WDS which is included as an example network in EPANET2 software package. The Net3 example is provided as a 24-hr extended period simulation (EPS) for an example calendar day.

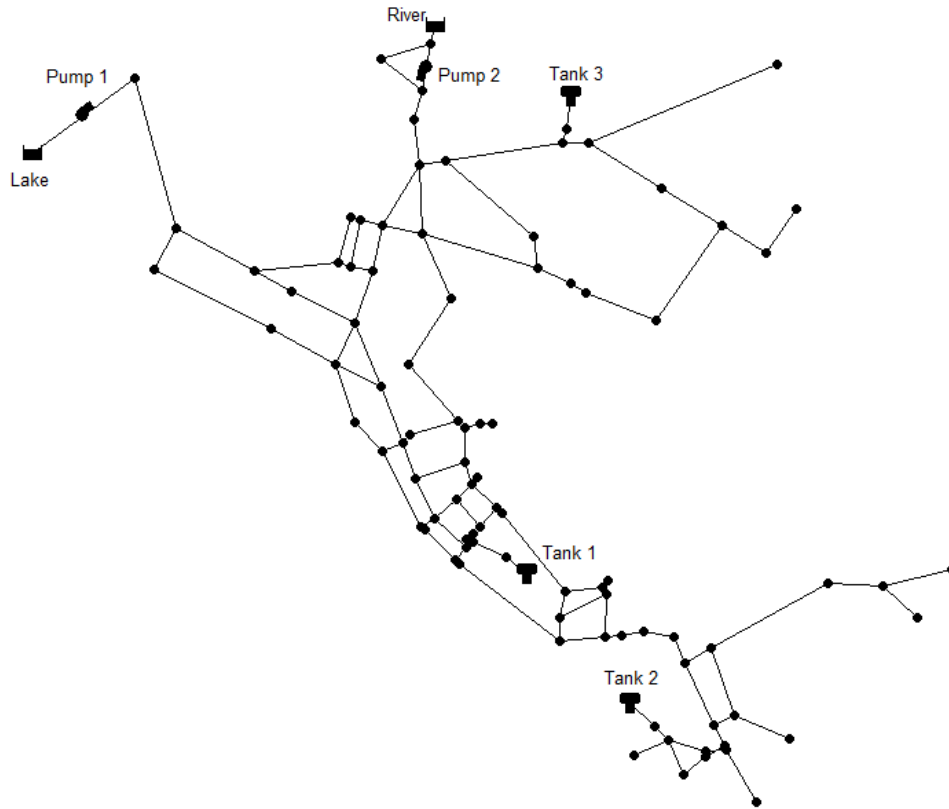


Figure 3-1. Net3 water distribution system layout

Net3 is considered to be calibrated and therefore the pipe diameters and other specifications are taken to be as realistic as possible. In other words, except for nodal demands, all the real characteristics of the network are known with certainty. Table 3-1, presents a brief description of Net3. In Net3, 59 of the 91 network junctions are demand junctions. Base demands for all the 59 junctions, for all time-steps, are given. The network is supplied by two sources: one lake and one river which are modelled as constant heads. The lake source operates only during a part of the day from 1:00 AM until 3:00 PM. There are two pumps in Net3. Pump 1 is fed by the lake. Pump 2 pumps water from the reservoir and is controlled by the water level in Tank 1; it is active or inactive if the water level is below 17.1 ft or above 19.1 ft, respectively. When pump 2 is closed, its bypass pipe is opened and vice versa. Units of the model are US Customary; flows are measured in gallon per minute (GPM), the diameter of pipes are in inches, elevations

in feet, pressures in psi, flow velocity in feet per second, and volume in cubic feet. Hazen-Williams equation is used to calculate head-loss in pipes. Emitter exponent for modelling leaks is assumed to be 0.5.

Table 3-1. Net3 specifications

EPANET2 Network Element	Count	Description
Junction	91	59 Demand Nodes
Reservoir	2	A lake and a river
Tank	3	Tank1, Tank2, Tank3
Pipe	117	Diameters ranging from 8 to 30 inches Roughness coefficient ranging from 110 to 141
Pump	2	Pump1, Pump2

3.4.1 No-Leak Scenarios

As the first step, a set of 30,000 random demand realizations were generated by sampling hourly demands randomly from normal distributions with means equal to the nominal demands and coefficient of variations of 30%. The multivariate sampling process follows the method introduced in the work of Filion et al. (2007). Figure 3-2 shows one demand realization (randomly picked out of the 30,000) along with the nominal demand of the network. Realizations are made in the absence of any leak in the network.

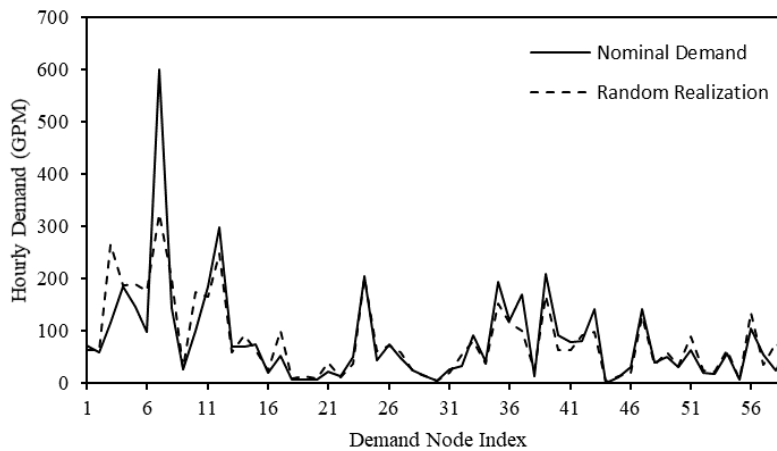


Figure 3-2. One random demand realization along with the nominal demand pattern

Using EPANET2, the network model was simulated for each demand realization and pressure residuals were generated for all the nodes over one time-step (an hour). The time step starts at 12:00 AM and then the randomly generated nodal demands are applied over the time step. End of time step pressure residuals (r_n) are obtained from Eq. (3-3), with respect to the nodal pressures at the corresponding time t under the nominal demand pattern.

$$r_n(t) = \hat{p}_{nd}^{nl}(t) - \hat{p}_{rd}^{nl}(t) \quad (3-3)$$

where $\hat{p}_{nd}^{nl}(t)$ and $\hat{p}_{rd}^{nl}(t)$ are the simulated pressure vectors at time t under no leak and nominal demand and no leak and random demand conditions, respectively. r_n is not to be conflated with Eq. (3-1) which is the pressure residuals taken from the unknown condition (i.e., leak or no-leak) and the simulated no leak pressure. r_n contains pressure responses of the network nodes to the noise in nodal demands in absence of a leak.

The experiment is done for the first and second time-steps which correspond to 12:00 AM to 1:00 AM and 1:00 AM to 2:00 AM, respectively. Figure 3-3 shows the histogram of pressure residuals at the first time step and for node number 1.

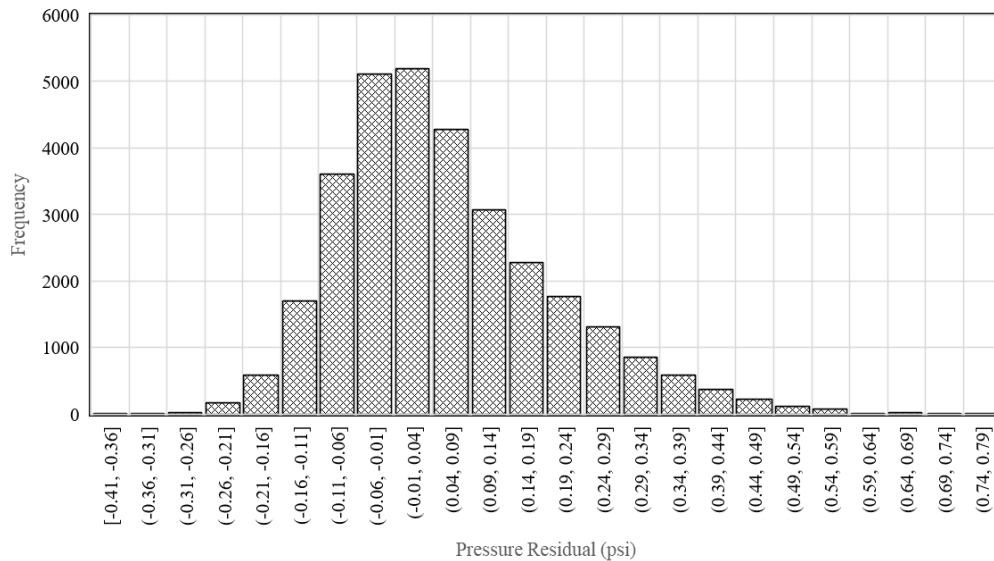


Figure 3-3. Histogram of pressure residuals at node #1 for time-step 12:00 to 1:00 AM

Figure 3-4 is prepared in an effort to visualize distributions for the 30,000 pressure residuals for each node in one plot for two example time-steps. The x-axis represents node numbers on which each tick-mark is for one node. The boundaries, median, and quantiles of each set of generated pressure residuals (per node) are defined in Figure 3-4-a for the first example time-step (1) and Figure 3-4-b for the second example time-step (2).

In both plots of Figure 3-4, the boundaries show the extent to which pressure residuals (r_n) could vary under influence of the uncertain demand in absence of any leak. The areas between the first and third quantiles and x-axis is darkened to present the most frequent residual values. The medians and boundaries are plotted by lines. Node indices are sorted on the x axis based on the magnitude of the range of each node's r_n distribution.

The aim is to investigate if the pressure residuals caused by an actual leak would be distinguishable from the residuals obtained under only demand fluctuation and no-leak. Later, pressure residuals under a leak are generated.

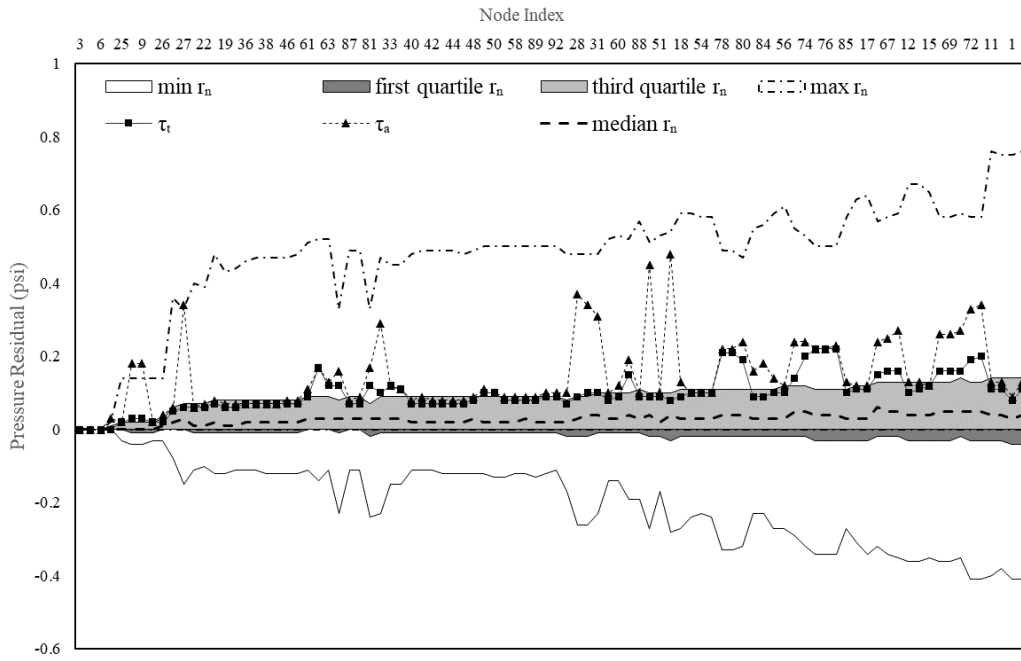
3.4.2 Leak Scenarios

As the next step, based on the nominal demands, pressure residuals for each node in response to a leak located on the same node were taken. Leak sizes were controlled by modifying emitter coefficients and hence precise leak flows could not be directly specified. Importantly, leak flows rather than flows resulting from pipe bursts were the target of this analysis. The resulting leak-flows from the nodes range from 0.87 to 3.65 LPS with an average of 2.56 LPS. The leak flow is on average equals to 2.7% of the total demand of the network. The leak used by Pérez et al. (2011) was in average 1.0 LPS and 3% of total network demand.

To obtain the residual values under leaks (Eq. (3-4)), the same pressure values from under the nominal demands were used. This means that to calculate the residuals, simulated nodal pressures under the leak and nominal demand condition were subtracted from pressures under no-leak and nominal demand condition. This is in line with Pérez et al. (2011) methodology to generate residuals.

$$r_l(t) = \hat{p}_{na}^{nl}(t) - \hat{p}_{na}^l(t) \quad (3-4)$$

a)



b)

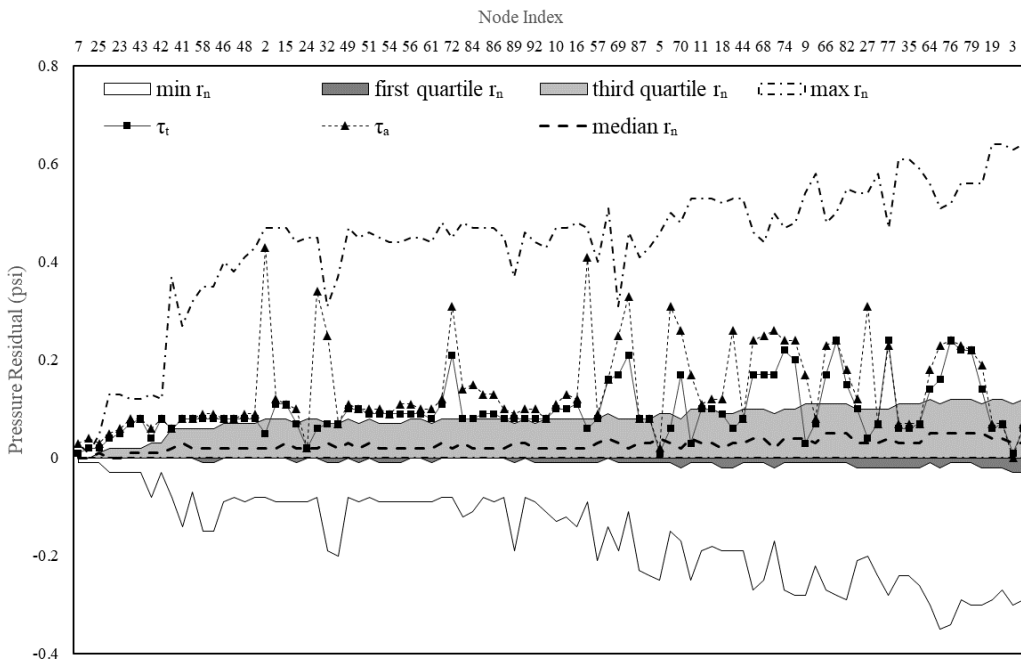


Figure 3-4. Pressure residuals variation per node for a) time-step 12 to 1 AM and b) time-step 1 to 2 AM (τ_a , and τ_t are explained in the following)

3.4.3 False Positives

False positive ratio is defined below as the empirical probability for a given threshold vector $\boldsymbol{\tau}$:

$$\varphi(\boldsymbol{\tau}) = Prob\{\boldsymbol{\tau} \leq \mathbf{r}_n\} \quad (3-5)$$

where \mathbf{r}_n is the vector of pressure residuals caused by the demand noise and nominal demand (depicted in Figure 3-4), $\boldsymbol{\tau}$ is the residual threshold. Higher values in $\boldsymbol{\tau}$, result in smaller $\varphi(\boldsymbol{\tau})$ and vice versa. The false positive ratio is calculated by dividing the number of items in \mathbf{r}_n that have exceeded in magnitude their corresponding threshold in $\boldsymbol{\tau}$.

To investigate the relationship between false positive ratio and threshold values, two scenarios for $\boldsymbol{\tau}$ are defined. In both scenarios, it is assumed that a leak is detected if any measured residual (at any available sensor location) exceeds its threshold.

Scenario 1)

In this scenario, each node has its threshold equal to its own pressure residual when the leak is at the same node:

$$\boldsymbol{\tau}_a = \mathbf{r}_l \quad (3-6)$$

To generate the series of pressure residuals under this scenario, for each node, the pressure drop resulted by the leak at the same node was reported. This series is plotted in Figure 3-4 to provide a comparison with the distribution of residuals under demand noise and no leak.

In this scenario, it is assumed that there always exists a sensor at the leak location so the residual at the node would always be available. Under this essentially unrealistic scenario (existence of sensors at each leak location), in the deterministic MFD approach, a leak at the node is always detected as it necessarily produces residuals that equals the node's threshold (assuming the same sized leak was utilized to generate the threshold). This scenario would produce the least (best) false positive ratios among the two because, under it, residuals smaller than the threshold may not falsely be picked up as a leak. However, in reality, this is not going to be the case because there will not be a sensor at every network junction.

Scenario 2)

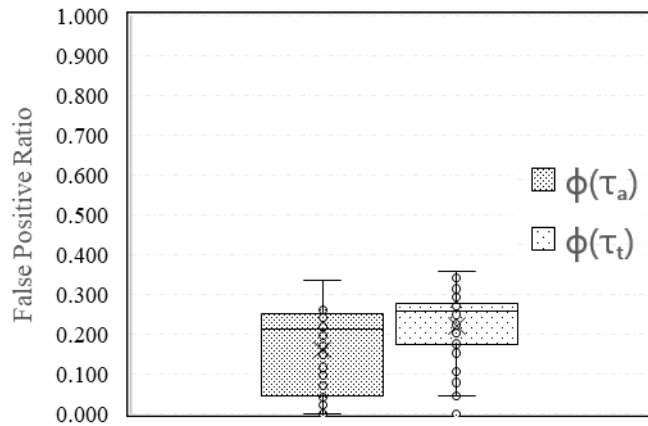
Another setup is defined in which the thresholds are determined based only on simulation experiments with nodes 15, 33, 50, 62, and 75. These nodes are arbitrarily chosen to provide a reasonable area coverage over the network map. This scenario is more realistic compared to the previous one. Under this scenario,

the threshold for each node is the highest pressure residual picked up by the sensor fleet in response to the leak at the node (Eq. (3-7)).

$$\tau_t = \max(r_l(15), r_l(33), r_l(50), r_l(62), r_l(75)) \quad (3-7)$$

The false positive ratio corresponding to each threshold scenario was calculated. For each scenario, a Box-Whisker plot of the false positive ratios for all the network nodes is presented in Figure 3-5 for two time-steps 1 and 2.

a)



b)

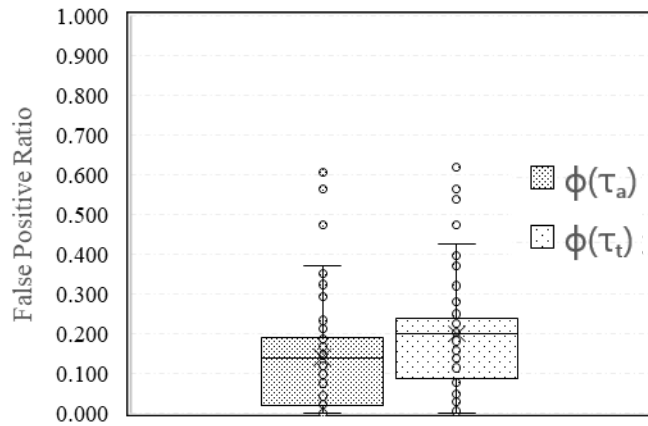


Figure 3-5. False positive ratios for different threshold scenarios at a) time-step 1 and b) time-step 2

Figure 3-5 shows that the false positives are generally more desirable under Scenario 1. Yet for the same scenario, more than half of the false positive ratios, in both time-steps, are larger than 10%. It can be seen

from Figure 3-4 that the leak residuals series (r_l), which is identical to τ_a , is enclosed by the boundaries of the demand-noise residuals r_n . This means that no matter where the leak is, its effect (i.e., pressure residuals) could be masked by the effects of uncertainty in nodal demands. This means that independent from the threshold, pressure changes under only demand uncertainty can significantly become larger than pressure variations as a result of a leak. It is also notable that for many nodes, the r_l is between the 25th and 75th quantiles (the denser parts of the distribution) of r_n . Less desirable false positive ratios (still better than the fix threshold scenario) are produced by the scenario of sensor fleet under which, the majority of false positive ratios are above 15% in both time-steps.

It is worth noting that, in order to faithfully replicate the deterministic MFD, random noise was not introduced into the demand patterns while producing r_l ; similar to the approaches reported in (Casillas et al. 2013b; Casillas, Garza-Castañón, PuigVargas-Martinez 2015; Casillas et al. 2015; Pérez et al. 2009; Pérez et al. 2011; Ponce et al. 2014) same nominal demand pattern were used to generate leak-influenced pressure residuals. This is under the perfect circumstances, which helps, unrealistically however, reduce false positive ratios. In a real system, these are not the residuals that would be compared. In reality, residuals measured in the field have noise around them.

3.4.4 The Absence of State Variables in the Comparison

Based on the previous implementations of the MFD method in the context of leak detection in WDS, each node is assigned with a threshold value for each time-step. Observed residuals are then compared with their corresponding time-dependent thresholds. Under this logic, clock-time becomes the essential base for comparison of observed residuals and thresholds. This means that the residuals for an observation would be compared with the threshold for the same clock-time with possibly completely different tank levels and pump statuses. This approach ignores that pressure drop, and thus the appropriate threshold value, are not functions of clock-time but functions of system state variables (i.e., total demand, tank levels, pumps and valve statuses). Physically, clock-time has no influence on the nodal pressure in WDS. Pressure drop in response to a leak would not be the same in two consecutive days at 2:00 PM, for example, if at those times tank levels are not the same on both days. A more reliable comparison scheme, as a means for leak detection, requires consideration of the state of the system.

3.4.5 The Absence of Total Demand in the Comparison

There is another potential disadvantage associated with the conventional application of MFD in the literature which is that known total demands of the system are not considered when generating the

residuals. Therefore residuals are calculated, in previous studies, by subtracting pressure values coming from different total demand conditions. On the contrary, to calculate residuals, pressure values should be compared when the total demand of the network with no leak is equal to the total demand of the network plus a specific leak. This is because, in reality, at the stage of detection, the operator would not know if the current total demand includes the leak flow or not because the existence of a leak is not known.

3.5 Conclusion

Effect of a leak, of around the same size as the one reported in Pérez et al. (2011), was investigated on the nodal pressure of Net3. It is shown that the pressure magnitude changes in absence of the leak and yet the presence of demand noise can easily exceed the size of pressure variations caused by the leak. This observation suggests vulnerability of the reported MFD studies in distinguishing between leaks and nodal demand fluctuations.

The conventional deterministic comparison is prone to generate false-positives at the first stage of leak diagnosis which is the detection. Those approaches are not robust in dealing with pressure variations as a result of the aleatory demand uncertainty. There is no study so far that considers demand uncertainty at the early stage of asserting the existence of an anomaly somewhere in the network (detection). Previous studies accept the idea of deterministic thresholds and build on that to perform localization and sensor placement. Some studies then try to address the issue of demand uncertainty by defining few demand realizations to serve as additional scenarios to establish a “robust” sensor placement and leak localization, which is still based on the deterministic detection assumption. Besides the unacceptable levels of false positive ratios for the leak, two potential issues associated with conventional methods, which are lack consideration of system state and system demand, were pointed out.

The proposed methodology of this thesis suggests replacing the deterministic comparison of pressure residuals with statistical tests performed based on the outcomes of residuals comparison under a controlled and plausible setup where the total demand of the network and other system state variables such as tank levels and pump statuses are taken into account. Only under such a comparison setup, can smaller leaks potentially be distinguished from demand fluctuations with minimal false positives. The process is illustrated over the next two chapters of the thesis.

Chapter 4

Exploratory Analysis on Pressure Signals Under Leak and Demand Noise

This chapter is based on the published article with the title of “Pressure-driven Leak and Burst Diagnosis under Demand Uncertainty in Water Distribution Networks” by Jahanpour. M., and Tolson B. A. in proceedings of WDSA/CCWI Joint Conference, July 2018. The content below is a slightly restructured presentation of that work. References are unified at the end of the thesis.

4.1 Summary

This chapter proposes a novel stochastic comparison framework which can be used to perform exploratory analysis on the pressure signals under leak and demand noise. Using the framework, observations from pressure sensors might be properly contrasted against the range and distribution of the expected and plausible nodal pressures under the no-leak condition. The framework serves as the initial step of the proposed uncertainty-incorporated MFD-based method for leak diagnosis in WDS. The incorporation of nodal demand uncertainty into the comparison framework requires describing nodal demands with a joint probability distribution which is illustrated in this chapter. To represent the uncertainty of demand in the network, Monte Carlo methods are employed to generate realistic demand realizations for the network which in turn are utilized to characterize the probability distributions of nodal pressures. The test framework is applied to Net3. The hydraulic analysis is performed by EPANET2. It will be shown that for a certain size of leak and larger, it is possible to distinguish between the observations resulting by a leak and those coming from the no-leak condition while considering significant uncertainty in the nodal demand. This achievement overcomes the shortcomings of the deterministic implementation of MFD demonstrated in Chapter 3. Unlike all previous MFD studies, this comparison framework is constructed to carefully respect observable or typically observed WDS variables that control the expected system behaviour.

4.2 Introduction

In this section, the steps to set up the stochastic comparison framework for pressure data under the leak and no-leak conditions in a WDS are described. It is assumed that the hydraulic model provided is correctly calibrated. Let us assume input data (shown in Table 4-1) at time-steps $t-1$ and t are accessible from supervisory control and data acquisition (SCADA).

Table 4-1. Required data for two consecutive time-steps

Observation at $t-1$	Observation at t
pump statuses	pump statuses
valve settings	valve settings
tank levels	tank levels
	nodal pressure: at sensor locations
	total demand/consumption between $t-1$ and t

Necessary deterministic data (e.g., pipe lengths, pipe diameters, node elevations, control policies) are also assumed to be available from the calibrated network model. Based on the data, the available calibrated hydraulic model is modified such that it represents the state of the system at $t-1$ named $\Psi(t - 1)$. Given this, the aim is to replicate the observed state of the system at time t , $\Psi(t)$, by simulating the system for one time-step.

Under the ideal situation; by running a hydraulic analysis on the model for one time-step, exact field predictions at the time-step t would be possible. This ideal situation infers the absence of both epistemic and aleatory uncertainties; when all nodal demands along with other system properties are known. However, vast uncertainties in the model do not allow the ideal situation to occur. For this reason, Monte-Carlo realizations of nodal demands are used to characterize a probability distribution of nodal pressures at each sensor location. Since information from time t is also available, those random realizations that do not generate simulated system-states similar enough to the observed (actual) state of the system at time t are filtered out. Although the above could be applied to additional uncertain system inputs, in this work only nodal demand is studied as the source of uncertainty.

The analysis in this chapter is based on a synthetic WDS and its corresponding monitoring system and does not utilize actual/observed data collected from the field (and thus available in a SCADA system). Nonetheless, the rest of this chapter refers to any synthetic observations from this synthetic WDS as simply observations or observed data. Initial analysis of the Net3 network yielded typical states at each hour of the simulation and thus the simulation experiments utilize these typical states for hydraulic model initialization.

First, the hydraulic model of the system is set up with the observations at $t-1$. Next, all nodal demand realizations are applied to the model where the realizations are constrained such that total nodal demands must equal the observed total demand over the time step. After each simulation, the

simulated system-state $\hat{\Psi}(t)$, is compared with the observed system-state at t , $\Psi(t)$. A realization (and thus the associated simulation results) is retained for analysis only if its simulated total demand and system-state at t both match synthetic observations (which would be available from SCADA in actual field applications).

After setting up an adequate number of random realizations, sets of simulated nodal pressures for each node of interest can be collected. Now, if the hydraulic model of the network did not simulate any leak, each obtained set of nodal pressures could be thought as a sample of nodal pressures under the no-leak case. Similarly, an independent sample of nodal pressures under the leak case can be generated when the hydraulic model simulates a leak. Distributions of nodal pressures under no-leak and leak condition can then be compared. In the practical adoption of the proposed comparison framework, it would be possible to compare the actual observations of nodal pressures at time t with the distribution of pressures under the no-leak case. The existence of an anomaly would be inferred if statistically significant deviations of observed nodal pressures from the distribution of the no-leak predictions are found in the comparison framework.

4.3 Random Demand Realizations

As in Chapter 3, the Poisson Rectangular Pulse model for nodal demands (Buchberger et al. 2003; Nilsson et al. 2005) is utilized; nodal demands are considered as rectangular pulses with widths equal to the hydraulic time-step and heights equal to the demand flow (M. Blokker et al. 2018). Realizations of demand flow across the network must be sampled from an assumed probability distribution. Again, hydraulics are simulated only over one time step, so there is no need to consider temporal nodal demand correlations.

A key piece of such a sampling approach is that even though individual nodal demands are uncertain, the total of all nodal demands for each realization has to match the actual observed total demand for the time step being analyzed, d_{total} , which is expected to be available from the municipalities' SCADA system. All previous deterministic MFD studies ignore this information when computing expected pressure responses (and instead utilize assumed nominal total demand) and only Goulet et al. (2013) begin to consider known total demands in a probabilistic approach to leak detection in WDSs.

To summarize, the assumptions to generate random demand realizations are as follows:

- Autocorrelation of nodal demands over time need not be modelled due to single hydraulic time step simulation
- Nodal demands can be spatially correlated.
- The shortest time interval between demand realizations is one hour.
- d_{total} is known from SCADA at any time a pressure sensor sample is picked up (e.g., water balance calculations for the entire WDS system are possible using tank levels and system inflows)

During design and/or calibration of a WDS, nominal demands for each time step are assigned. In EPANET2, these nominal demands are the product of a scalar nominal demand for each junction node and a demand multiplier that follows a pattern over time. One way to define the nominal demands is by using billing information of each particular consumption type. In reality, the nominal demands over time reflect average behaviour and for any time step, the actual demands can be viewed as a random variable related to the corresponding nominal demand. The cumulative actual consumption for any time step, here referred to as total demand d_{total} , is distributed among demand nodes. In Eq. (4-1), \mathbf{D}_{nom} is the vector of nominal demands for all M demand nodes in the network for a given time step:

$$\mathbf{D}_{nom} = \begin{bmatrix} d_{nom}(1) \\ \vdots \\ d_{nom}(M) \end{bmatrix} \quad (4-1)$$

where $d_{nom}(j)$ is the nominal demand of node j .

The aim is to, based on \mathbf{D}_{nom} , generate random demand realizations so that for each realization:

- Total demand equals the observed d_{total} for a time step
- Spatial correlation between nodal demands can be considered
- Non-demand nodes get only zero demand values
- Demand nodes get assigned with non-negative demand values
- EPANET2 solver can solve the network's hydraulics while
 - all pumps and valves can still deliver enough flow or head
 - negative pressures do not occur at any node

Most of the WDS literature generating random nodal demands is not in the context of leak/fault detection studies (with the exception of Goulet et al. (2013)). Goulet et al. (2013) sample demand realizations from an exponential distribution with the mean equal to the minimum total water demand divided by the number of demand nodes. They chose the exponential distribution to best represent the situation where most consumptions are regular yet there are few high consumption locations. Branisavljević et al. (2009) used the knowledge of system inflow as a constraint in WDS optimization modelling. They took into consideration the uncertain nodal demands, and using this constraint reduced the uncertainty of the model output. They used fuzzy sets to represent the uncertain demands and used modified genetic algorithms to find the optimal solutions. Similar approaches to demand uncertainty characterization will also be considered in this research. Choosing the probability distribution from which random demand multipliers will be sampled is subjective and case study dependent. Eck et al. (2015) report various sampling methods to produce demand scenarios with the aim of uncertainty analysis study of WDS. Filion et al. (2007) generated random realizations of nodal demands by sampling from a normal multivariate distribution with a coefficient of variation of 0.15. In their work, normal demands were considered to hold spatial cross-correlation which was presented in a matrix form.

In this thesis, similar to Branisavljević et al. (2009) Monte-Carlo methods are employed to generate demand realizations conditioned on known total demands while allowing for possible the spatial correlation between demand nodes. The realizations are generated by drawing random samples from a multivariate Gaussian distribution which in turn calls for the covariance matrix of the random variables. Covariance matrix is described in Eq. (4-2):

$$Cov(D_i, D_j) = \rho(D_i, D_j)Cv_{D_i}Cv_{D_j}\mu_{D_i}\mu_{D_j} \quad (4-2)$$

where D_i, D_j are random variables for nodal demands at node i and j at the time-step of interest; ρ is the Pearson's correlation coefficient between two random variables; and Cv and μ are the coefficient of variation and mean of each random variables, respectively. Ideally, ρ for each couple of demand nodes, and Cv and μ for each node, would be obtained directly from nodal demand field records. However, in absence of data, values for those quantities need to be identified. Nodal nominal demands at the time step of interest are taken from the calibrated hydraulic model and assigned as the mean values for each node in Eq. (4-2). Based on Filion et al. (2007), a $Cv = 0.3$ was assigned for all the nodes. Cv and μ , however, can be updated by monitoring nodal demands in the field (Eck et al. (2015)). Both Cv and ρ are unitless quantities. The nodal demands are assumed uncorrelated across the nodes in this study (it is acknowledged

that this may not be true in some systems but in absence of field data, an assumption such as this is mandatory).

In order to respect the condition that random nodal demands adhere to the known total consumption, an iterative sampling procedure is implemented as follows to generate a candidate demand realization for the network. Nodal demand samples must generate the simulated end of time-step system states that are consistent with known system states as described in Section 4.4. Also, they need to closely match the known total demand during the time-step. In an effort to generate similar magnitude leak flows during leak scenarios, some candidate realizations with large leak flow relative to the nodal demands are discarded. Note that when a leak is simulated, the total nodal demands including the leak flows also need to be equal to the total consumption. Similar to the iterative sampling approach described above, for every required nodal demands realization, candidate demand realizations are sampled until consistent system states are achieved.

The above conditional sampling of nodal demands is applied until a set of η demand realizations, $\mathbf{D}(\Psi(t), d_{total})$, across all M nodes for a given time-step is obtained from the above described random sampling procedure, where each realization successfully satisfies the required conditions for total demands and for system states. These demand realizations are provided in Eq. (4-3).

$$\mathbf{D}(\Psi(t), d_{total}) = \begin{bmatrix} d(1,1) & \dots & d(1,\eta) \\ \vdots & \ddots & \vdots \\ d(M,1) & \dots & d(M,\eta) \end{bmatrix} \quad (4-3)$$

where $\mathbf{D}(\Psi(t), d_{total})$ is a $M \times \eta$ matrix within which each column is one demand realization, and $\Psi(t)$ is the state of the system that realizations in $\mathbf{D}(\Psi(t), d_{total})$ replicate.

For each system state, a certain number of demand realizations that match with total demand of the state are generated. This number is identified with η . With $\mathbf{D}(\Psi(t), d_{total})$, a series of η single time step hydraulic simulations are conducted and the resulting nodal pressures are a sample from the probability distribution of nodal pressures under the no-leak condition (or leak condition).

4.4 System States

A system-state, noted by Ψ , is a database of system's state variable values at a given time. System-state consists of three sets of variables concerning the network at a specific time:

1. set of water levels in tanks,

2. set of pump statuses, and
3. set of valve statuses.

Intuitively, system states and system responses (e.g., nodal pressures) at time t are a function of system states in the previous time step and nodal demands over the time step. In the previous chapter, it was demonstrated that characterizing expected system behaviour using nominal demands in a deterministic MFD-framework was problematic because the actual demands at the time of the anomaly analysis, were unknown but inconsistent with nominal demands. In this chapter, this inconsistency idea is expanded to incorporate system states such that expected system responses are recognized to be conditional on the observable and known system states. In all past deterministic MFD studies (Casillas et al. 2013b; Casillas, Garza-Castañón, PuigVargas-Martinez 2015; Casillas et al. 2015; Pérez et al. 2009; Pérez et al. 2011; Ponce et al. 2014), the observable system states at or just before the time pressure residuals are not accounted for. Instead, and at most, the time of day was used as a proxy for system states such that the pressure residual was computed for the same time of day and under nominal demands for that time of day.

In this study, it is recognized that deviations from expected nodal pressures must be evaluated conditional on system states in the field matching system states in the hydraulic model. This is possible because in modern distribution systems, the three components of system states are typically monitored and available in real-time for some or all locations in the network. Such a conditioning requires two parts. Firstly, the observed system states must be used as initial values in the hydraulic model simulation. This is straightforward in EPANET2 as users must assign these initial states to simulate any system. Secondly, the simulated system states at the end of a hydraulic simulation, corresponding to the time of day of the observed nodal pressure being assessed, should also be consistent with the observed system states at that time. Ensuring this consistency is not as straightforward and the approach to doing this is detailed below.

4.4.1 Consistency Criteria Between Simulated and Observed System States

After the hydraulic simulation under a randomly sampled candidate demand realization (produced by the sampling procedure described in the previous section), the consistency between simulated and observed system states must be evaluated. If there is an inconsistency in any state variables, the sampled demand realization is discarded or filtered out of the analysis and demands are resampled and the process is repeated.

The criteria for consistency in pump statuses and valve statuses are relatively simple in this study since only constant speed pumps and partially open valves are included in the selected WDS case studies. In

each of these cases, a pump is either on/off and a valve is either open or closed. The simulated and observed status of all pumps and valves must be the same, otherwise, the simulated and observed system states are deemed inconsistent.

The criteria for consistency of tank levels is more complex because tank levels vary continuously between an upper and lower physical limit. If the discrepancy in simulated and observed water level in tank i does not exceed a threshold value defined in Eq. (4-4) then simulated and observed levels of tank i are deemed consistent.

$$\text{for each Tank } i: \quad \frac{|L_{T_i}^1 - L_{T_i}^2|}{(L_i^{max} - L_i^{min})} \leq \text{tol}_i \quad (4-4)$$

where $L_{T_i}^1$ and $L_{T_i}^2$ are water levels in the tank i taken from system-states $\Psi(t)$ and $\hat{\Psi}(t)$, respectively; L_i^{max} and L_i^{min} are fixed and known values that define the range in which water level may change inside tank i ; and tol is a tolerance defined as a ratio that limits the relative deviation. A small value such as 0.01 allows for only minor relative differences in tank levels. Definition of tol , for each tank, could benefit from knowledge about the diameter, or more generally the geometry, of the tank; the same value of tol could translate into significantly different volumes of water in tanks of different geometry.

4.5 Case Study Net3

Net3 model network, previously introduced in Chapter 3, was used as the case study to develop the comparison framework. Sets of simulated leaks under the leak as well as no-leak conditions were generated during the first time-step (from 12:00 AM to 1:00 AM). Three nodes (node 14, 28, 61) with non-zero water demands were selected for pressure analysis and as the location of the leaks. These nodes are highlighted in the network map (Figure 4-1) by their index number in red.

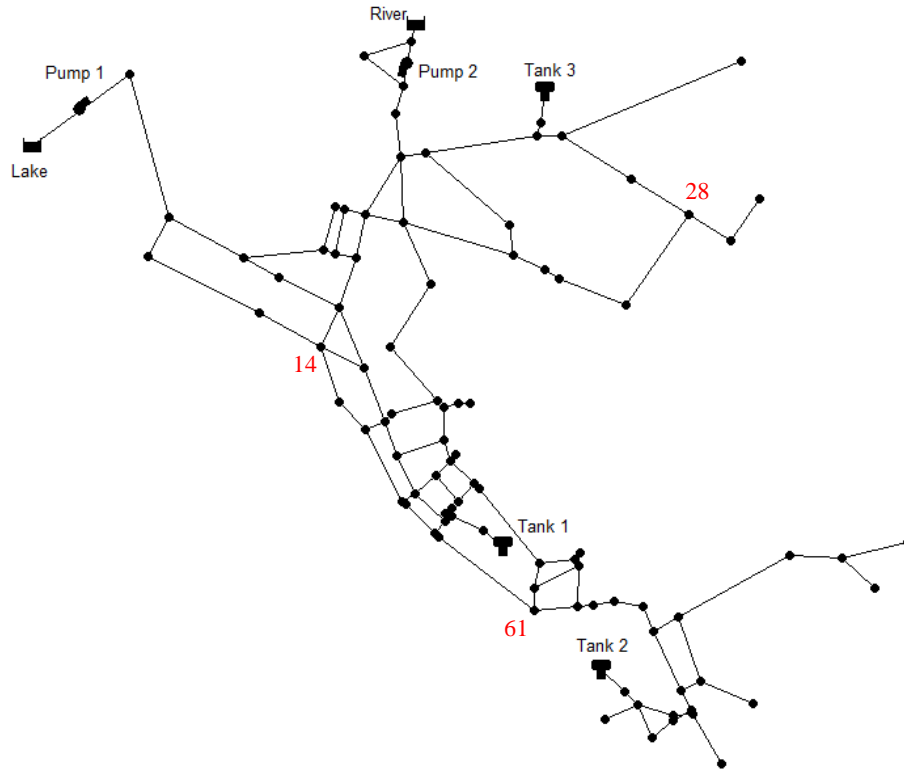


Figure 4-1. Location of the selected nodes for pressure analysis in Net3

Monte-Carlo sampling was performed to create $\eta=1000$ simulated pressures for sets of the leak and no-leak conditions. Emitters were adopted to simulate leakages in the junction nodes. Emitters are devices associated with junctions that model the flow through a nozzle or orifice that discharges to the atmosphere. Four values for the emitter discharge coefficient (EDC) were evaluated (0, 7, 15, 30). Smaller EDC values generate smaller leak-flows. In order to gain a better insight into the magnitude of the leak flow, the leak flow ratio (LFR) was calculated as the leak-flow divided by the maximum diurnal demand of the node (under no leak). Medians of the leak and no-leak simulated pressure sets alongside other metrics calculated from the results of the simulations are reported in Table 4-2.

Table 4-2. Results of the simulations under the leak and no-leak conditions for Net3 network.

Node	14					28					61				
→															
EDC↓	LF	LFR	ML	MNL	PV	LF	LFR	ML	MNL	PV	LF	LFR	ML	MNL	PV
0	000.0	0.0	66.80	66.80	0.99	000.0	0.0	73.22	73.22	0.56	000.0	0.0	65.75	65.75	0.24
7	54.7	0.1	66.63	66.7	0.00	59.7	3.4	72.74	73.15	0.00	56.7	0.5	65.60	65.66	0.00
15	122.3	0.3	66.44	66.58	0.00	127.4	7.2	72.16	73.07	0.00	121.3	1.0	65.43	65.57	0.00
30	243.8	0.6	66.06	66.37	0.00	253.0	14.3	71.15	72.93	0.00	242.1	2.1	65.11	65.39	0.00

LF: leak flow which is the volume of the water exiting the system during the time, in GPM.

LFR: leak flow ratio which is the leak flow divided by the maximum diurnal demand at the node.

ML, MNL: median of the set of simulated pressures (psi) in the presence and absence of the leak, respectively.

PV: p-values of the Student's t-test

To test for the deviation between the leak and no-leak sets, a two-sided Student's t-test was carried out. The null hypothesis of the t-test was that the two averages are not significantly different. This test assumes the two sets have identical variances which was the case with the results. Based on the test, small p-values (less than the level of significance) indicate the difference in means is significant. Figure 4-2 shows histograms for the sets of simulated pressures under the leak and no-leak conditions.

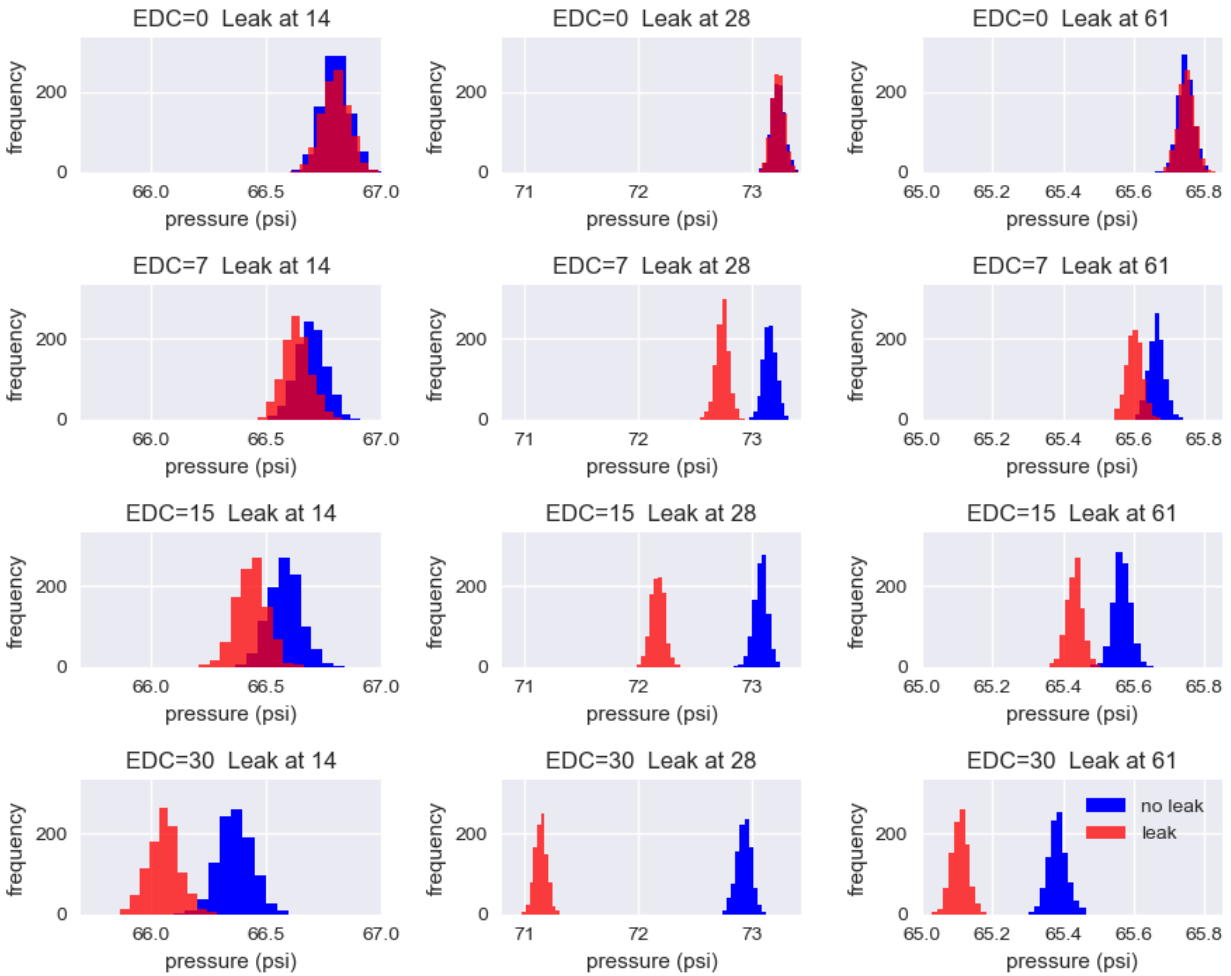


Figure 4-2. Histograms of nodal pressure responses with and without a leak at various sensor locations and leak magnitudes (the leak is located at the sensor locations)

As presented in Figure 4-2, for all EDC-node cases, the distribution of the leak-influenced pressures (coloured in red) are at lower pressures than the no-leak condition distributions (coloured in blue). For each node, the gap between the two distributions increases with the EDC. The t-test results show that the red and blue distributions are statistically distinguishable for all three nodes and all non-zero EDC values. This is promising proof of concept showing that small leaks have the potential to be detected if multiple pressure observations are taken. On the contrary, deterministic MFD methods rely on only one demand realization to simulate the no-leak and leak nodal pressures and then use it as the base of comparison. It can be detected from Figure 4-2, that some pressure distributions overlap (for example, both distributions overlap in a pressure range of 66.1 to 66.25 psi when a leak with EDC=30 is on Node 14). This indicates

there exist demand realizations that replicate system-state and total demand under both leak and no-leak conditions but can also cause pressure variations on the node contrary to expectations. This suggests that results of comparison could be misled by such pressure observations when using MFD methods in a deterministic setting.

To get around this problem, some studies (Casillas et al. 2013b; Casillas, Garza-Castañón, PuigVargas-Martinez 2015; Casillas et al. 2015; Pérez et al. 2009; Pérez et al. 2011; Ponce et al. 2014) utilized a threshold value to check the significance of the discrepancy between pressures. Two concerns are raised here about this strategy. First, those studies choose arbitrary values for the threshold without conducting uncertainty analysis on nodal pressures. As shown in Figure 4-2, for a certain increase in the leak-flow, Node 28, shows a relatively larger pressure-drop from its no-leak condition in comparison to the other two nodes. This means there are nodes in the network that, compared to other nodes, experience smaller pressure drops in response to the same amount of water loss. Such nodes will only show large pressure drops when larger leak-flows occur. Ignoring this fact, the deterministic MFD studies consider a fixed threshold value for all the nodes while it seems necessary to adjust the threshold for each node. This is because the relationship between pressure-drop and leak-flow is different among the network nodes. Another concern is that the threshold also functions to filter out pressure variations induced by relatively small leaks which cannot be properly distinguished from the effect of regular demand variations on pressure. Considering a threshold effectively ignores the smaller leak-flows and focuses on bigger ones and functions to reduce the false-positive rate at the expense of increasing the rate of non-detection.

Correlation between the leak-flow and the discrepancy between the medians of the leak and no-leak scenarios (MNL-ML) was evaluated by calculating Pearson's correlation coefficient. Results, shown in Figure 4-3, revealed a very strong positive linear correlation for all the three nodes, which demonstrates the linear response of the nodal pressure-drop to the leak-flow.

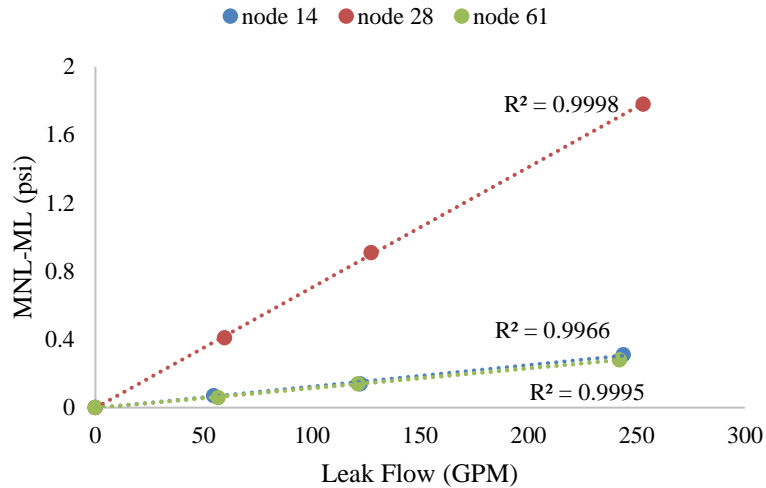


Figure 4-3. Variation of pressure drop by the leak flow

4.6 Case Study C-Town

C-Town is a significantly larger case study in comparison with Net3. It is introduced in Ostfeld et al. (2011) for Battle of the Water Calibration Networks and later on by Giustolisi et al. (2014) under the Battle of Background Leakage Assessment for Water Networks in 2014. While Ostfeld et al. (2011) provide a comprehensive description of the network model, Table 4-3 shows an overview of the network elements.

Table 4-3. C-Town specifications

EPANET2 Network Element	Count	Description
Junction	388	333 Demand nodes
Reservoir	1	
Tank	7	Diameters ranging from 65 to 132 meters
Pipe	432	Diameters ranging from 51 to 610 millimetres Roughness coefficients ranging from 5 to 139 Lengths varying from 4 meters to 1.2 km
Pump	11	
Valves	1	One shutoff (gate) valve

Figure 4-4 presents a layout of C-Town network along with the location of the four nodes (207, 239, 69, 265) selected for pressure analysis.

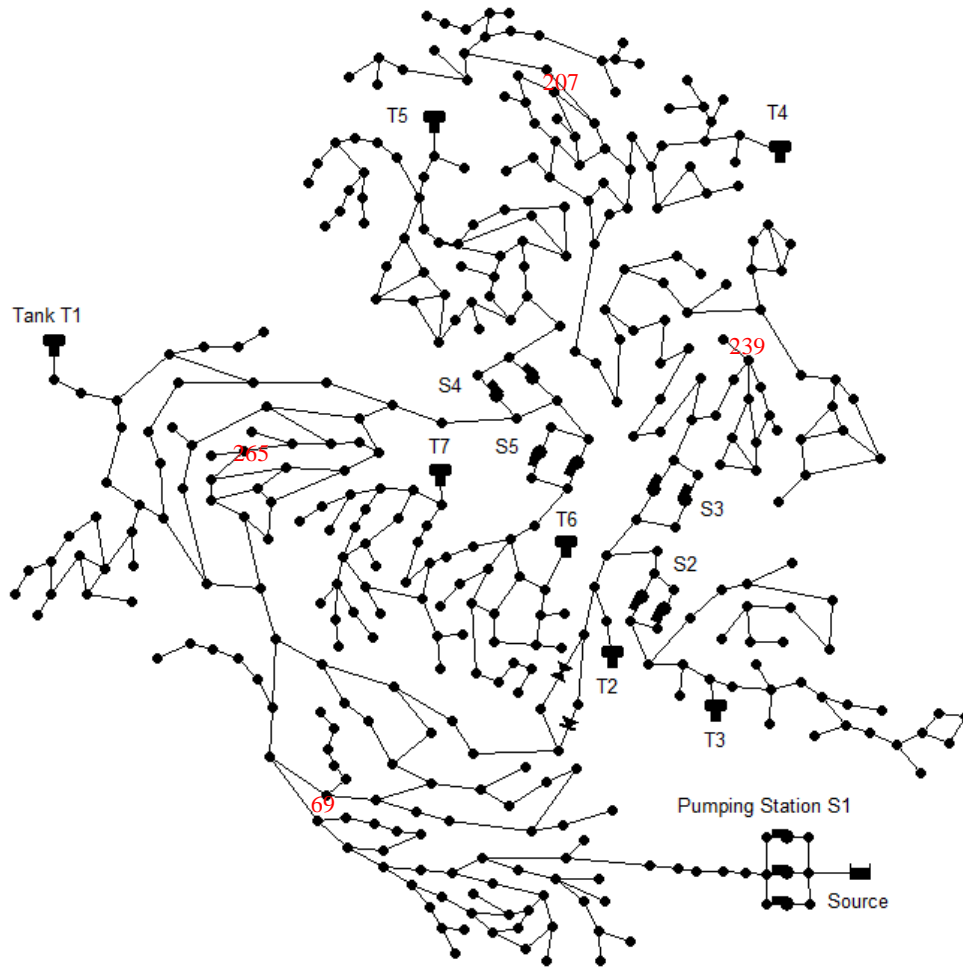


Figure 4-4. C-Town WDS layout

Sets of simulated pressures under the leak and no-leak conditions, with $\eta=50$, were generated during the first time-step (from 12:00 AM to 1:00 AM) for four network nodes (207, 239, 69, and 265). This procedure, which is similar to the case of Net3. Results of nodal pressure analysis for the four mentioned nodes under the effect of network-wide demand uncertainty are presented in Table 4-4 and Figure 4-5.

Four *EDC* values (0, 0.01, 0.05, 0.1) were evaluated for C-Town. Similar to the case of Net3, smaller *EDC* values generate smaller leak-flows and leak flow ratios (leak-flow divided by the maximum diurnal

demand of the node). Medians of the leak and no-leak simulated pressure are reported in Table 4-4. The P-values of the two-sided Student’s t-test indicated the existence of stochastically significant differences between the means of the simulated pressure sets under the leak and no-leak conditions for $EDC > 0$ (non-zero leak flows).

Table 4-4. Results of the nodal pressure simulations under the leak and no-leak conditions (C-Town)

Node →						Node →				
207						239				
EDC↓	LF	LFR	ML	MNL	PV	LF	LFR	ML	MNL	PV
0.00	0.00	0.00	70.11	70.11	0.11	0.00	0.00	89.90	89.89	0.20
0.01	0.13	2.32	70.00	70.09	0.00	0.14	13.64	89.82	89.88	0.00
0.05	0.42	7.40	69.80	70.08	0.00	0.47	47.36	89.65	89.86	0.00
0.10	0.83	14.75	69.53	70.03	0.00	0.95	94.56	89.43	89.83	0.00

Node →						Node →				
69						265				
EDC↓	LF	LFR	ML	MNL	PV	LF	LFR	ML	MNL	PV
0.00	0.00	0.00	67.58	67.58	0.50	0.00	0.00	62.63	62.63	0.91
0.01	0.13	2.35	67.54	67.57	0.00	0.13	2.53	62.62	62.63	0.00
0.05	0.41	7.41	67.46	67.57	0.00	0.40	7.77	62.59	62.62	0.00
0.10	0.82	14.81	67.35	67.55	0.00	0.79	15.51	62.56	62.62	0.00

LF: leak flow which is the volume of the water exiting the system during the time-step, in LPS.

LFR: leak flow ratio which is the leak flow divided by the maximum diurnal demand at the node.

ML, MNL: median of the set of simulated pressures (meters) in presence and absence of the leak, respectively.

PV: p-values of the Student’s t-test

The frequency bar plots for sets of simulated pressures under the leak and no-leak conditions are presented in Figure 4-5.

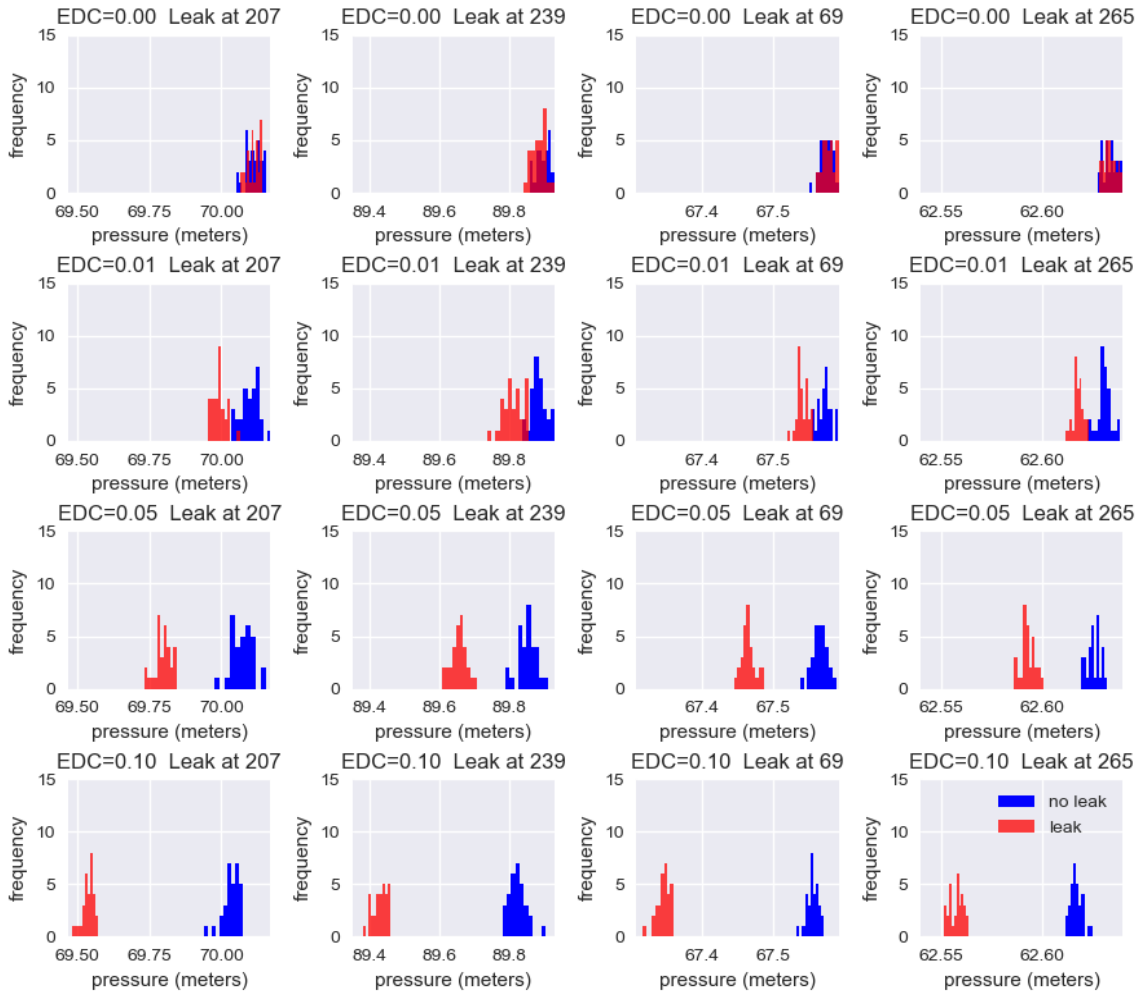


Figure 4-5. Histograms of nodal pressures with and without a leak at various sensor locations and leak magnitudes (C-Town)

Similar to the case of Net3, it can be seen in Figure 4-5 that nodal pressures under leak are distinguishable from the no-leak condition (visually and also based on the P-value of the t-test). It is also notable that for all the four nodes, by increasing the leak flow the median of leak distributions moves further away (to the left) from the median of nodal pressures under no-leak condition. Trends observed in the C-Town results closely match the ones from Net3; therefore, the pressure analysis framework may be reliably used in the leak detection test which is performed in the next step.

4.7 Conclusion

The comparison framework presented in this chapter serves as a base to quantitatively account for the uncertain nodal demands as well as known system states any time a pressure measurement is used in the MFD analysis. To set up the framework, a hydraulic model of the network and SCADA data for pumps, tanks, and valves of the network is expected. It is further assumed that the system-wide water consumption (i.e., leak flow plus actual demands) plus system states (such as pump and valve statuses, tank levels) are available from SCADA at any time a pressure sensor sample is picked up. Results show that under a range of small leak sizes, the probability distribution for nodal pressure under the leak is distinguishable from the probability distribution for the corresponding nodal pressure under no-leak condition.

The above proof of concept finding is important to demonstrate the utility of the comparison framework. In reality, a deterministic pressure observation from the field is collected (rather than a probability distribution characterizing the observation). As such, the comparison framework must be adapted to account for this and then aggregate evidence of a leak across multiple pressure observations at the same sensor. This adaptation and formalization is described in Chapter 5 and results in a new leak detection method.

Chapter 5

Leak Detection Methodology

5.1 Summary

A novel leak detection methodology, which is based on a nightly sampling of nodal pressures, built on statistical analysis is presented in this chapter. This method is able to compare observations (from a leak or no-leak scenario) with probability distributions under the no-leak condition and then make a judgment on the existence of a leak in the system by performing a statistical test. Other typical pressure-based leak studies utilize a single observation of pressure to determine if a leak is present. Viewing multiple observations as a statistical sample as it is done in this study is a new approach. Furthermore, the concept of false positive is being introduced for the first time as a performance metric for a stochastic MDF detection method and later on sensor placement. This chapter explains the general workflow of the proposed leak detection methodology. The statistical test, its design (sampling frequency and schedule), and control metrics (false positive and false negative ratios) are explained in this chapter. This chapter also presents a step-by-step demonstration of the application of the proposed leak detection methodology on two (one medium and one large size) network models, taken from the literature. First, for verification purposes, the results of the smaller network are discussed thoroughly. Next, the results of the larger network are discussed in a more brief manner. In both cases, the variation of false positive and false negative with respect to design parameters (ΔT and S) are investigated and discussed.

5.2 Introduction

The exploratory analysis on pressure signals under leak and demand noise in the format of a comparison framework (proposed in Chapter 4) provides insight into the range of plausible variations in nodal pressure in both absence and presence of any leak size at any location in the network. It was shown that the framework could be used to compare nodal pressure measurements with probability distributions that characterize pressures expected under no-leak condition. This comparison forms the base for the statistical detection methodology proposed in this chapter.

5.3 Proposed Leak Detection Method

A hypothesis test is proposed to detect the existence of a leak (detection rather than localization) based on the incoming data from sensors and the plausible distribution of pressures under the no-leak condition which are derived from Monte Carlo simulation using a hydraulic model. However, this no-leak pressure distribution could also be taken from a database of historical pressure measurements at the current sensor locations (with the caveat that all such utilized historical samples represented what were believed to be no leak conditions).

In the following, first, the sampling schedule is explained. Next, the structure of the hypothesis test is demonstrated. This chapter ends by providing a guideline on steps to adapt the detection test to each specific case study by introducing methods to choose the design parameters which are scheduling factors and locations of the sensors.

5.3.1 Observation Pairs Schedule

To be consistent with other works in the field, night time was chosen for sampling nodal pressures (Alkassseh et al. 2013; B. Farley et al. 2010; Z. S. Kapelan et al. 2003; Liemberger and Farley 2004; Puust et al. 2010; Sanz et al. 2015; Zhang et al. 2017). The proposed methodology suggests nightly observation pairs where the k^{th} observation pair is made of two nodal pressure samplings at t_k^o and t_k' .

One pressure observation is not enough to identify a moderate or small leak. Evidence should be aggregated across multiple observations through time since leaks persist and will theoretically reduce pressures for as long as the leak persists. At each night, N^1 observation pairs with a frequency of ΔT are made. The sampling pattern repeats for S consecutive nights resulting in a total $N = S \times N^1$ observation pairs. The N observation pairs form the statistical sample used to make a judgment about the existence of a leak.

Π is defined as the set of night hours on which sampling is regarded appropriate. Π is defined with attention to the network total demand profile; those hours with the lowest total demand are more suitable for inclusion in Π . This network dependent set serves as the decision space in the search for clock-times to initiate the sampling of the observation pairs. Observation pairs may only occur beginning at hours pre-defined in Π .

Repeating at every night, the first observation pair is made starting at time $\Pi[1]$ (i.e., the initial element of Π) followed by the next observation pair after ΔT where ΔT is the sampling frequency at which observation pairs are made. ΔT is not to be conflated with t_h which is the hydraulic time-step of the

network model used in the comparison framework to characterise probability density functions (PDF) of nodal pressures under demand uncertainty and the no-leak condition. ΔT is in units of the simulation time steps which is often hourly. For example $\Delta t = 5 \text{ hours}$ and $t_h = 1 \text{ hour}$ describe a situation where observation pairs are made every 5 hours in a night while the time between actual pressure observations in each observation pair is 1 hour.

Λ is a set containing all possible values of ΔT . Practical considerations may guide the definition of Λ . Based on the value of ΔT , different patterns and different numbers of observation pairs per night (N^1) can be sampled. Based on the above definition, the number of observations per night N^1 is obtained from below.

$$N^1 = \left\lfloor \frac{\text{size of } \Pi - 1}{\Delta t} \right\rfloor + b \quad (5-1)$$

$$b = \begin{cases} 0, & \left\lfloor \frac{\text{size of } \Pi - 1}{\Delta t} \right\rfloor = \frac{\text{size of } \Pi - 1}{\Delta t} \\ 1, & \text{otherwise} \end{cases} \quad (5-2)$$

$$N = S \times N^1 \quad (5-3)$$

where S is the number of successive nights that observations take place through which a total number of N observation pairs are collected.

Figure 5-1 illustrates an example timing structure for nightly sampling. It shows how observation pairs and sampling times look like in one night under $\Delta T = 3$ and $\Pi = [1,2,3,4,5,6]$.

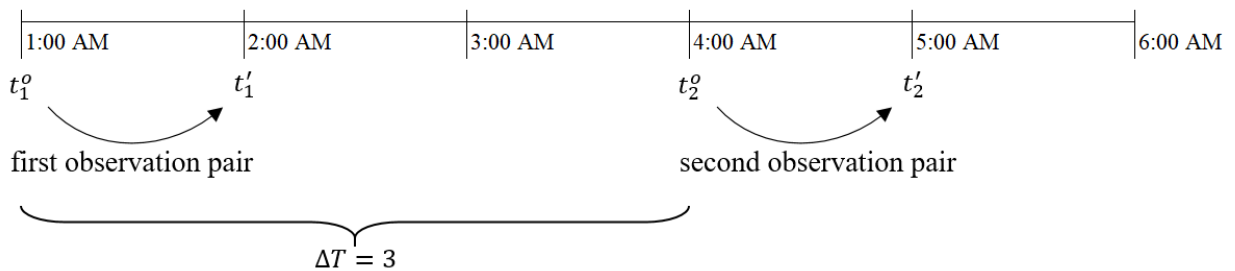


Figure 5-1. Timing structure for one night of pressure observations to include in proposed leak detection analysis

The set up the timing framework, one needs to first make assumptions about Π (and thus the initiation time) and Λ . Next, a decision needs to be made over the observation frequency $\Delta T \in \Lambda$, and also over S , which is the number of sampling nights. The design of the schedule is discussed in the following sections and the impact that these design variables have on the proposed hypothesis test is parametrically evaluated in numerical experiments.

5.3.2 The Hypothesis Test for Leak Detection

The main idea in the proposed leak detection method is to aggregate evidence from contrasting the set of observations against their probability distributions under the no-leak condition. Such a set of evidence, conceptually depicted in Table 5-1, could then be used in a hypothesis test to determine if the set of sampled pressures appear anomalous. With that purpose, a hypothesis test is suggested that uses evidence obtained from comparing N observation pairs from a sensor with their corresponding conditional probability distributions for pressure under the no-leak condition. A graphical presentation of an example comparison is illustrated in Table 5-1.

Table 5-1. Illustration of evidence accumulated over time in one night from the i^{th} sensor, in the proposed leak detection approach

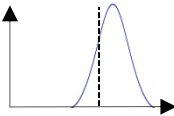

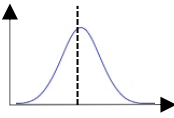
Observation pair # k	Time of k-th observation pairs (t_k^o, t_k^l)	Probability distribution of the uncertain simulated pressures, \hat{p}_i under no leak at end of time-step	Graphical comparison of observation to simulated pressure uncertainty under no leak
1	t_1^o $t_1^l = t_1^o + t_h$	$f_i(\hat{p}_i \Psi(t_1^o), \Psi(t_1^l), D_1)$	 $p_i(1)$
2	$t_2^o = t_1^o + \Delta T$ $t_2^l = t_2^o + t_h$	$f_i(\hat{p}_i \Psi(t_2^o), \Psi(t_2^l), D_2)$	 $p_i(2)$
...			
N^1	$t_N^o = t_{N^1-1}^o + \Delta T$ $t_N^l = t_{N^1}^o + t_h$	$f_i(\hat{p}_i \Psi(t_{N^1}^o), \Psi(t_{N^1}^l), D_{N^1})$	 $p_i(N^1)$

Table 5-1 only shows the accumulated evidence over N observations for one sensor. Note that there might be more than one sensor available in the network.

For the k th observation pair, the probability distribution of pressure for node i at the end of time step under the no-leak condition, (Eq. (5-4)), is obtained from the Monte-Carlo sampling and conditional single time step hydraulic simulation process explained in Chapter 4.

$$f_i(\hat{p}_i | \Psi(t_k^o), \Psi(t_k^1), D_k) \quad (5-4)$$

Each PDF represents η pressure values obtained from simulations that given the state of the system at the start of the time step, $\Psi(t^o)$, replicate (closely enough) the observed state of the system at the end of the time step $\Psi(t^1)$ and also the total demand consumption during the time step (between t^o and t^1). In Eq. (5-4), \hat{p}_i is the nodal pressure at node i at t^1 in the absence of any leak.

One challenging aspect of this comparison is that the PDFs are functions of time and thus uniquely paired to each observation time. The proposed comparison approach is to assess each observation against the median of its corresponding PDF: if there was no leak, and the PDFs reasonably depicted the uncertainty in the nodal pressures, then one would expect to see 50% of the observations below the median and 50% above the median. More than 50% below the median indicates an anomalous result consistent with the impact of a leak. Each comparison in this approach is thus a Bernoulli trial with probability of success (defined as an observation less than the median), $p = 0.5$ and the binomial probability distribution can be used to describe the probability of seeing x successes out of N trials. The binomial probability mass function in this case defining the probability of seeing x successes out of a total of N observation pairs is given in Eq. (5-5).

$$P(X = x) = b(x; N, 0.5) = \binom{N}{x} 0.5^x 0.5^{N-x} \quad (5-5)$$

A hypothesis test on a single proportion can be used to evaluate the aggregated evidence. The P_{value} based hypothesis test procedure for such a test is given in Walpole and Myers (1985) and Eq.(5-6) gives the P_{value} used for the hypothesis test.

$$\begin{aligned} P_{value} &= P(X \geq x \text{ when } p = 0.5) \\ &= b(x; N, 0.5) + b(x+1; N, 0.5) + \dots + b(N; N, 0.5) \\ &= 1.0 - F(x-1; N, 0.5) \end{aligned} \quad (5-6)$$

where $F()$ is the cumulative distribution function for the binomial probability distribution and the P_{value} is the probability of seeing equal or stronger evidence of a leak assuming the null hypothesis of no leak ($p=0.5$) is true. The hypothesis test characteristics are as follows:

1. $H_0: p = 0.5$ is the null hypothesis; this means the sampled pressure values are not meaningfully less than the corresponding predicted median pressures under no leak.
2. $H_1: p > 0.5$ is the alternative hypothesis; which means the sampled pressures tend to be lower than the corresponding predicted median pressures under no leak. This shows a systematic pressure drop that is consistent with the existence of a leak.
3. Level of significance equal to α is assumed.

The test statistic is the observed value of x for the binominal random variable, X , and the P_{value} is then computed with $p = 0.5$ from Eq. (5-6). Then the existence of a leak is asserted based on the comparison of the P_{value} and the level of significance, α :

$$p_{value} < \alpha \quad (5-7)$$

This test is performed for all the nodes where a sensor is installed (the sensor fleet). Finally, a leak is deemed to exist if at least for one sensor, Eq. (5-7) holds.

As an example, let us assume a situation where 2 observations are made during 5 consecutive nights which gives $N=10$ observation pairs. Assume, for example, 9 out of the 10 showed pressures smaller than the median of their corresponding predicted pressures under no leak. The P_{value} is the probability of seeing an equal or more extreme result under the null hypothesis of no leak and is computed using Eq. (5-6) as follows:

$$P_{value} = P(X \geq 9 \text{ when } p = 0.5) = b(9; 10, 0.5) + b(10; 10, 0.5) = 0.0107$$

The P_{value} is smaller than the level of significance $\alpha = 0.1$, and so this is evidence to reject the null hypothesis ($p = 0.5$, no leak) and conclude the alternative hypothesis is true ($p > 0.5$, a leak exists in the network). This means that during the sampling time, that specific sensor, independent from other sensors, is showing evidence for the existence of a leak somewhere in the network. If there is no sensor that satisfies the inequality in Eq. (5-7), the conclusion is that there is no evidence for the existence of a leak in the network. Note that each sensor in the sensor fleet has its own and only one P_{value} ; P_{value} is not calculated based on the observations from different sensors.

Note that the detection test described above employs the median of the distribution of no-leak nodal pressures; however, there is no assumption made on the type of the distribution itself. In other words, the methodology is agnostic towards any other characteristics of the distributions besides the median.

5.3.3 Dependency of Random Variables

The hypothesis test used above assumes independence of the random variable which in this case is the Boolean outcome of the comparison between observed nodal pressure with the median of its corresponding predicted pressures under the no-leak condition. The validity of this assumption is hereby investigated using a Runs-Test (Bradley 1968) on time-series of results of the test when applied on no-leak condition on Net3.

A 960-hour (40 days) long random demand realization ($Cv = 0.3$) dataset was generated and used to simulate the network in absence of any leak. Next, using the comparison framework (explained in Chapter 4), for all time-steps, the pairs of simulated nodal pressure versus the median of the expected pressures under no-leak (using $\eta = 150$) were obtained. For each time-step, the nodal pressures were compared with the corresponding median of its no-leak PDF. Results of the comparison for each node and for each ΔT , were recorded in integer format (-1 if the simulated pressure is greater than the median and 1 otherwise). To perform the Runs-Test on each of the integer series (for each node representing an example sensor location), the number of runs were counted. Number of runs in a dichotomous sequence is the number of times the values of two adjacent elements change.

The idea of the Runs-Test is based on the fact that if a set of data is generated in a random manner, the probability that the $(I+1)^{\text{th}}$ value in the sequence is larger or smaller than the I^{th} value follows a binomial distribution. The test's null hypothesis is that the data set is generated randomly and so its alternative hypothesis is that the sequence is not generated randomly. The test statistic, Z , is defined as a function of the number of existing and expected runs in the data set, respectively noted by R and \bar{R} , the standard deviation of the number of runs, noted by s_R , and the number of positive and negative values in the mapped sequence, respectively noted by n_1 and n_2 (Eq.(5-8) to Eq. (5-10)).

$$Z = \frac{R - \bar{R}}{s_R} \quad (5-8)$$

$$\bar{R} = \frac{2n_1n_2}{n_1 + n_2} + 1 \quad (5-9)$$

$$s_R = \sqrt{\frac{2n_1n_2(2n_1n_2 - n_1 - n_2)}{(n_1 + n_2)^2(n_1 + n_2 - 1)}} \quad (5-10)$$

Z would be compared to the standard normal table. A significance level of 0.05 was considered for the tests based on which the test statistics Z would be compared with 1.96. The null hypothesis is rejected if

$|Z| > 1.96$ indicating the data set are generated in a non-random manner. Results of the tests, for three independent trials, are shown in Table 2-1.

Table 5-2. Number of nodes (from a total of 91 nodes) showing non-randomness

ΔT	Number of the nodes with $ Z > 1.96$		
	Trial 1	Trial 2	Trial 3
1	3	2	1
2	1	2	2
4	1	1	0
24	1	2	3

The Runs test results show that for each test (on each ΔT) there were very few nodes (maximum three) for which the test statistic was greater than the critical value derived from the level of significance of 0.05, which means the test did not show non-randomness in the time series. It is concluded therefore that the random variable shows no evidence of non-independence and thus can be used in the leak detection hypothesis test defined in 5.3.2.

5.4 Leak Detection Method Performance Assessment

False positive and false negative ratios are introduced to evaluate the accuracy/performance of the detection hypothesis test when applied on a set of the leak and no-leak scenarios. In order to calculate the false positive and negative rates, multiple leak and no-leak scenarios must be defined.

5.4.1 Leak and No-leak Scenarios and No-leak PDF Generation

An exhaustive database of experiment detection method results is defined as a set of the leak and no-leak synthetic scenarios $\mathbf{X}(\Omega, \Gamma, Cv, EDC, \eta)$ which holds in it pressures generated as a function of a set of Ω leak and Γ no-leak demand scenarios. The synthetic actual demands are generated using an assumed coefficient of variation Cv while synthetic actual leak flows are generated using an emitter discharge coefficient of EDC . Note that Ω should be selected as an integer multiple of the number of network nodes in order to always evaluate leak detection rates with the same number of scenarios for each node. The database also holds in it, for every synthetic scenario pressure value, the corresponding median of the

conditional probability distribution of pressure resulting from η single time step hydraulic simulations under conditionally sampled random demand realizations. Note that this database approach enables easy post-processing of results for a thorough exploratory analysis while minimizing database size (e.g., system states for scenarios are not saved and the resulting probability distribution for pressure under no-leak is summarized only by the median).

Following the approach detailed in Chapter 3, no-leak scenarios are clones from the base network model where nodal demands are replaced with a time-series of random demands sampled from a multivariate distribution. Leak scenarios are generated in the same way as no-leak scenarios except that a non-zero EDC is assigned to a node where a leak is meant to be and each and every node is simulated as a leak location. Note multiple simultaneous leak scenarios were not considered. The conditional Monte Carlo sampling to characterize the no-leak condition probability distributions of pressure are carried out as described in Chapter 4.

Leakages are modelled using emitter element in a junction node. Emitters are essentially devices associated with junctions that model the flow through a nozzle or orifice that discharges to the atmosphere. The flow rate through the emitter varies as a function of the pressure available at the junction node (Eq. (2-9)).

$$q_j(t) = EDC \times \hat{p}_j(t)^\gamma \quad (5-11)$$

where $q_j(t)$ and $\hat{p}_j(t)$ are leak flow rate and simulated pressure at the junction node j at time t , respectively; EDC is emitter discharge coefficient and γ is emitter pressure exponent which following EPANET2 default, is assumed to be 0.5 in all cases

The synthetic scenarios generate network states and pressures that are the synthetic equivalent of what could happen and be observed in an actual WDS. This synthetic system behavior is based on $\text{Max}(S)$ (e.g., 9 for Net3 case study) day extended period simulations of EPANET2 at an hourly time step. The leak detection methodology is repeatedly applied to each synthetic scenario based on a selected subset of synthetic observations to evaluate methodology performance under various settings. Evaluating over multiple scenarios yields a statistical sample of detection methodology performance.

5.4.2 False Positive Assessment

False positive rates are computed using the Ω synthetic no-leak scenarios. For the database of detection method assessment experiment results, \mathbf{X} , $\varphi_{sf}(\Delta T, S, \alpha, \mathbf{sf}, \mathbf{X})$ is the false positive ratio evaluated by sensor fleet \mathbf{sf} , when sampling frequency and the number of consecutive sampling nights are ΔT and S ,

respectively and α is the significance level of the hypothesis test for each sensor location. φ equals the number of no-leak scenarios that were incorrectly deemed to be a leak scenario divided by the total number of no-leak scenarios.

5.4.3 False Negative (i.e., Leak Detection Accuracy) Assessment

False negative rates are computed using the Ω synthetic leak scenarios. For detection experiment results database \mathbf{X} , $\omega_{sf}(\Delta T, S, \alpha, \mathbf{sf}, \mathbf{m}, \mathbf{X})$ is the false negative ratio evaluated for nodal leak locations in \mathbf{m} (leak locations are specified by node locations in \mathbf{m}) by sensor fleet \mathbf{sf} , when sampling frequency and the number of consecutive sampling nights are ΔT and S , respectively, and α is the significance level of the hypothesis test for each sensor location. ω equals the number of leak scenarios that were not detected divided by the number of total leak scenarios.

The application of the detection methodology to any *one* of these leak scenarios requires a substantial number of hydraulic simulations. The total number of single time step hydraulic simulations per leak scenario is the number of observation pairs in the hypothesis test multiplied by the η demand realizations.

5.5 Detection Hypothesis Test Design

In the real implementation of this methodology on a WDS, below steps are taken:

1. A fleet of pressure sensors (\mathbf{sf}) need to be installed on certain nodes in the network,
2. the operator should be provided with values of ΔT and S , as the nightly schedule, to take the pressure samples,

By design of detection hypothesis test, it is meant to identify most desirable values for $\Delta T, S$ and number and location of the pressure sensors (\mathbf{sf}). The ideal situation would be that with the minimum number of sensors (and thus hardware-associated costs), minimum φ and ω are obtained with the minimum number of samples (i.e., maximum ΔT and minimum S). It might be clear initially that some of these mentioned objectives are competing; for example, having a fewer number of sensors conflicts with getting smaller false negative ratios. However, the effect of the design parameters on φ and ω need to be explored. Under any specific detection experiment results database \mathbf{X} , this exploratory study is done in two steps:

1. As the first step, a parametric study on ΔT and S under the effect of different values of α is performed and these design variables are fixed. This step is detailed in the rest of this chapter.

2. Based on the results of the previous step, iteratively search for the optimum configuration of \mathbf{sf} to obtain the best values of φ and ω (sensor placement). This step is detailed in Chapter 7 where the configuration of \mathbf{sf} is optimized.

5.6 Step 1: Examining the Effect of ΔT and S

Depending on the definition of Π and Λ , a certain number of $(\Delta T, S)$ pairs are formed. Sampling under the condition of each $(\Delta T, S)$ pair results in different values of φ and ω in an detection experiment results database. The aim in this step is to perform a comprehensive study over the response of false positive and false negative ratios to different $(\Delta T, S)$ pairs. The knowledge can then be practiced to choose the most desirable pair as the first part of the design of the leak detection hypothesis test (this is also the outcome of this step). More specifically, in this step below questions are dealt with:

- What does happen to φ and ω when S increases with a constant, reasonable ΔT ?
- What does happen to φ and ω when leak flow increases with a fixed $(\Delta T, S)$?
- What does happen to φ and ω when leak sensor location moves away from a leak with a fixed $(\Delta T, S)$?

5.7 Case Study Net3

A full description of this small literature network is provided in Chapter 3.

5.7.1 Observation Pairs Schedule

The total hourly nominal demand of the Net3 WDS case study is shown in Figure 5-2. Based on this time series, experiments using Net3 define $\Pi = [1,2,3,4,5,6]$.

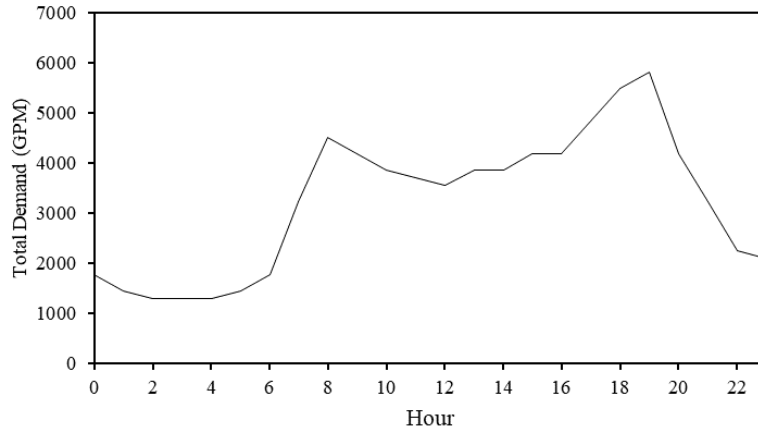


Figure 5-2. Total hourly demand of Net3

For Net3, $\Lambda = [1,2,3]$ was chosen. For example, based on the aforementioned assumptions of Π and Λ for Net3, the number of observation pairs and their starting time in one night is demonstrated in Table 5-3.

Table 5-3. Demonstration of ΔT , and N^1 variations for Net3

Observation frequency (ΔT)	Starting time of the observation (t_1^0)	Number of observations per night (N^1)
1	1, 2, 3, 4, 5	5
2	1,3,5	3
3	1,4	2

Therefore, observation pairs schedule for Net3 is based on $\Pi = [1,2,3,4,5,6]$ and $\Lambda = [1,2,3]$ which as shown in Table 5-3, results in N^1 (number of observations per night) to range from 2 to 5, depending on the values of ΔT and S .

5.7.2 Experiment Definition

To perform the parametric study, the first step is to define an experiment which refers to detection experiment results database. Based on the network model of Net3, below experiment was designed:

$$\mathbf{X1} = \mathbf{X}(\Omega = 65,520, \Gamma = 24,000, \mathbf{m} = \mathbf{M}, Cv = 0.3, EDC = 5, \eta = 150)$$

Experiment **X1** is the detection experiment results database for $\Omega = 65,520$ leak and $\Gamma = 24,000$ no leak scenarios, respectively. The leak is of the size $EDC = 5$ and all the leak location will be applied to

all nodes, one node at a time ($\mathbf{m} = \mathbf{M}$). For each leak or no-leak scenario, $\eta = 150$ demand realizations are sampled from a multivariate normal distribution with ($Cv = 0.3$) to characterise the distribution of nodal pressure under no-leak condition.

From the 65,520 leak scenarios, each of the 91 nodes gets around $\frac{65,520}{91} = 720$ leak scenarios. The maximum number of nights for sampling is assumed to be 9 (i.e., $1 \leq S \leq 9$). Based on $\Lambda = [1,2,3]$ and the range defined for S , a total of 24 ($\Delta T, S$) pairs can be defined (listed in Table 5-4). To produce these scenarios, the evaluation period was set to 9 days.

To evaluate sensor level false positive and false negatives ratios under each ($\Delta T, S$) pair, the total number of the leak and no-leak scenarios are distributed among these pairs. The 720 leak scenarios for each node, are distributed equally between 24 ($\Delta T, S$) pairs, imparting each pair 30 specific leak scenarios. The 24,000 no-leak scenarios are similarly distributed equally between 24 ($\Delta T, S$) pairs, giving each 1000 specific scenarios. For each of the 24 pairs of ΔT and S , the corresponding false positive and false negative ratios can then be empirically calculated from the results of the detection test on 1000 non-leak scenarios and 30 leak scenarios per node.

In the next section, the effect of different values of ΔT , S and α on false positives and false negative ratios in presence of a 30% uncertainty in the nodal demand is discussed.

5.7.3 Examining the Effect of ΔT and S

A study over the response of sensor level false positive and false negative ratios to ΔT and S is performed and results, grouped by a number of sensors and leaks, are presented in this section.

5.7.4 Single Sensor and Single Leak Location

False positive and false negative ratios are evaluated for detection experiment results database **X1** assuming only one sensor (on the same node where the leak is) and under the conditions below:

- each 9-day scenario was only utilized for a single detection test per sensor location thus yielding only one P_{value} per sensor location
- to calculate the false negative ratio, only the leak scenarios on the same node (where the sensor is installed) are taken into account.

A p_{value} was calculated for each node and for all pairs of ($\Delta T, S$). Next, the p_{value} was compared to two level of significances of $\alpha = 0.01$ and $\alpha = 0.1$ to obtain the false positive and false negative ratios.

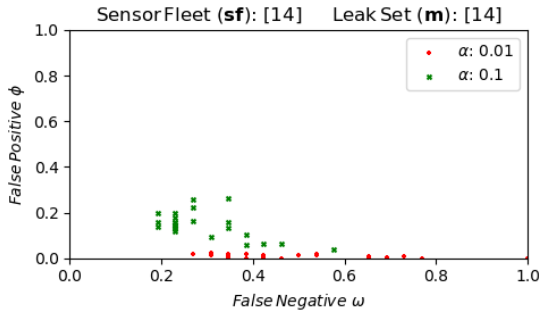
The results corresponding to all $(\Delta T, S)$ pairs, but only for two nodes in the network, are presented in Table 5-4 and Figure 5-3.

Table 5-4. False positive (φ) and false negative (ω) ratios under the single sensor and single leak condition (Net3)

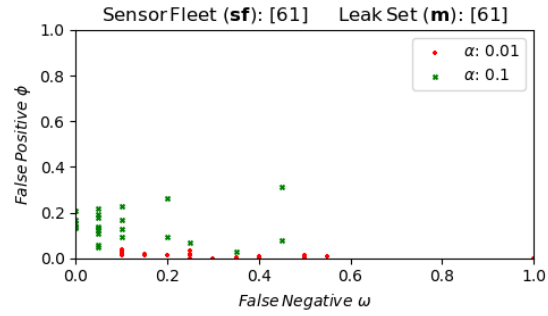
ΔT - S pair #	ΔT	S	N^1	N $= S \times N^1$	$\alpha = 0.01$				$\alpha = 0.1$			
					Node 14		Node 61		Node 14		Node 61	
					φ	ω	φ	ω	φ	ω	φ	ω
1	1	1	5	5	0	1	0	1	0.264	0.346	0.311	0.45
2	1	2	5	10	0.002	0.692	0.01	0.55	0.257	0.269	0.264	0.2
3	1	3	5	15	0.018	0.538	0.031	0.25	0.197	0.231	0.218	0.05
4	1	4	5	20	0.02	0.385	0.023	0.1	0.164	0.269	0.193	0.05
5	1	5	5	25	0.023	0.308	0.032	0.1	0.159	0.231	0.168	0
6	1	6	5	30	0.019	0.346	0.03	0.1	0.127	0.231	0.131	0
7	1	7	5	35	0.015	0.308	0.04	0.1	0.199	0.192	0.209	0
8	1	8	5	40	0.016	0.308	0.019	0.1	0.16	0.192	0.152	0
9	1	9	5	45	0.017	0.269	0.015	0.1	0.137	0.192	0.139	0
10	2	2	3	6	0	1	0	1	0.062	0.423	0.08	0.45
11	2	3	3	9	0.008	0.731	0.015	0.5	0.221	0.269	0.227	0.1
12	2	4	3	12	0.012	0.538	0.009	0.4	0.159	0.231	0.166	0.1
13	2	5	3	15	0.015	0.5	0.013	0.25	0.143	0.231	0.127	0.1
14	2	6	3	18	0.013	0.423	0.012	0.25	0.117	0.231	0.094	0.1
15	2	7	3	21	0.004	0.346	0.015	0.2	0.18	0.231	0.176	0.05
16	2	8	3	24	0.001	0.385	0.016	0.15	0.15	0.231	0.134	0.05
17	2	9	3	27	0.006	0.346	0.012	0.15	0.135	0.231	0.109	0.05
18	3	3	2	6	0	1	0	1	0.037	0.577	0.028	0.35
19	3	4	2	8	0.01	0.654	0.003	0.4	0.064	0.462	0.07	0.25
20	3	5	2	10	0.001	0.769	0.003	0.5	0.103	0.385	0.094	0.2
21	3	6	2	12	0.004	0.654	0.003	0.35	0.16	0.346	0.126	0.05
22	3	7	2	14	0.006	0.423	0.016	0.25	0.132	0.346	0.137	0.05
23	3	8	2	16	0	0.462	0.001	0.3	0.06	0.385	0.05	0.05
24	3	9	2	18	0.005	0.423	0.001	0.25	0.093	0.308	0.058	0.05

Figure 5-3 presents $\varphi - \omega$ scatter plots where each point in the plot corresponds to a $(\Delta T, S)$ pair. Figure 5-3.a and Figure 5-3.b show the cloud of the nodes for all the 24 $(\Delta T, S)$ pairs and for two nodes 14 and 61, respectively. Figure 5-3.c and Figure 5-3.d present only $(\Delta T, S)$ pairs with non-dominated values of φ and ω (smaller φ and ω are desirable) including data-label of each point in the format of “ $\Delta T.S$ ”.

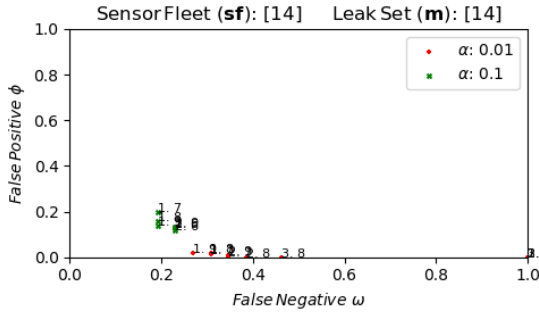
a)



b)



c)



d)

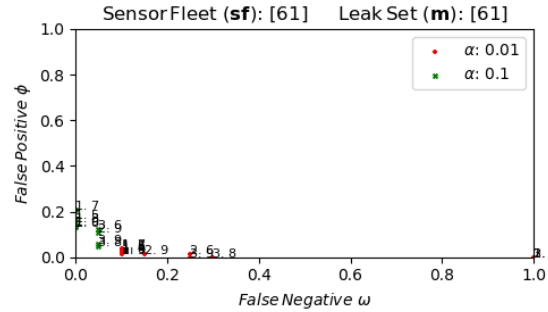


Figure 5-3. Scatter plots of false positive and false negative ratios under example single sensor locations and single location leak conditions (Net3)

5.7.4.1 ϕ and ω Variation as a Function of S (fixed ΔT)

The first attempt for verification of the results is to investigate the variation of false negative values by increasing S . Figure 5-4 and Figure 5-5 show this trend for node 14 and 61, respectively, considering both $\alpha = 0.1$ and $\alpha = 0.01$ and all values of ΔT .

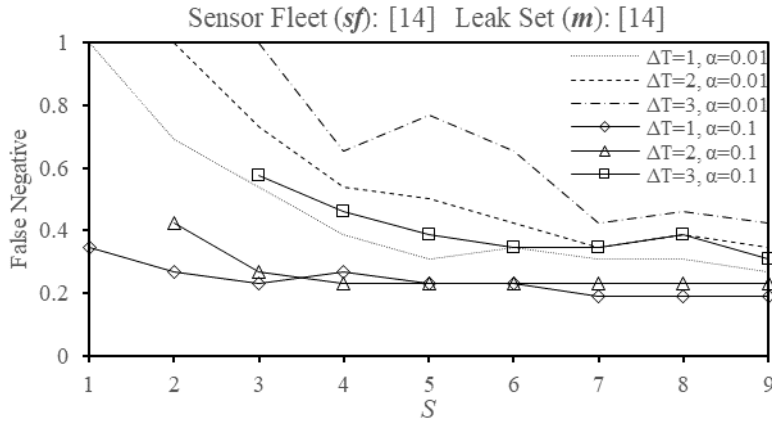


Figure 5-4. False negative variation by *S* for node 14 (Net3)

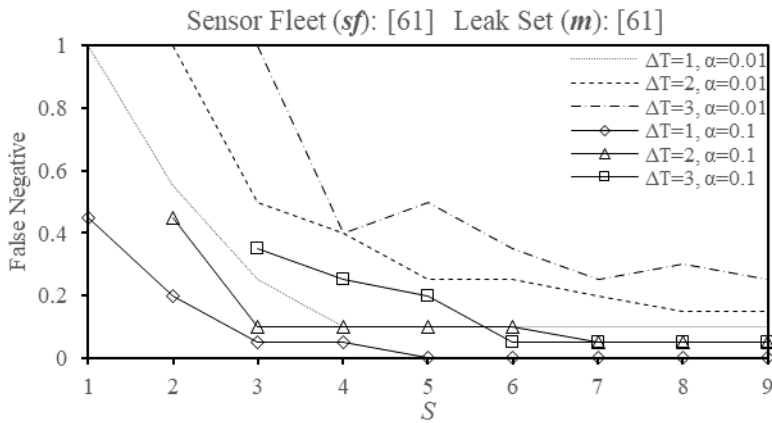


Figure 5-5. False negative variation by *S* for node 61 (Net3)

As illustrated in Figure 5-4, for any constant value of ΔT , as *S* increases, the associated false negative rate shows a generally decreasing trend. This is the case for both α values. Smaller ΔT , in both nodes, results in better false negatives. These observations are in line with the logical anticipation that more observations result in better detection of leaks (smaller false negative ratios). More observation in this context means smaller ΔT (more frequent sampling) and larger *S* (more nights to perform sampling). It can as well be seen in those plots that $\alpha = 0.1$ produces generally better false negatives when compared with $\alpha = 0.01$.

Results of the same analysis on false positive is presented in Figure 5-6 and Figure 5-7. In comparison to the false negative, false positive rates show a more uniform behaviour as *S* rises. Figure 5-6 and Figure 5-7 show that false positive values vary around the value of the level of significance based on which they

are calculated. This is the case for both nodes and for all the three cases of ΔT . This observation verifies the expected behaviour of a properly structured hypothesis test where the empirical values of false positives reasonably approximate the applied level of significance in the stochastic test. A lower (better) false positive is obtained by employing $\alpha = 0.01$ rather than $\alpha = 0.1$.

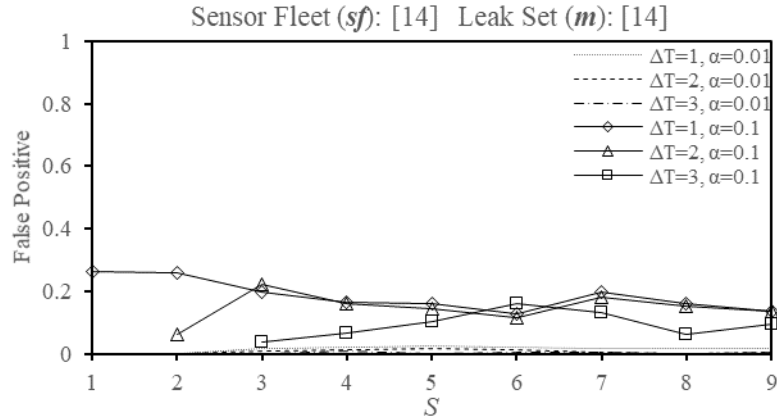


Figure 5-6. False positive variation by *S* for node 14 (Net3)

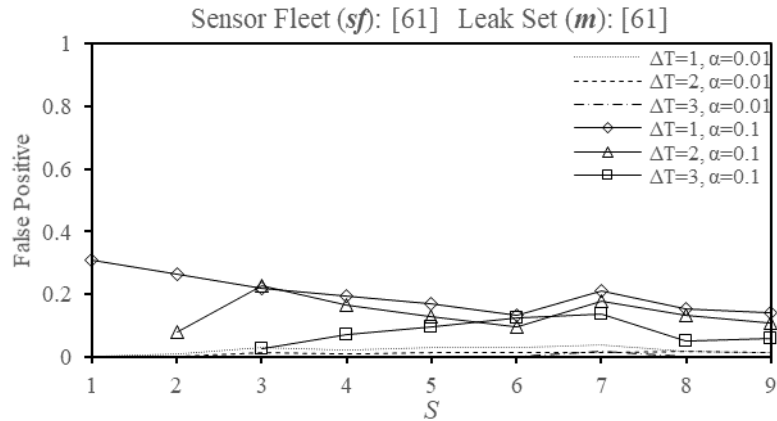


Figure 5-7. False positive variation by *S* for node 61 (Net3)

It can be concluded that better false negative values in this detection experiment results database are obtained with more samples and larger α , while false positive is only a function of α . Therefore, any attempt to improve false negative by increasing α directly results to weaken the false positive values. Very similar patterns are observable in plots of other network nodes.

5.7.4.2 ϕ and ω Variation by Leak Flow (fixed ΔT and S)

To investigate the influence of the leak flow size, three new groups of leak scenarios with different EDC equal to 6, 7, and 10 were created and added to experiment **X1** (temporarily for this analysis only). False positive and false negative, again for one node at a time, were calculated (Figure 5-8).

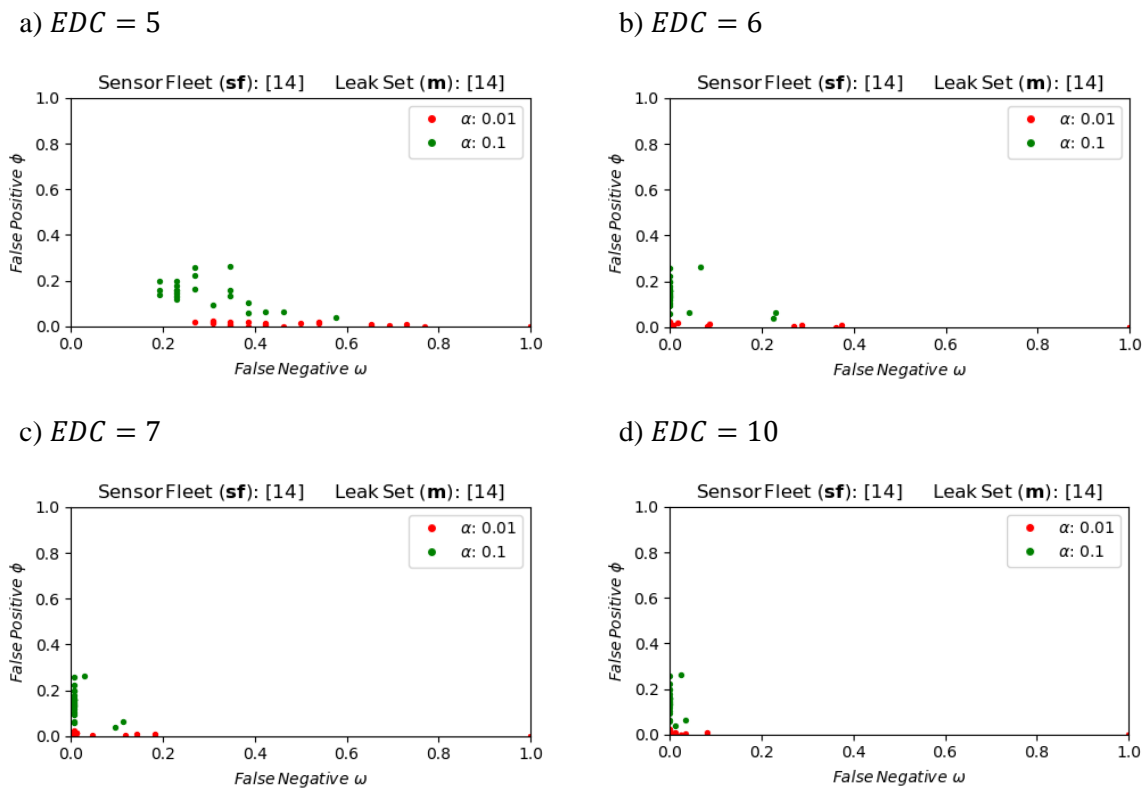


Figure 5-8. Scatter plots of false positive and false negative ratios under example single sensor location and single location leak condition for different leak flows (Net3)

Figure 5-8 shows that the cloud of $\phi - \omega$ points for all the $(\Delta T, S)$ pairs shifts toward the left corner of the plot ($\phi = 0, \omega = 0$) as leak flow increases. This means that both false positive and false negative ratios improve as the leak flow increases. This observation is expected as larger leak flows ought to be detected easier thus generating smaller (better) false negative ratios.

Figure 5-9 shows the effect of the number of samples on false negative and leak flow simultaneously. This plot only shows results for the case of $\alpha = 0.01$ and $\Delta T = 1$; however, similar trends were obtained

from other values of α and ΔT . It can be seen from Figure 5-9 that for the leak with $EDC=5$, the higher number of samples does not significantly improve the false negative after the fifth night; whereas, in the case of leaks with $EDC > 5$, false negative gets close to zero (best possible value for false negative) after only 3 nights of sampling. This shows that larger leak flows are being detected faster by the detection test.

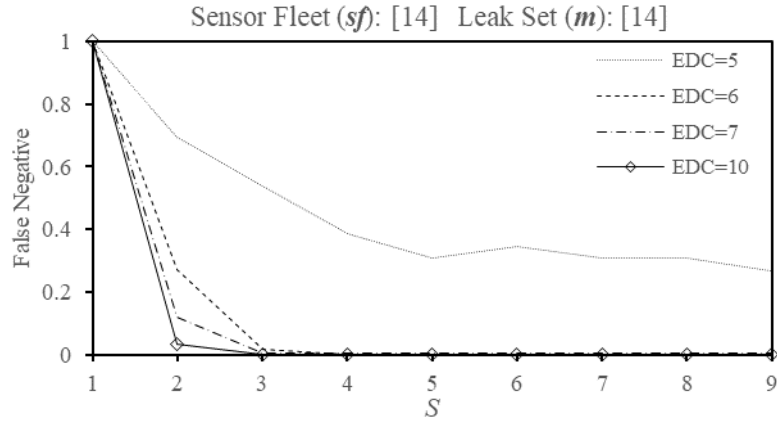


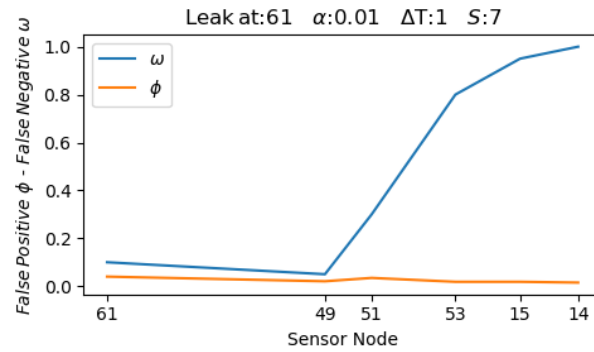
Figure 5-9. False negative variation with S (number of days of observation pairs), for different leak flows, for node 14 (Net3)

5.7.4.3 φ and ω Variation by Sensor Location (Fixed Leak Location and Size, ΔT and S)

In this section, the effect of the distance between leak location and the sensor on the false positive and false negative rates is investigated. First, a node is assigned to have a leak on it. Next, a series of nodes with locations moving away from the leak location is selected to have a sensor on them and ω and φ are calculated for each sensor node in response to the leak. This is done by adapting a fixed α , ΔT , and S .

As an example of this investigation, a leak with $EDC = 5$ was introduced to node 61. Nodes 49, 51, 60, 53, 15, 14 (which are respectively farther away from node 61) were chosen to have sensors one at a time. Node 49 is the closest and node 14 is the farthest to the leak location. ω and φ were calculated for, $\Delta T = 1, S = 7$ (Figure 5-10a) and $\Delta T = 3, S = 9$ (Figure 5-10b), both with $\alpha = 0.01$. The x-axis in Figure 5-10 plots reflects, in scale, the actual distant between the nodes.

a)



b)

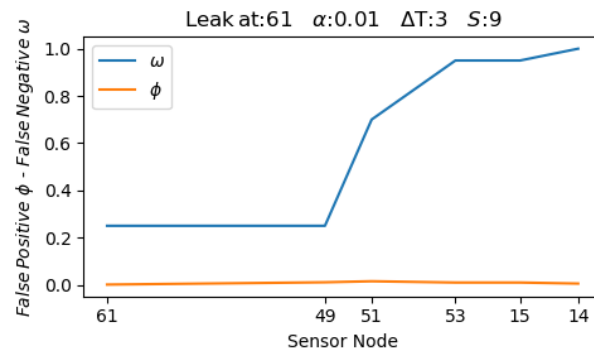
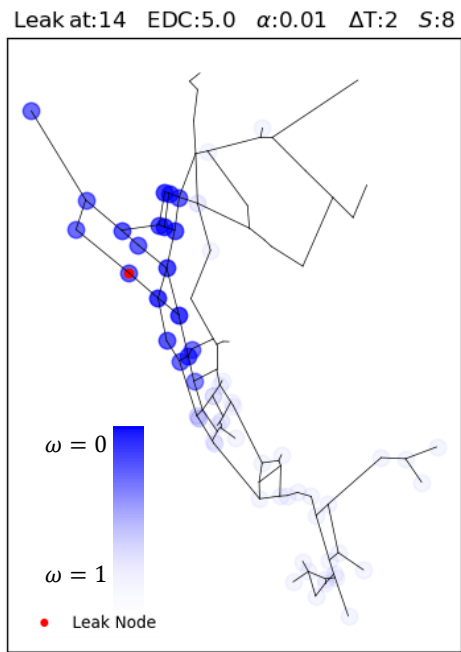


Figure 5-10. Sensor performance as a function of distance from a leak on node 61 (Net3)

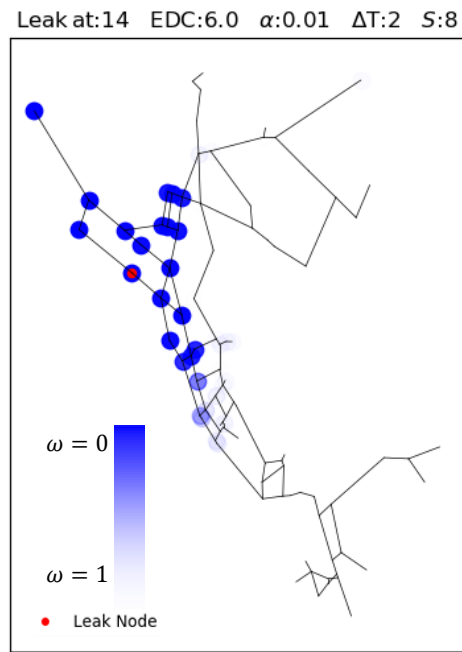
It can be seen from Figure 5-10, in both cases, as the sensor location goes farther away from the leak location, the false negative rate increases (deteriorate) generally. False positive ratios, however, regardless of the distance, keep a value around α . Similar patterns are observed for different leak node locations and sensor node combinations. This shows that the ability of a sensor to generate small (less than α) p-values and thus assert the existence of a leak is a function of its distance to the leak location.

To further investigate the influence of distance, false negative ratios were calculated in response to a fixed leak at node 14 each time using one, and only one, sensor moving on all the nodes in the network. Results are presented in a scatter heat map (Figure 5-11) where the colour intensity is for $1 - \omega$ (i.e., the detection ratio). In those plots, ω for each node is obtained from the results generated by having a sensor on that node. Solid blue and white colors correspond to $\omega = 0$ and $\omega = 1$, respectively, in the plots of Figure 5-11.

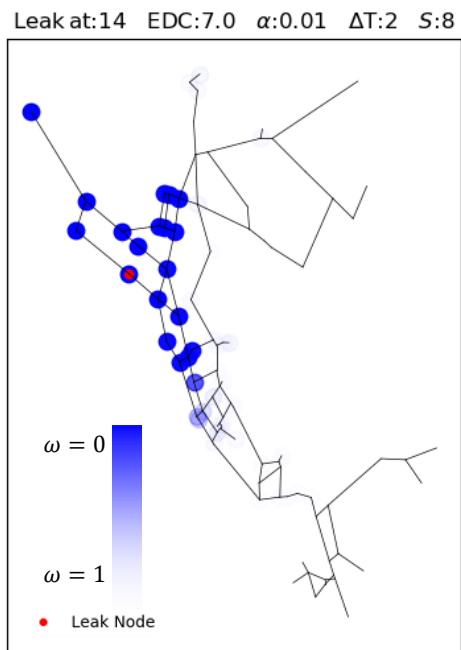
a)



b)



c)



d)

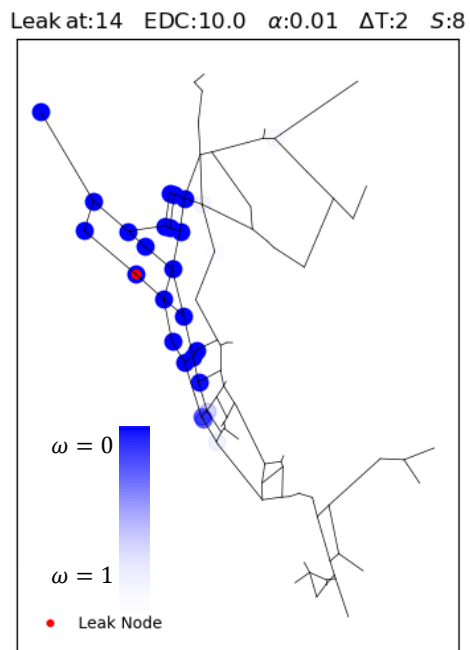


Figure 5-11. False negative scatter heat map for four leak sizes on node 14 (Net3)

It can be observed from Figure 5-11 that false negative is a nonlinear function of sensor distance. For smaller leak sizes (Figure 5-11.a) the false negative tailed off with distance and even the farthest sensors still have some minor false negative values. For larger leaks (Figure 5-11.d) however, false negative shows a more spatially abrupt behaviour where false negative is very low in a certain neighbour around the leak location but suddenly increases dramatically outside that area.

5.7.5 Single Sensor and All Leak Scenarios

Investigation on the effect of ΔT and S is continued in this section by now considering all leak scenarios as opposed to scenarios for only one leak node which was the focus of the previous section. In this section, the leak is assumed to exist in all nodes ($m=M$). Note that this does not mean that more than one leak exists in the network at a time; it means that all leak scenarios (each with one leak on some node) are included in the calculation of false negative. This is different from the previous section where the ratio would be calculated by including leak scenarios of a certain node only.

Keeping the format of Figure 5-3, plots in Figure 5-14 show false positive and false negative values of the cloud and dominating configurations of all $(\Delta T, S)$ pairs while including all leak scenarios for every node in the network. A visual comparison between the plots of Figure 5-3 and Figure 5-14 shows an overall increase (deterioration) in the false negative when more leak scenarios are considered. This is an expected behaviour because more leak scenarios produce an accumulated false negative effect. False positives, however, more or less keep the same range (around α) and position in the $\varphi - \omega$ space.

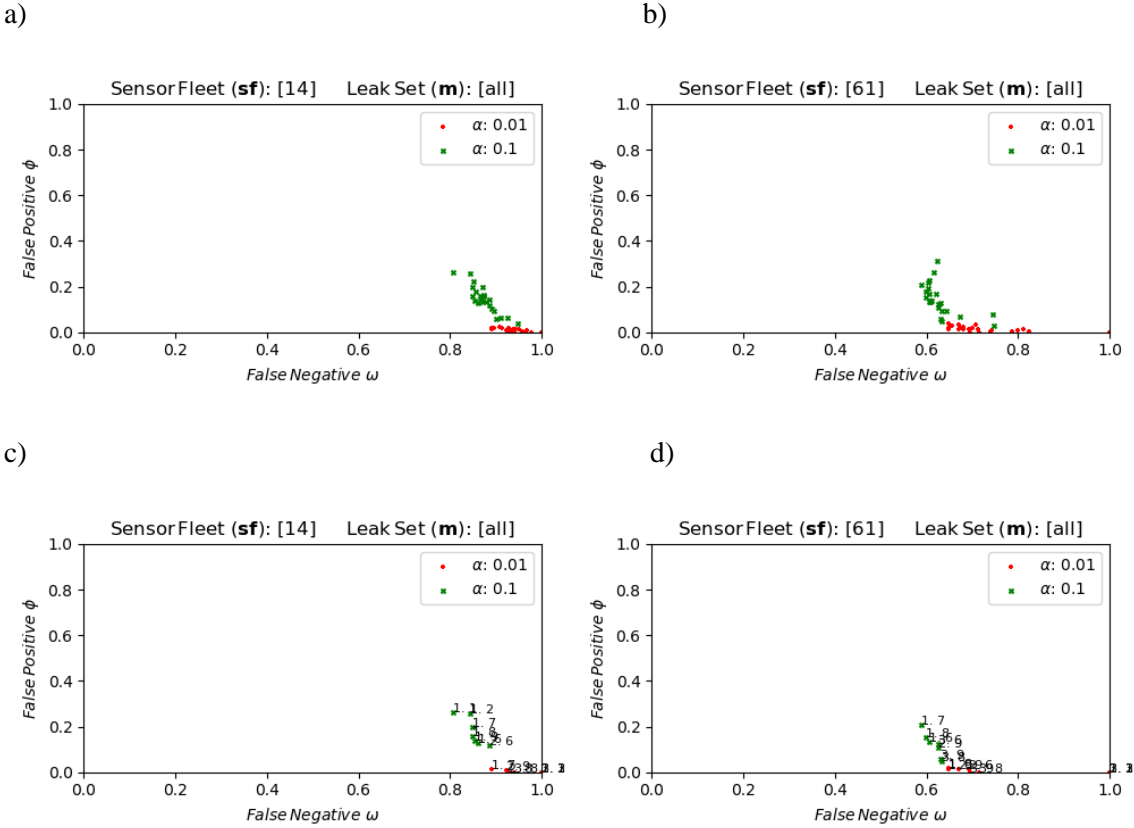


Figure 5-12. Scatter plots of false positive and false negative ratios under example single sensor location and all leak scenarios (Net3)

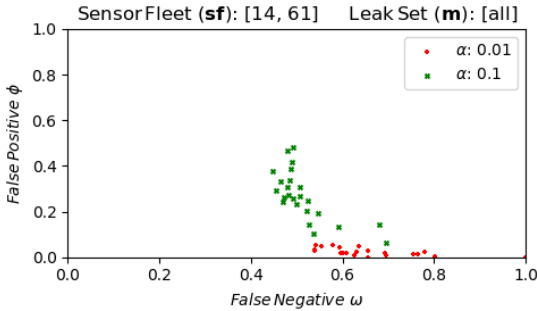
5.7.6 Multiple Sensors and All Leak Scenarios

The experiments in the previous system evaluate *sensor level* false positive and false negative ratios. In this section, the focus is on characterizing *system level* false positive and false negative ratios for a given sensor fleet. Performance assessment at the system level evaluates if at least one sensor detected the leak in a leak scenario (measured by system false negative ratio) and if one or more sensors incorrectly detects the presence of a leak when none are present (measured by system false positive ratio).

Figure 5-13 shows example system level performance results for the cases of two sensors and all leak scenarios. From a comparison of the relative position of the cloud of points in Figure 5-13 and Figure 5-3, it can be seen that by adding the second sensor, the false positive increases (gets worse). However, the second sensor helps to improve the false negative. System level performance is not great for these two example sensor locations. There are likely a better set of two sensor locations than the ones in Figure 5-13

and this introduces the idea that where and how many sensors should be placed is a multi-objective optimization problem.

a)



b)

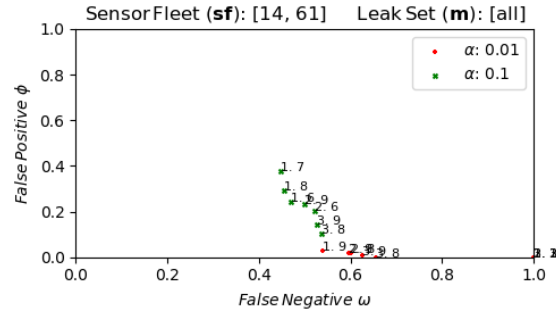
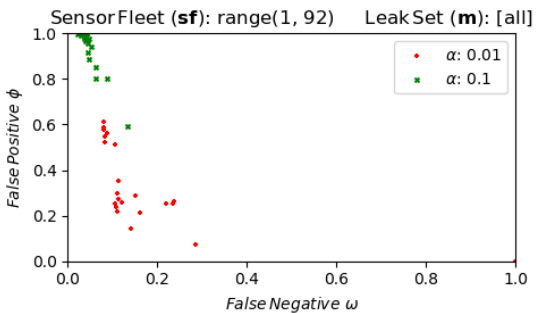


Figure 5-13. System level performance for an example sensor fleet in Net3 network. Scatter plot of false positive and false negative ratios (panel a) under two example sensors and all leak scenarios and the subset of detection method configurations that are non-dominated (panel b).

To consider some bounding performance for a sensor fleet, the same analysis is performed on the case of including all leak scenarios and having sensors on every node in the network (Figure 5-14).

a)



b)

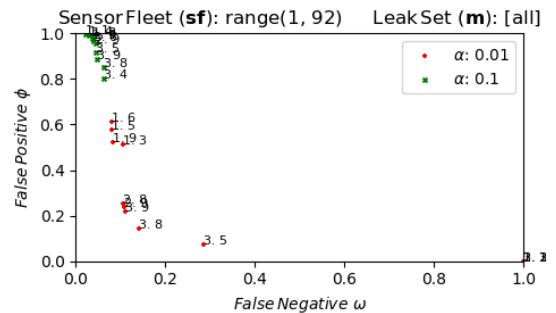


Figure 5-14. System level performance for an exhaustive sensor fleet (sensors on every node) in Net3 network. Scatter plot (panel a) under all sensors and all leak scenarios and the subset of detection method configurations that are non-dominated (panel b).

By adding more sensors (Figure 5-14), the same pattern of increasing false positive and decreasing false negative (improving) repeats. The worst false ϕ positive and best false negative ratios are obtained by

having sensors on every node. The larger in size sf becomes, the cloud covers a wider area between the two extremes. The more sensors, the false positives generated by each node stacks up and becomes larger. Following a basic probability argument, assuming sensor level false positives are independent, it is expected that the system level false positive ratios are inflated when multiple sensors are utilized.

Results under the condition of all leak scenarios and all sensors are presented in Table 5-5. Under the same condition, the variation of false negative and false positive ratios with the number of sampling nights are as well presented in Figure 5-15 and Figure 5-16, respectively.

Table 5-5. System level false positive (φ) and false negative (ω) ratios given sensors at all nodes and all leak scenarios condition for Net3 network.

ΔT - S pair #	ΔT	S	N^1	N $= S \times N^1$	$\alpha = 0.01$		$\alpha = 0.1$	
					φ	ω	φ	ω
1	1	1	5	5	0.000	1.000	0.996	0.021
2	1	2	5	10	0.255	0.234	0.995	0.031
3	1	3	5	15	0.512	0.106	0.998	0.036
4	1	4	5	20	0.562	0.088	0.991	0.029
5	1	5	5	25	0.575	0.080	0.986	0.042
6	1	6	5	30	0.610	0.079	0.974	0.042
7	1	7	5	35	0.588	0.080	1.000	0.036
8	1	8	5	40	0.549	0.083	0.987	0.037
9	1	9	5	45	0.521	0.082	0.976	0.037
10	2	2	3	6	0.000	1.000	0.803	0.087
11	2	3	3	9	0.261	0.238	1.000	0.028
12	2	4	3	12	0.288	0.151	0.999	0.033
13	2	5	3	15	0.260	0.120	0.976	0.046
14	2	6	3	18	0.297	0.111	0.944	0.053
15	2	7	3	21	0.274	0.112	0.989	0.037
16	2	8	3	24	0.253	0.107	0.988	0.039
17	2	9	3	27	0.236	0.108	0.955	0.044
18	3	3	2	6	0.000	1.000	0.592	0.135
19	3	4	2	8	0.254	0.220	0.801	0.062
20	3	5	2	10	0.076	0.285	0.918	0.045
21	3	6	2	12	0.211	0.161	0.965	0.041
22	3	7	2	14	0.351	0.113	0.985	0.042
23	3	8	2	16	0.145	0.142	0.850	0.061
24	3	9	2	18	0.219	0.110	0.887	0.048

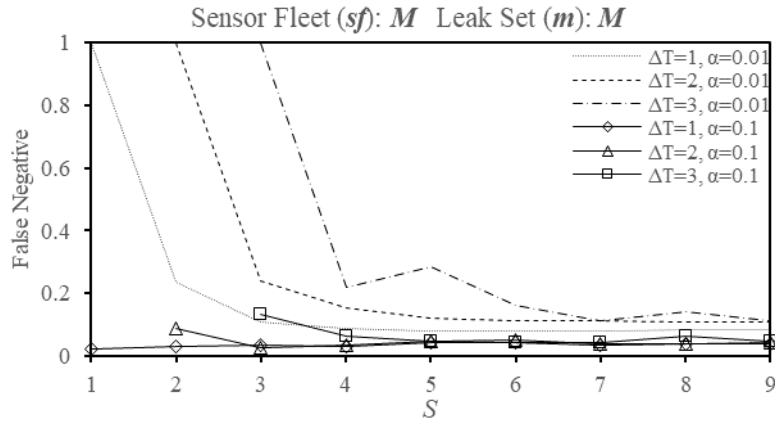


Figure 5-15. System level false negative variation with days of sampling (S) for the all sensor condition for Net3 network

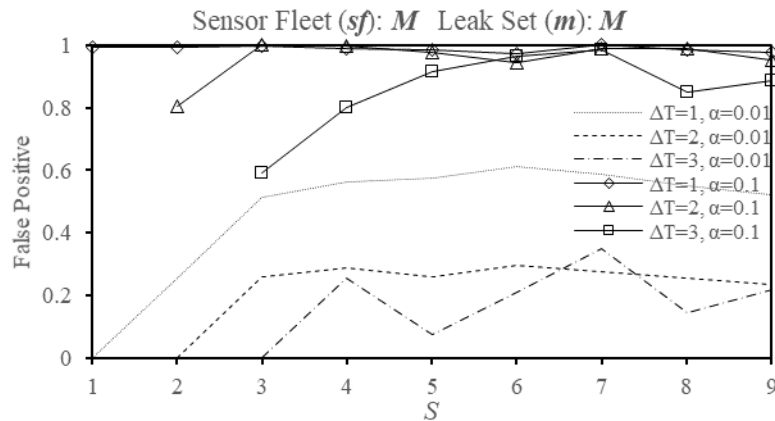


Figure 5-16. System-level false positive variation with days of sampling (S) for the all sensor condition for Net3 network

It can be observed from earlier results in Figure 5-15 that for one sensor, more observation pairs (smaller ΔT and larger S values), result in smaller (better) false negative ratios. False positive values were found to be more or less around the chosen α value and thus indifferent toward ΔT , and S . Therefore, in the case that the sensor fleet was meant to consist of only one sensor, the most desirable design of the detection hypothesis test would be to have the minimum value of ΔT and the maximum value of S , apart from the location of the sensor. However, the sensor fleet is meant to include a variable number of sensors in it. Results for multiple sensors (Figure 5-16) indicate that system level false positive ratio is no longer fixed around the level of significance for each sensor-based hypothesis test. Instead, the false positive

ratios for all configurations show a steep initial increase and then they reach a constant value (which depends on the ΔT and S pair) after 3-5 days of sampling. However, false negative, similar to the case of one sensor, decreases with more observations (Figure 5-15). It can be concluded then that increasing the number of observation pairs, improves false negatives remarkably and does not result in significantly worse false positives. So, for the case of Net3, the smallest value of ΔT defined in Λ , and the largest permitted value of S are recommended for these design parameters (Eq. (5-12)).

$$\begin{aligned}\Delta T &= \min(\Lambda) = 1 \\ S &= \max(S) = 9\end{aligned}\tag{5-12}$$

The above-recommended design parameters are based on the results from Net3 and are used in the optimal sensor placement problems solved for this network (Chapter 7). In general, the determination of ΔT and S for a net network would ideally be done by repeating the above investigations or via the alternative method explained in the following section.

5.7.7 Alternative Method for Choosing ΔT and S

The non-dominated front presented in Figure 5-14.b can be of interest to a decision maker for choosing ΔT and S . This multi-objective decision-making problem can also be solved by selecting the solutions that has the minimum Euclidian distance to the theoretical ideal point $((\omega, \varphi) = (0,0))$.

Note that the detection experiment results database under which the front is generated considers sensors on every node and thus the p_{value} of all the nodes participate in the comparison test. In order to use this approach, or more generally the results in Figure 5-14, to determine ΔT and S prior to sensor placement location optimization, the results must be assumed to hold to all cases where less sensors are deployed as opposed to the case of sensors deployed everywhere.

As an example of this method, it can be seen in Figure 5-14.b that when ΔT and S are taken to be 3 and 9 respectively, and $\alpha = 0.01$, relatively small values of false positive and false negatives could be obtained for when $m=M$ and there are sensors on all nodes. These values, from Table 5-5, are $\varphi = 0.219$ and $\omega = 0.110$.

5.8 Case Study C-Town

5.8.1 Observation Pairs Schedule

For simplicity, the observation pairs schedule for C-Town is taken to be identical to Net3:

$$\Pi = [1,2,3,4,5,6]$$

$$\Lambda = [1,2,3]$$

5.8.2 Experiment Definition

Due to intractable computational load and to keep consistency with the Net3 case study, only 91, out of the 388 nodes of C-Town, were considered in this experiment. Experiment **X2** is defined per below:

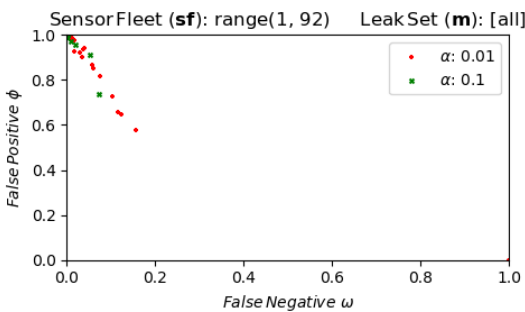
$$\mathbf{X2} = \mathbf{X}(\Omega = 65,520, \Gamma = 3,120, \mathbf{m} = \mathbf{M}, Cv = 0.3, EDC = 0.05, \eta = 30)$$

Experiment **X2** includes $\Omega = 65,520$ leak and $\Gamma = 3,182$ no-leak scenarios, respectively. The leak is of the size $EDC = 0.05$ and all the nodes in the network will have it once at a time ($\mathbf{m} = \mathbf{M}$). For each leak or no-leak scenario, $\eta = 30$ demand realizations are sampled from a multivariate normal distribution with ($Cv = 0.3$) to characterise the distribution of nodal pressure under the no-leak condition. From the 65,520 leak scenarios, each of the 91 nodes get around $\frac{65,520}{91} = 720$ leak scenarios which gives 30 scenarios for each of the 24 $(\Delta T, S)$ pairs. The 3,120 no-leak scenarios are also equally distributed among the 24 $(\Delta T, S)$ pairs imparting each with 130 scenarios.

5.8.3 Results

Figure 5-17.a presents $\phi - \omega$ scatter plots for all the 24 $(\Delta T, S)$ pairs when all nodes are having a sensor and all the leak scenarios (for all the nodes) are included. Figure 5-17.b presents only $(\Delta T, S)$ pairs with non-dominated values of ϕ and ω including data-label of each point in the format of “ $\Delta T.S$ ”.

a)



b)

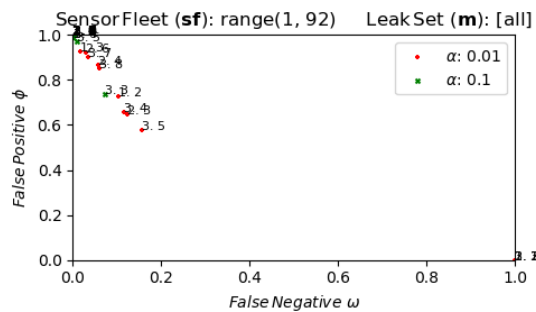


Figure 5-17. System level performance for an exhaustive sensor fleet (sensors on every node) in C-town network. Scatter plot (panel a) under all sensors and all leak scenarios and the subset of detection method configurations that are non-dominated (panel b).

It can be seen from Figure 5-17 that the cloud of points is concentrated on the left-top side of the plot area which corresponds to high false positives (undesirable) and low false negative ratios (desirable). The much better false negative ratios (in comparison to Net3) indicate the leak flow is larger and thus easier to be sensed in this experiment. The associated leak flow ratio (LFR) for a leak with EDC=0.05 in C-Town is often much larger than the LFR of the leak used in Net3 which had an EDC of 5. LFR is defined as the leak flow divided by the maximum diurnal demand at the node. LFRs are reported in Table 4-4 and Table 4-2 for C-Town and Net3, respectively.

Following the design instructions suggested in 7-3, the smallest value of ΔT defined in $\Delta T = 1$, and the largest S , $S = 9$ are also selected for C-Town sensor placement optimization.

5.9 Conclusion

In this chapter, the proposed leak detection method was introduced. The method was implemented and thoroughly verified by solving Net3 and then successfully applied to a second larger network. The flexible structure of the proposed stochastic detection test allows customized sampling schedule and level of significances. As expected, results show larger leaks are easier to detect than smaller leaks but leaks just under 3 LPS were also detected. It was shown that more samples improves the false negative rate and does not deteriorate the false positive rate. Also, the adverse effect of distance on false negatives was demonstrated. This chapter essentially focused on the first step of the detection test design which is scheduling the sampling. The outcome of this chapter are ΔT and S for the case studies and in general, two approaches for determining ΔT and S .

The next step in any leak detection design is to identify the locations for a set of pressure sensors (i.e., sensor placement). This is done by picking up a certain subset of M via solving an optimization problem. The objective functions of this minimization problem are the two control metrics established above as the false positive and false negative ratios for a set of leak and no-leak synthetic scenarios. The slow evaluation of these objective functions combined with the vast search space size (e.g. 2^{91} possible sensor fleets for Net3) make the optimization process intractable unless an efficient solver is used which is able to probe the decision space properly and reach/approach the true Pareto front in a minimum calls of the objective function evaluation process. Without an efficient solver, for the reasons mentioned, the optimization problem of sensor placement cannot be solved during an acceptable time for any real network. A comprehensive study on the identification, configuration, and application of the most efficient

multi-objective optimization solvers in the field of WDS is therefore studied in Chapter 6 before the sensor placement optimization problem is presented and solved in Chapter 7.

Chapter 6

PADDS Algorithm Assessment for Biobjective Water Distribution System Benchmark Design Problems

This chapter is based on the published article with the title “PADDS Algorithm Assessment for Biobjective Water Distribution System Benchmark Design Problems” in the Journal of Water Resources Planning and Management, by Jahanpour M., Tolson, B. A., and Mai, J. December 28, 2017, volume 144, issue 3, in 12 pages. References are unified at the end of the thesis.

6.1 Summary

The need to identify the most efficient multi-objective optimization algorithm available to solve the problem of sensor placement was discussed in Chapter 5. A survey into the literature reveals a large variety of gradient-free multi-objective solvers that have been used in the context of water distribution network optimization in different aspects such as design, operation, calibration and anomaly detection. Furthermore, there exist benchmarking studies that focus on the efficiency of the solvers in solving WDS-related problems. The benchmarking studies are of particular interest when it comes to adopting a multi-objective solver. This chapter presents a benchmarking study to compare six algorithms in solving 12 WDS multi-objective design problems. The results of this chapter in terms of the best multi-objective solver provide the basis for multi-objective solver selection in Chapter 7 where the optimization problem computational burden precludes any sort of algorithm testing and configuration work done in this chapter. Among the benchmarked solvers is the Pareto archived dynamically dimensioned search (PADDS) algorithm. PADDS using two different selection metrics are applied to 12 water distribution system design benchmark problems. Convex hull contribution (CHC) and hypervolume contribution (HVC) are the PADDS selection metrics compared in this chapter. Past research applied five state-of-the-art multiobjective evolutionary algorithms (MOEAs) to these 12 benchmark problems to generate the best-known Pareto fronts (PFs). PADDS-CHC and PADDS-HVC both find all solutions on the known true PFs of the first three problems. Together, both PADDS results augment the previously best-known PFs in nine other benchmark problems with new PF solutions to define updated best known PFs. Compared with other MOEAs, PADDS algorithms identify the highest percentage of solutions in the updated best-known PFs in 11 out of 12 problems. Overall, PADDS-CHC outperforms PADDS-HVC. Compared with PADDS-HVC, the effective archive size of PADDS-CHC is typically about an order of magnitude

smaller. In fact, the PADDs-CHC algorithm generates candidate solutions from a surprisingly small effective archive size which ranges from only from 16 to 73 solutions across the 12 benchmark problems.

6.2 Introduction

The multiobjective optimization (design, calibration, operation) of real-world, large-scale water distribution systems (WDS) are challenging problems for multiobjective optimization (MOO) algorithms such as multiobjective evolutionary algorithms (MOEAs). Cost is often among the multiple objectives in this context and millions of dollars could be saved taking, for example, design decisions on the basis of a superior approximate Pareto front (PF). Past research efforts toward identification and development of MOO algorithms that are capable of good performance on WDS optimization problems are common (Asadzadeh and Tolson 2012; Marques et al. 2010; Moosavian and Lence 2016; Prasad and Park 2004; Yazdi 2016). Performance comparisons of MOO algorithms in dealing with WDSs of various sizes is a critical component of such research.

Wang et al. (2015) set up an archive of 12 benchmark bi-objective WDS design problems from previously published WDS optimization literature. The design objectives in each benchmark problem are to minimize total pipe material costs and maximize the system resilience calculated according to Wang et al. (2015). The benchmark problems range in network size from 8 to 3032 pipes and 8 to 567 integer decision variables associated with defining the pipe diameters of some or all pipes in the network. Wang et al. (2015) aimed to obtain the best-known PFs for those benchmark problems given extensive computational budgets and applied five different MOEAs. The MOEAs used in Wang et al. (2015) were AMALGAM (Vrugt and Robinson 2007), Borg (Hadka and Reed 2013), NSGA-II (Deb et al. 2002), epsilon-MOEA (Deb et al. 2005), and epsilon-NSGA-II (Kollat and Reed 2006).

The well-organized set of WDS benchmark design problems presented by Wang et al. (2015), and the corresponding reported best-known PFs for those problems, have been utilized by other researchers. In a study by Zheng et al. (2016), they use the reference fronts for calculation of six PF quality metrics in order to investigate the run-time behaviour of various MOEAs solving six of the 12 benchmark problems. Bi et al. (2016) also used the best-known PFs from Wang et al. (2015) to calculate PF quality metrics which are used to investigate the improvement by their proposed method for identifying high-quality initial populations. As Wang et al. (2015) mentioned, their work enhances future comparative MOEA performance studies using PF quality metrics that require reference PFs.

The main motivation of this study was to use Pareto archived dynamically dimensioned search (PADDs) (Asadzadeh and Tolson 2009) to resolve the 12 benchmark problems and compare the algorithm performance with the other MOEAs. As a side-product of this work, the best-known PFs for these problems will be updated by the solutions obtained from PADDs.

The PADDs algorithm is a multi-objective adaptation of the single-objective dynamically dimensioned search algorithm (DDS) originally introduced by Tolson and Shoemaker (2007). Tolson et al. (2009) introduced the hybrid discrete dynamically dimensioned search (HD-DDS) algorithm, which is a modified version of DDS algorithm, to solve single-objective WDS design problems with discrete (integer) decision variables. They compare HD-DDS with Genetic Algorithm, ant colony, and particle swarm optimization on four WDS problems and conclude that HD-DDS outperforms the three other algorithms in terms of searching ability and computational efficiency. Inspired by the multi-objective Pareto Archived Evolution Strategy (PAES), Asadzadeh and Tolson (2009) used DDS as the search engine to develop PADDs; a parsimonious multi-objective optimization algorithm with only one algorithm parameter which scales the search procedure based on the computational budget defined by the user. Having solved test problems, they report the promising performance of PADDs relative to NSGA-II and AMALGAM.

Subsequent versions of PADDs are applied to WDS design problems in (Asadzadeh and Tolson 2012; Marchi et al. 2014) and found to produce good quality results. Asadzadeh and Tolson (2012) hybridized PADDs by a discrete local search and used it to solve five benchmark WDS design problems to compare its performance with NSGA-II and SPEA2 (Zitzler et al. 2001). Results of their study indicated high potential of hybridized PADDs for approximating the true PFs despite its simplicity and limited computational budget. In a study by Khedr et al. (2015), the WDS calibration problem for the Town of X in Ontario, Canada was solved firstly by engineers using expert-based approaches and secondly by PADDs considering the problem as a three-objective optimization problem. PADDs obtained a total of 24 design solutions which dominated the manually calibrated design suggested by engineers familiar with the system. Tolson et al. (2012) utilize PADDs as the optimization algorithm in the Battle of the Water Networks II multiobjective WDS design competition (Marchi et al. 2014) and their results ranked 2nd overall.

PADDs relies on a roulette wheel approach to select a solution from the set of archived, nondominated solutions which is then perturbed to generate a new candidate solution. The selection probability of archived solutions determines their chance to be selected by roulette wheel in each iteration. To assign selection probability to the archived solutions, a number of selection metrics have been introduced and tested for PADDs. The first version of PADDs (Asadzadeh and Tolson, 2009) used the crowding distance

selection metric introduced in Deb et al. (2002). Asadzadeh and Tolson (2013) later demonstrate that hypervolume contribution metric, as in Knowles et al. (2003), is more effective for PADDs compared to crowding distance and uniform random selection where each solution in the PADDs archive has an equal probability of selection. Most recently, Asadzadeh et al. (2014) introduce the convex hull contribution (CHC) metric and compare against the hypervolume contribution (HVC) for several benchmark mathematical problems and several hydrologic model calibration problems. Asadzadeh et al. (2014) demonstrate that PADDs using CHC shows improved performance over PADDs using HVC in some situations. In this chapter, PADDs-CHC and PADDs-HVC refer to PADDs using CHC and HVC as selection metrics, respectively.

Given the predominantly convex shape of the best known PFs for all 12 benchmark problems in Wang et al. (2015), these benchmarks are excellent examples to more robustly test CHC versus HVC in the context of WDS multiobjective optimization.

This chapter directly follows the problems and analysis of the original benchmark paper in Wang et al. (2015). Thus, minimum benchmark problem details are presented here and readers therefore are encouraged to refer to Wang et al. (2015) for full details. The remainder of the chapter is organized as follows. The Methodology section describes further details of PADDs, the decision variable definitions, the computational experiment outline and the inter-algorithm results comparison approach. The Results section reports on all experimental results and in particular highlights the excellent quality PADDs results compared to the five benchmark algorithms from Wang et al. (2015) and closely compares PADDs-CHC versus PADDs-HVC performance for a range of computational budgets.

6.3 Methodology

In this section, procedures to design and solve the optimization problems, including definition of objective functions, decision variables, and constraints followed by procedures for post-processing of raw results to generate the best-known PFs are explained. Details about how the PADDs algorithm works are provided in Appendix A.

6.3.1 Benchmark Problems and Decision Variables

The decision variables in all 12 WDS design problems in this study are of integer type with predefined ranges and function to specify the diameter of individual pipes in the network. Each network problem comes with a specific list of available pipe diameters, which may be used in the design of pipes in that network. In addition to alternative pipe diameters, in some problems, some pipes can be left alone (do

nothing) or duplicated. For PADDs, decision variables are defined as an integer pipe option ID number for each pipe where the list of possible ID or option numbers for a given pipe is defined as consecutive integers such as 0, 1, 2, ... $n-1$, where n is the number of options. The design options for each pipe are sorted based on costs such that option 0 has the lowest pipe upgrade costs and option $n-1$ has the highest costs.

The 12 WDS problems in this study fall into two categories: design problems and extended design problems. Design problems include the two-loop network (TLN) (Alperovits and Shamir 1977), BakRyan network (BAK) (S. Lee and Lee 2001), Blacksburg network (BLA) (Sherali et al. 2001), Hanoi network (HAN) (Fujiwara and Khang 1990), GoYang network (GOY) (Kim et al. 1994), Fossolo network (FOS), Pescara network (PES), and Modena network (MOD), the latter three are taken from (Bragalli et al. 2008), and the Balerma irrigation Network (BIN) (Reca and Martínez 2006). In design problems, a set of integer option numbers, each assigning a diameter to an individual new link (pipe) in the network, is considered as the vector of decision variables. Note that not all the pipes in a network are necessarily involved in the design procedure. Thus, the number of decision variables in a design problem is less than or equal to the total number of pipes in the network. For example, TLN network has eight pipes, which all are involved in the design, and there are 14 different diameter options available for each pipe in this network. Therefore, the number of decision variables, their range and the search space size in the TLN problem are 8, [0, 13] and 8^{14} respectively. In the BAK network, although there are 58 pipes in the network, only 9 are included in the design process and thus the design problem has only 9 decision variables.

Extended design problems, on the other hand, are the two-reservoir network (TRN) (Gessler 1985), New York tunnel Network (NYT) (Schaake and Lai 1969) and Exeter network (EXN) (Farmani et al. 2004). They are 'extended' problems because they involve making decisions beyond pipe sizing for new links. For example, decisions on how to modify existing pipes/links in the network are required. For the TRN network, the first 5 decision variables are regular design variables for new links which determine the diameter of a pipe in the network while the remaining 3 decision variables are extended decision variables and can equal 0, to leave the pipe unchanged, 1, to clean the pipe, and an integer in range [2, 9] to duplicate the pipe with a pipe having a range of possible diameters. A zero value for a decision variable in NYT is considered as an extended design parameter and indicates that the pipe should be left unchanged. Other non-zero values for NYT, which range in [1, 15], assign a different pipe diameter to the corresponding duplicated pipe in this network. EXN is the largest network and has 3032 pipes. The decision variable vector has 567 elements and there are 10 available pipe duplication diameters. A zero value for a decision variable in EXT is considered as an extended design parameter and indicates that the pipe should be left

unchanged. Other non-zero values for EXT, which range in [1, 10], each assign a different pipe duplication diameter to the corresponding duplicated pipes in this network.

It is worth mentioning that the procedures to ultimately generate integer pipe options are different in PADDs compared to the MOEAs in Wang et al. (2015). In Wang et al. (2015), MOEAs initially generate real-value decision variables which are next rounded down to integer values; whereas, PADDs has the capability of directly generating and working with integer decision variables. This strategy in PADDs ensures the algorithm tracks and perturbs the precise, integer-valued decision variables.

6.3.2 Objective and Constraint Evaluation

When it comes to comparison of MOO algorithms, it is of prime importance to make sure that the objective functions (and constraints) are being identically simulated/calculated when called by all the MOO algorithms being compared. The objective functions under consideration in the benchmark problems are to 1) minimize the total cost, TC , of the network design in millions of dollars, defined by Eq. 6-1, and 2) minimize the negative value of the network resilience index, $-NR$ defined by Eq. 6-2. The total cost, TC , of a design solution contains expenditures of pipe components such as installing new pipes and/or cleaning existing ones.

$$TC = a \sum_{i=1}^{np} D_i^b \times L_i \quad (6-1)$$

where np is the number of pipes potentially modified; a and b are constants depending on a specific problem; D_i is the diameter of pipe i ; and L_i is the length of pipe i .

Network resilience index introduced by Prasad and Park (2004), is a resilience-base index which improves the resilience indicator by taking into account the uniformity of pipes connected to demand nodes.

$$-NR = - \frac{\sum_{j=1}^{nd} \left(\left(\frac{\sum_{i=1}^{np_j} D_i}{np_j \times \max\{D_i\}} \right) Q_j (H_j - H_j^{min}) \right)}{\left(\sum_{k=1}^{nr} Q_k H_k + \sum_{i=1}^{npu} \frac{P_i}{\gamma} \right) - \sum_{j=1}^{nd} Q_j H_j^{min}} \quad (6-2)$$

where nd is the number of demand nodes; Q_j , H_j , and H_j^{min} are the demand, simulated head, and minimum required head of node j , respectively; nr is the number of reservoirs; Q_k and H_k are the discharge and simulated head of reservoir k , respectively; npu is the number of pumps; P_i is the power of pump i ; γ is

the specific weight of water; np_j is the number of pipes connected to node j ; and D_i is the diameter of pipe i connected to demand node j . Eq. 6-1 and Eq. 6-2 are both taken from Wang et al. (2015).

Each benchmark problem has a corresponding set of hydraulic constraints which must be met. These constraints are all nonlinear functions of the decision variables. Interested readers are referred to Wang et al. (2015) for detailed constraint specifications. Note that all benchmarks have pressure constraints, i.e. all nodes must meet some minimum specific pressure. Additionally, some of the networks have further constraints on maximum nodal pressures as well as minimum and/or maximum flow velocities.

Wang et al. (2015) published the source code to evaluate the objective functions and constraints for a candidate solution for all benchmark problems. This code sets up, runs, and gathers results from EPANET2 programmer's toolkit (Rossman 2000) and finally calculates and reports numeric values of both objective functions plus any constraint violations. This source code, which in this paper will be briefly referred to as the simulation model, was directly compiled and used for simulation of solutions in this study. However, it was verified that the same simulation model outputs (objective function values and constraint satisfaction) as Wang et al. (2015) are obtained for a suite of example solutions. EPANET2 programmer's toolkit version 2.00.12 was compiled under Linux and utilized within the simulation model to perform the hydraulic analysis.

A design solution is considered infeasible if any constraint is not satisfied or if EPANET2 terminates due to computational instability and/or returns an error value. The constraint handling approach in this work is consistent with the penalty function free approach that was used by Wang et al. (2015) for all the algorithms they implemented. Wang et al. (2015) utilized the constrained-domination principle introduced in Deb et al. (2002). The main idea of constraint handling in this work is to make sure that any infeasible solution will be dominated by any feasible solution and thus removed from the archive, provided a feasible solution is already found. This is done by assigning infeasible solutions with objective functions worse than the objective function values of any feasible solution. In the benchmark WDS design problems, the worst possible cost feasible solution is known as the cost of the solution specifying all pipes at their maximum diameter.

Pseudocode in Figure 4-1 describes the objective and constraint handling logic used in this study. After a feasible solution is found by PADDs, infeasible solutions are shifted to a point in the objective space, called terminal point, where both objectives have values greater (worse) than their worst possible feasible values. Coordinates of the terminal point were chosen arbitrarily to be $[10^5, 10^5]$, which are reliably worse values for the cost (in millions of dollars) and the negative resilience (defined to have a maximum of 0)

objectives. The terminal point is not to be confused with the Nadir point which is the point in the objective space defined by the individual objectives at their worst possible, yet feasible values.

```

Simulate  $x^p$ 
Get total_cost, network_resilience, and constraint_violation values from simulation model results
 $\mathbf{F}[1] = \text{total\_cost} / 10^6$ 
 $\mathbf{F}[2] = -1 \times \text{network\_resilience}$ 
IF (constraint_violation = 0):
     $x^p$  is feasible
    feasible_solution_yet = True
ELSE:
     $x^p$  is not feasible
    IF (feasible_solution_yet = True):
         $\mathbf{F} = [10^5, 10^5]$ 
    ELSE:
        IF (EPANET2 has crashed):
             $\mathbf{F} = [10^5, 10^5]$ 
        ELSE:
             $\mathbf{F}[1] = \text{constraint\_violation} + \text{Cost}_{max}$ 
             $\mathbf{F}[2] = \text{constraint\_violation} + 1.0$ 
RETURN  $\mathbf{F}$ 
END procedure

```

Figure 6-1. Pseudocode for Calculation of Objective Functions for Network Design

Note: *constraint_violation* is a positive real number showing the total value of violations of constraints calculated by the model. Zero value of this variable means there has been no violation and x^p is feasible; \mathbf{F} is vector of objective function values; *feasible_solution_yet* is a global Boolean variable, which retains its value throughout the optimization trial, has an initial value of False and functions to track if the algorithm has identified any feasible solution found yet; Cost_{max} , in millions of dollar, is the maximum possible cost of the network design.

6.3.3 Computational Experiments

Table 6-1 summarizes the PADDs computational budgets used in this study for each benchmark problem. The PADDs computational budget(s) were assigned to be equal to the budgets used in Wang et al. (2015). Wang et al. (2015) allocated a certain number of maximal solution evaluations (NSE) to each network problem. The NSE defined their MOEA computational budget for solving the problem in each optimization trial and each MOEA was only terminated after this budget was exhausted. The first set of PADDs algorithm experiments were conducted under the full budget (equal to the maximum NSE in Wang et al. (2015) which ranges from 600,000 to 2,000,000 across the problems). A second set of PADDs experiments was conducted at a partial budget (1/100th of full budget).

Table 6-1 Specifications for benchmark design problems. All specifications based on or taken from (Q. Wang et al. 2015).

Network	# of DVs	PADDSD V range	SS size	NSE	CE	RE	Cost _{max}	EFE
TRN	8	[0, 9]	3×10^7	10^5	10^{-2}	10^{-3}	5.525	N/A
TLN	8	[0, 13]	1×10^9	10^5	10^{-2}	10^{-3}	4.400	True
BAK	9	[0, 10]	2×10^9	10^5	10^{-3}	10^{-3}	1.389	True
NYT	21	[0, 15]	2×10^{25}	6×10^5	10^0	10^{-3}	294.156	True
BLA	23	[0, 13]	3×10^{26}	6×10^5	10^{-3}	10^{-3}	1.299	False
HAN	34	[0, 5]	3×10^{26}	6×10^5	10^{-1}	10^{-3}	10.970	True
GOY	30	[0, 7]	1×10^{27}	6×10^5	10^{-3}	10^{-3}	0.330	True
FOS	58	[0, 21]	7×10^{77}	10^6	10^{-3}	10^{-3}	1.662	True
PES	99	[0, 12]	2×10^{110}	10^6	10^{-2}	10^{-3}	19.004	False
MOD	317	[0, 12]	1×10^{353}	2×10^6	10^{-2}	10^{-3}	28.083	False
BIN	454	[0, 9]	1×10^{455}	2×10^6	10^{-2}	10^{-3}	21.642	True
EXN	567	[0, 10]	3×10^{590}	2×10^6	10^{-2}	10^{-3}	97.501	False

DV = decision variables; SS = search space; NSE = number of solution evaluations (computational budget); CE = cost epsilon; RE = resiliency epsilon; Cost_{max} = maximum cost in millions of dollars corresponding to the extreme design (highest cost decision variable option selected); EFE = Boolean variable checking if the extreme design of a network is a feasible solution.

Consistent with Wang et al. (2015), PADDSD solves each benchmark problem with a total of 30 independent optimization trials. In the full budget case, this means PADDSD and the Wang et al. (2015) MOEAs utilize the same number of total NSEs, and thus results are directly comparable. Note that Wang et al. (2015) designed experiments with three different configurations of each MOEA, each with a different population size but all configurations used the same maximum NSE. Each of the three configurations were applied 10 times each time using a different random initial seed, resulting in a total of 30 optimization trials for each MOEA to optimize a network.

PADDSD has a single algorithm parameter which has a well-defined default value of 0.2 that developers suggest does not need to be tuned to each new problem. Hence, the 30 PADDSD optimization trials only differ regarding their random seeds. Two versions of PADDSD are applied to solve the problem: PADDSD-CHC and PADDSD-HVC. Each of the optimization trials terminates with an approximate Pareto front composed of points or solutions defined by the pair objective function values. The only stopping criterion in the MOEAs used in Wang et al. (2015) and in both PADDSD algorithms was the maximum allowable NSE.

6.3.4 PADDs Result Post-Processing and Comparisons

In this work, there were 12 network problems, 2 PADDs algorithms and 2 computational budget groups, resulting in $12 \times 2 \times 2 = 48$ sets of algorithm results, each containing 30 optimization trials. Each of the 48 sets of optimization trials was post-processed as follows. First, all obtained solutions of the trial set were rounded according to the epsilon precisions based on Wang et al. (2015) for the corresponding network (see Table 6-1 column for CE). Second, solutions from all 30 trials of the trial set were merged into one list of unique and nondominated solutions. The remaining solutions form an approximate aggregate PF for the respective set of optimization trials. In total, 48 such approximate aggregate PFs are created.

The best known PF for each problem from Wang et al. (2015) are augmented with the approximate full budget PADDs PFs generated via the procedure in the previous paragraph. The augmentation involved merging the best known PF from Wang et al. (2015) with the approximate full budget PADDs PFs to form one list of unique and nondominated solutions. Consistent with Wang et al. (2015), the primary metric used here for comparing algorithm performance is the contribution percentage (%C). The %C for a specific MOO algorithm is defined as the percentage of solutions contributed to the best-known PF by that algorithm.

PADDs is a stochastic MOO algorithm and thus, even solving the same problem, different results are expected by changing the random seed used to initialize the search Asadzadeh and Tolson (2013). Zitzler et al. (2008) state that any statement about the performance of a randomized optimization algorithm is probabilistic in nature. Relying on a single approximate PF, to represent behavior of a MOEA in solving a problem should therefore be considered as a last option in the process of comparison. A comprehensive examination of stochastic search algorithms requires taking into account results from multiple runs each based on a different random seed. To do this, the individual optimization trial results from PADDs-CHC and PADDs-HVC are compared based on the normalized hypervolume (NHV) multiobjective algorithm performance metric from Deb (2001) which is based on NHV as introduced by Zitzler and Thiele (1998). Hypervolume of an approximate PF measures the confined volume of objective space between the front and a reference point. Normalized hypervolume is computed in objective space normalized on the range of 0 to 1 with a corresponding reference point of (1, 1). NHV for an approximate PF is calculated by dividing the hypervolume of the approximate front by the hypervolume of the best-known front of that problem. NHV values therefore range from 0 to 1. A higher value of NHV is desirable, yet different approximate PFs could have very close NHV values thus making interpretation of different NHV values not always straightforward (Asadzadeh and Tolson 2012).

6.3.5 Effective Archive Size of PADDs

The PADDs archive size is unbounded and every nondominated solution found by the algorithm is added to the archive. Each PADDs selection metric (i.e., CHC and HVC) follows a specific procedure to calculate and assign selection probabilities to solutions archived by PADDs, in every iteration. The selection probabilities are subsequently used by a roulette wheel to select a solution from the archive. The selected solution is then perturbed and referred to as the next candidate solution. The detailed search process of PADDs is described by Asadzadeh and Tolson (2013). To better investigate the behavior of CHC and HVC in assigning selection probabilities to the archived solution through iterations, which in turn directs the PADDs search, an innovative metric called effective archive size (EAS) is introduced in this study. The EAS of a set of archived solutions is defined as the minimum number of archived solutions with cumulative selection probability value greater or equal to 0.99. For example, an EAS value of 2 for an archive that contains 50 solutions, means that among all archived solutions, there are two solutions with a total probability of selection of 0.99 or higher of one of them being selected by the roulette wheel during the next iteration; leaving a very small chance for all other 48 solutions in the archive to be selected for generating the new solution. For CHC, nondominated solutions that are not on the convex hull are assigned a selection probability of 0, while for HVC, all nondominated solutions are assigned a non-zero probability of selection. Relative EAS is introduced as a ratio obtained by dividing EAS value by the total number of solutions in the archive.

6.4 Results

6.4.1 Best-Known Pareto Fronts

Optimization trials for the 12 benchmark problems were conducted following the configuration described in the methodology section. Raw results were post-processed as explained in result data post-processing section. The outcome was approximate PFs for 12 benchmark problems, obtained by PADDs-CHC and PADDs-HVC using full and partial computational budget. The best solutions found for the benchmark problems are completely documented and provided in the Supplemental Online Materials associated with Jahanpour et al. (2017).

With a full computational budget considered for each network problem (see Table 6-1), there were two approximate PFs obtained from PADDs algorithms plus five others by MOEAs used in Wang et al. (2015). Results from all MOEAs (i.e. PADDs-CHC, PADDs-HVC, AMALGAM, Borg, NSGA-II, epsilon-MOEA, epsilon-NSGA-II) were used to generate updated best-known PFs (relative to Wang et al.

(2015)) for each network problem by merging all solutions together and removing duplicate and/or dominated ones. Remaining solutions formed the updated best-known PFs for each network problem. Each PADDs algorithm found all solutions on the known true PFs of the first three problems. Together, the PADDs algorithm results augment the best-known PFs in all 9 other benchmark problems with new PF solutions, some of which dominate previous best-known PF solutions. Henceforth, the updated best known PFs are simply referred to as the best known PFs.

The portion of the PADDs computational budget spent in each problem to obtain the first feasible solution was identified to ensure the constraint handling strategy (explained in Figure 4-1) functioned appropriately. This portion was found to be always less than or equal to 0.5% of the full budget in first 11 networks of Table 6-1 and 3.2% for last network, which is the largest problem solved in this study. These very small values indicate that the constraint handling strategy in PADDs enabled the algorithm to very quickly navigate to the feasible region of decision space.

6.4.2 Contribution of Each MOEA

With updated best-known PFs due to PADDs, the contributions of each MOEA to the best known PFs need to be updated from those published in Table 5 of Wang et al. (2015).

Table 6-2 in this chapter uses the same format of Wang et al. (2015) and shows the updated contribution percentages (%C) for the five MOEAs used in Wang et al. (2015) and the %C for the PADDs algorithms. The %C value of a specific MOEA in the best-known PF of a network is calculated by dividing the number of solutions contributed by that MOEA by total number of solutions in the front.

Table 6-2 shows that in 11 of 12 networks, one of the PADDs algorithms contributed the maximum number of solutions in the best-known PF. NSGA-II results for the FOS network are the only case where another algorithm outperformed both PADDs implementations (NSGA %C=30.6 versus PADDs %C=19.4 in both implementations). PADDs-HVC and PADDs-CHC both contribute 100% of the best known PF solutions in each of the first four problems (smallest networks) and are the only algorithms to have achieved that in the NYT problem. PADDs-HVC and PADDs-CHC %C values are quite similar to each other (within 6%) for the BLA, HAN, FOS networks. PADDs-HVC clearly outperforms PADDs-CHC on the GOY and PES networks while PADDs-CHC performs substantially better than PADDs-HVC on the three largest networks (MOD, BIN, EXN). In fact, PADDs-HVC identified 0% of the solutions on the best-known PF for the three largest networks.

Table 6-2 Percentage of Solutions Contributed to the Best-Known PF via each MOO algorithm. Highest percentage for each benchmark network are bolded.

Network	MO Algorithm						
	AMALGAM	Borg	NSGA-II	epsilon-MOEA	epsilon-NSGA-II	PADDS-CHC	PADDS-HVC
TRN	100.0	90.3	100.0	91.4	36.6	100.0	100.0
TLN	97.4	83.1	100.0	83.1	83.1	100.0	100.0
BAK	100.0	76.3	100.0	73.8	76.3	100.0	100.0
NYT	90.3	20.0	91.0	17.9	24.8	100.0	100.0
BLA	86.8	26.3	74.3	28.3	24.3	94.1	100.0
HAN	84.6	25.6	94.9	20.5	23.1	94.9	97.4
GOY	80.9	22.1	41.2	2.9	52.9	55.9	86.8
FOS	7.6	21.5	30.6	6.9	7.6	19.4	19.4
PES	16.4	0.0	5.3	12.4	2.2	34.7	49.8
MOD	21.3	4.6	31.5	2.5	0.0	50.8	0.0
BIN	10.4	0.0	5.6	2.6	0.7	86.2	0.0
EXN	0.0	41.9	0.0	0.0	6.7	54.2	0.0

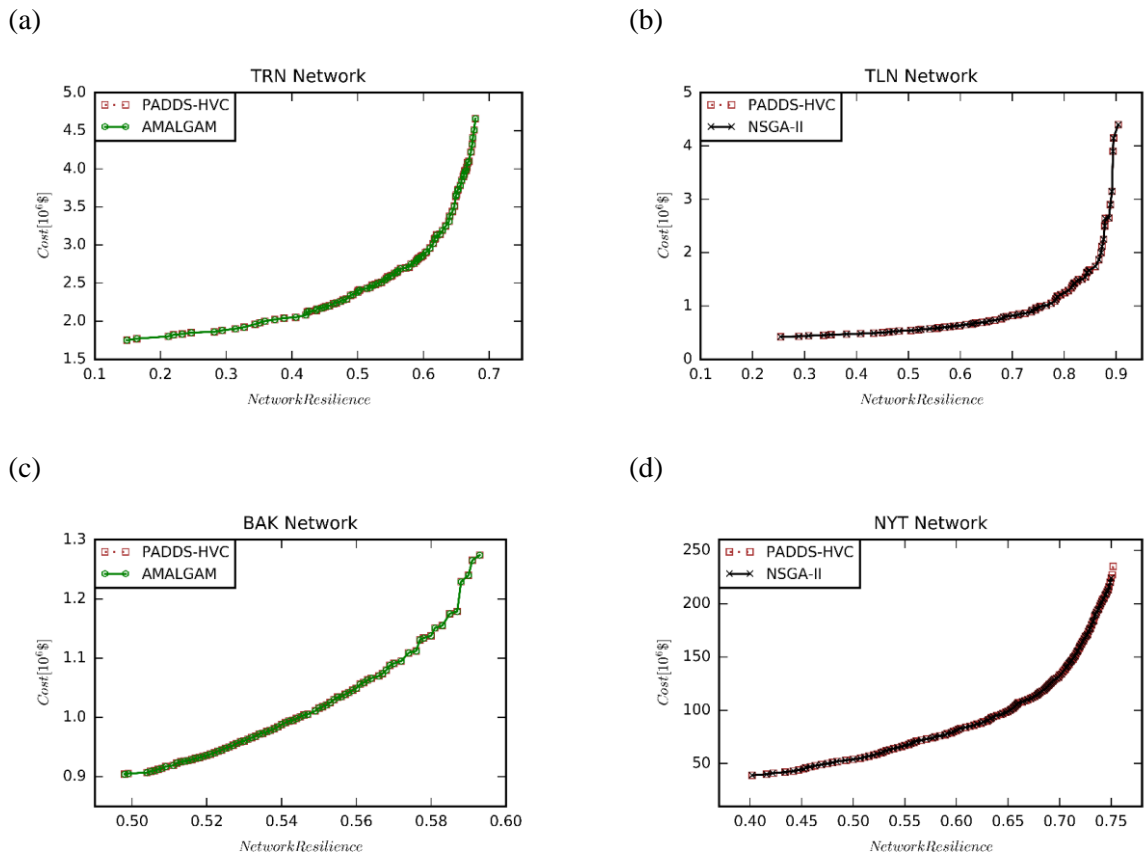
The %C is only one of many PF quality metrics introduced in the literature and refers to the performance of a MOO algorithm to provide nondominated solutions. A more robust comparison between MOO algorithms needs consideration of results from individual trials, which were run based on different random seeds, rather than aggregate approximate PFs. However, raw results for optimization trials in Wang et al. (2015) study were not available.

Figure 6-2 shows approximate PFs by selected MOEAs for all 12 benchmark problems. For the sake of clarity and to keep the algorithm results distinguishable, the panels in Figure 6-2 do not include the approximate PFs from all seven algorithms (all PADDs algorithm generated solutions in best-known PFs of all network problems are provided as supplemental data file S1). Instead, for the first 11 problems, the best MOEA result from Wang et al. (2015) is compared with the best PADDs result (in terms of the %C in

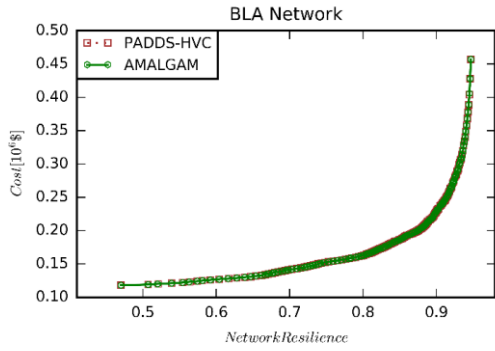
Table 6-2). For the largest network (EXT), since the algorithm specific aggregate PFs are generally distinguishable, results from all seven MOO algorithms are compared in Figure 6-2 PADDs-HVC is compared to AMALGAM or NSGA-II in panels (a) to (e) and results are indistinguishable for these smaller networks. For the HAN and GOY networks in panels (f) and (g), slight differences begin to be noticeable with the PADDs algorithms generating more solutions on the best-known PF. More pronounced differences between algorithms are apparent for the larger networks depicted in panels (h) through (l). For example, for the PES, MOD and BIN networks in panels (i) to (k), PADDs results better characterize the bulge or knee Das (1999) of the approximate PFs while the best MOEA from Wang et al. (2015) better characterizes the extreme solutions on the right-most (max cost) end of the approximate PFs.

Solutions in knee region tend to keep a balance between objective values and are key points estimating the approximate PF; therefore, decision makers are regularly more interested in the knee part of PFs. Note that the FOS network is the only case where neither of the PADDs algorithms contributed the most of solutions in the best-known PF; however, PADDs-HVC (and PADDs-CHC although results not shown) were able to contribute almost all of the dominating solutions in the knee region.

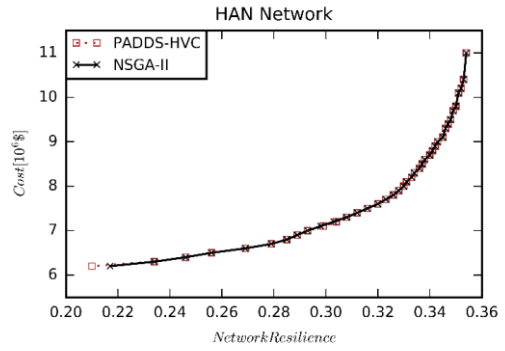
Figure 6-2 Select approximate Pareto fronts generated by PADDs algorithms and multiobjective evolutionary algorithms used by Wang et al. (2015)



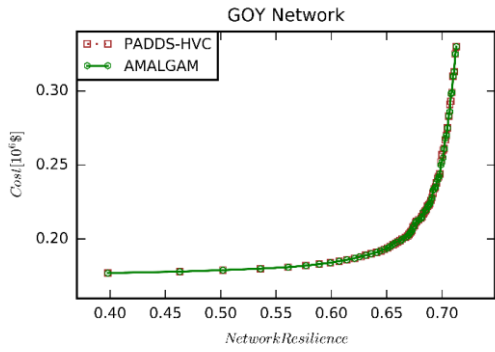
(e)



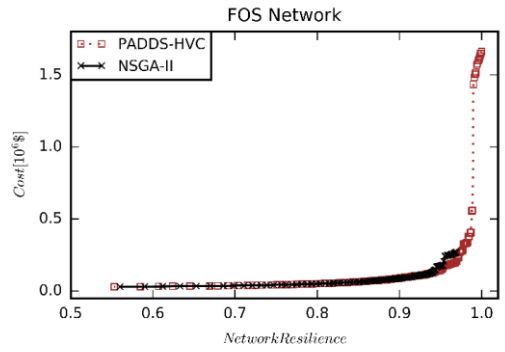
(f)



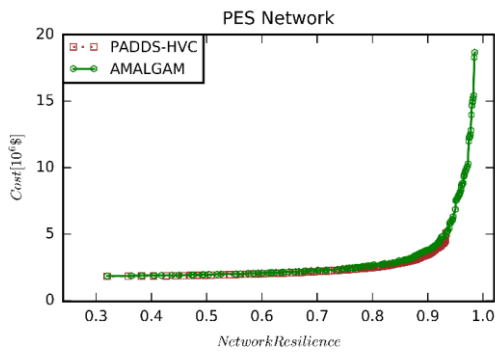
(g)



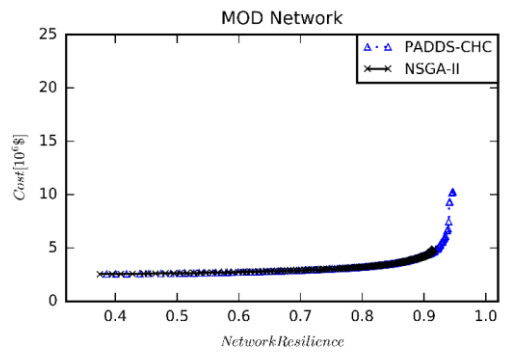
(h)



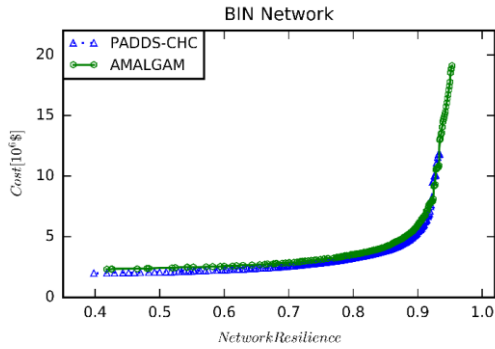
(i)



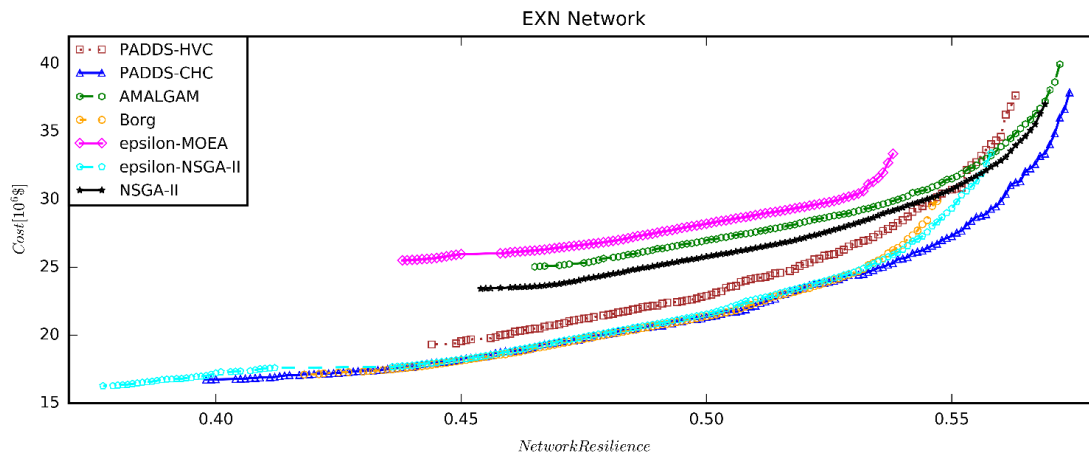
(j)



(k)



(l)



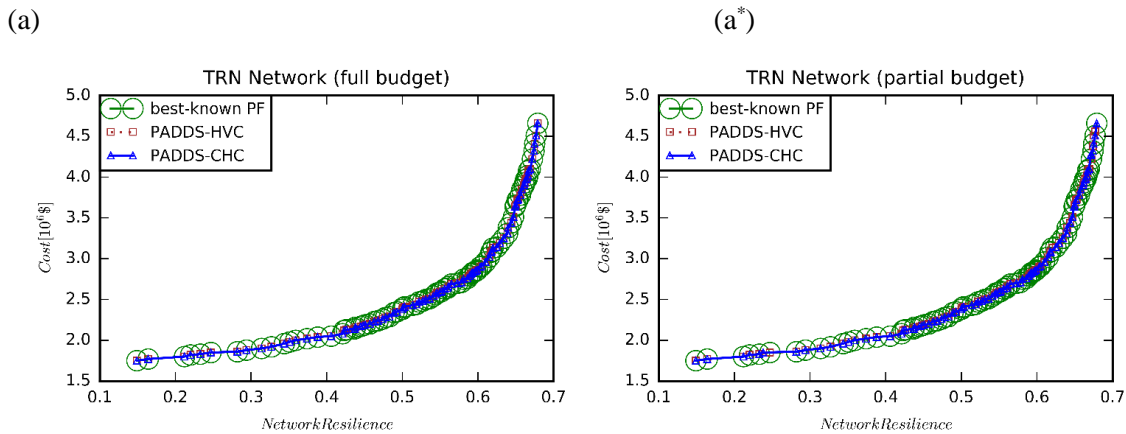
For the EXN problem, all seven MOEAs are shown in Figure 6-2(1). In the right side and upper knee region of the PF, PADDs-CHC produced significantly less expensive solutions (at the same resilience) compared with previously best-known PF. For example, if a decision maker wanted to achieve a network resilience of 0.56 for the design of the EXN network, the results obtained from PADDs-CHC suggest a design solution about \$3 million cheaper than the solution from previously best-known PF. In the rest of the knee region, solutions from PADDs-CHC, Borg, and epsilon-NSGA-II are very close together. PADDs-CHC and epsilon-NSGA-II each contribute roughly half of the solutions on the left side of the best known PF. AMALGAM, NSGA-II, epsilon-MOEA and PADDs-HVC are not contributing any nondominated solution for the EXN network.

6.4.3 PADDs Selection Metrics Comparison

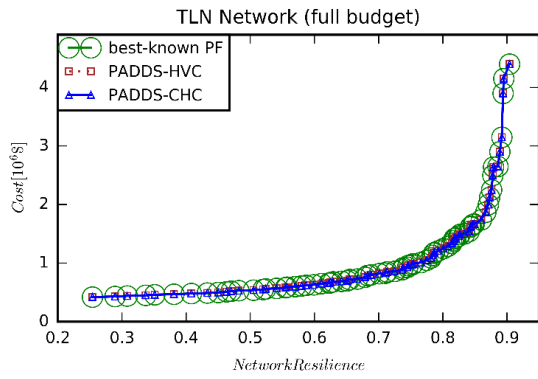
Figure 6-3 compares the influence of computational budget on PADDs performance in terms of the final algorithm-specific approximate PFs for each network. Note that the raw PADDs results were post-processed as explained in Result Data Post-Processing section. The left-side panels in Figure 6-3 are the final approximate PFs for the full budget optimization trials (e.g., same results appearing in

Table 6-2) and the right-side panels are for the partial budget (1/100th of full budget) sets of optimization trials. At both budgets, panels (a)-(f) and then (a*)-(f*) show that for the first six networks, both PADDs algorithms generate approximate PFs that are virtually indistinguishable from the best known PFs. The PADDs results become different in panels (g)-(l) and (g*)-(l*). In general, PADDs-CHC is better characterizing the knee of the best known PFs in comparison with PADDs-HVC. This difference is more pronounced with a limited budget as shown in panels (g*)-(l*). Overall, given a sufficiently large computational budget, PADDs-HVC and PADDs-CHC tend to yield the same quality approximate aggregate PFs which are generally equivalent to the best known PFs. However, with a relatively limited budget, results clearly indicate PADDs-CHC is preferred.

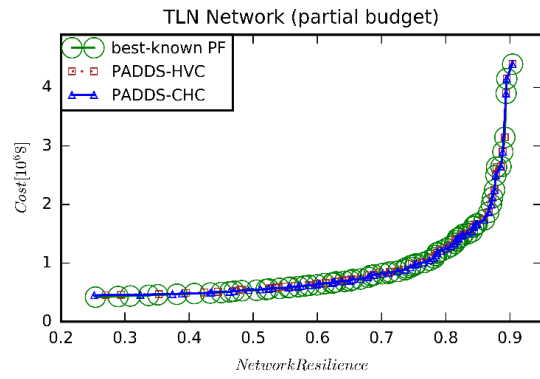
Figure 6-3 Approximate Pareto fronts (PFs) obtained by PADDs algorithms the aggregated results from 30 optimization trials with the full NSE budgets listed in Table 6-1 (left column) and partial budgets (right column) using 1/100th of the full NSE budgets.



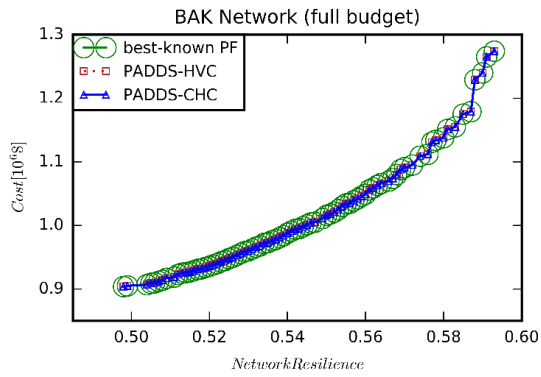
(b)



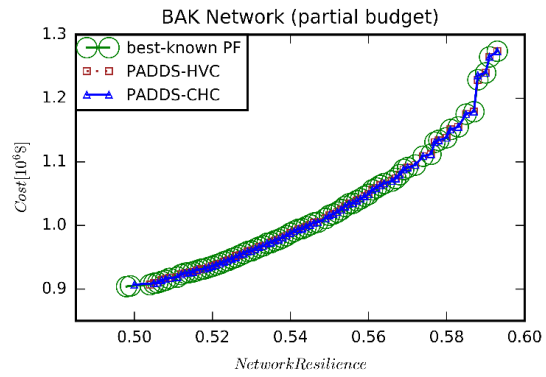
(b*)



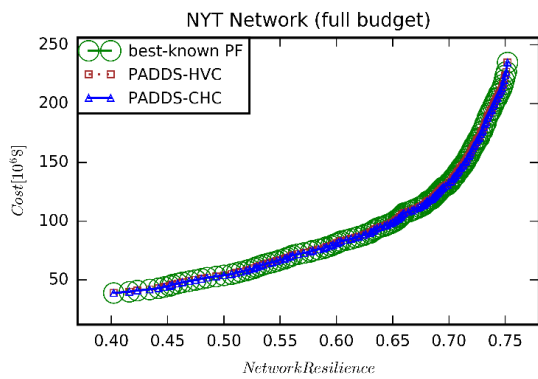
(c)



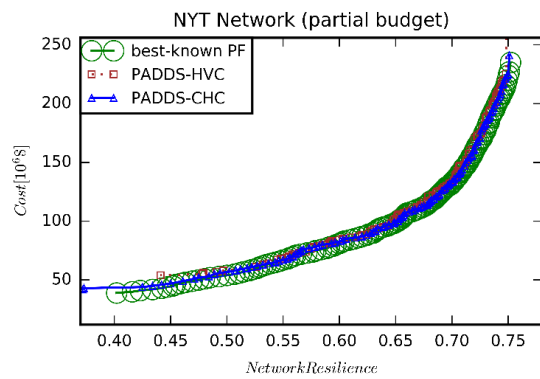
(c*)



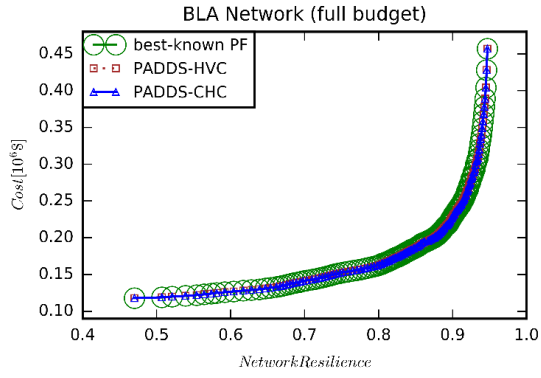
(d)



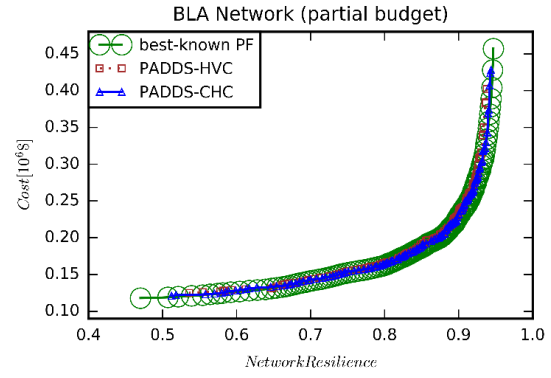
(d*)



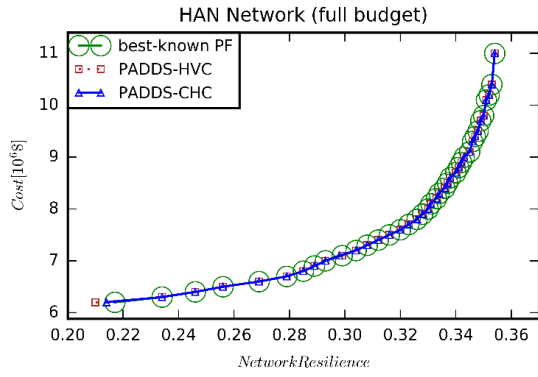
(e)



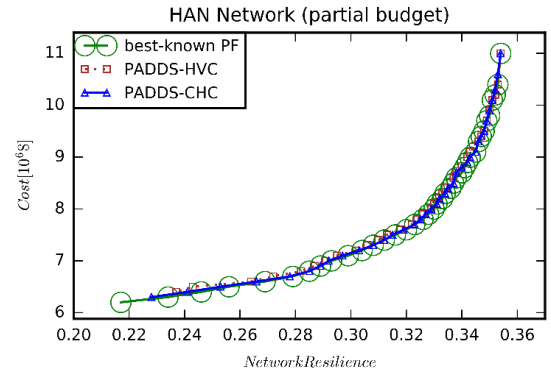
(e*)



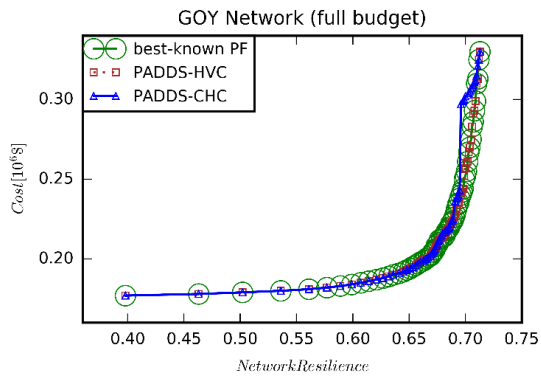
(f)



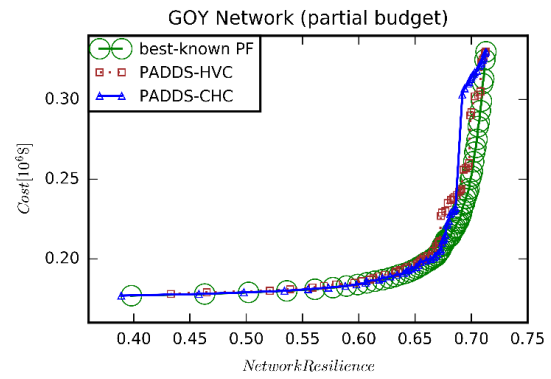
(f*)



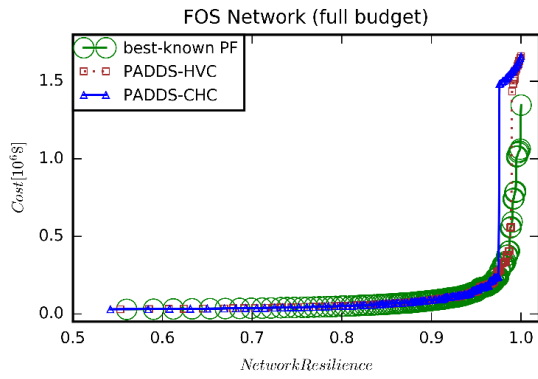
(g)



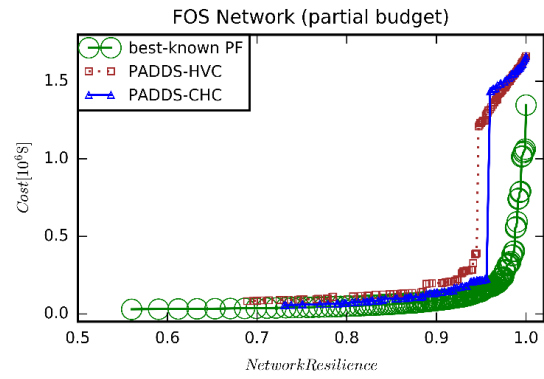
(g*)



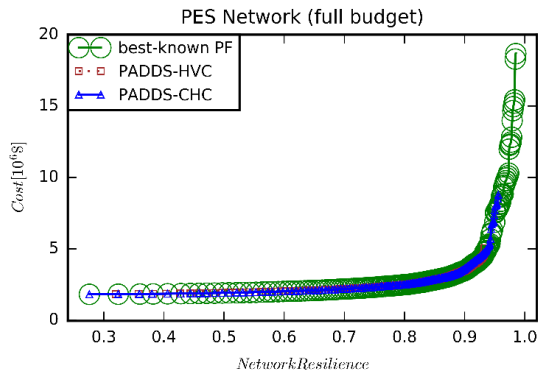
(h)



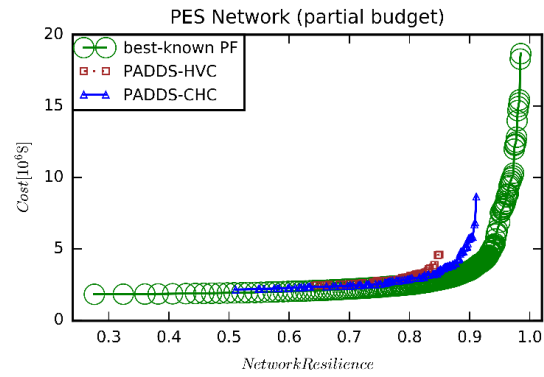
(h*)



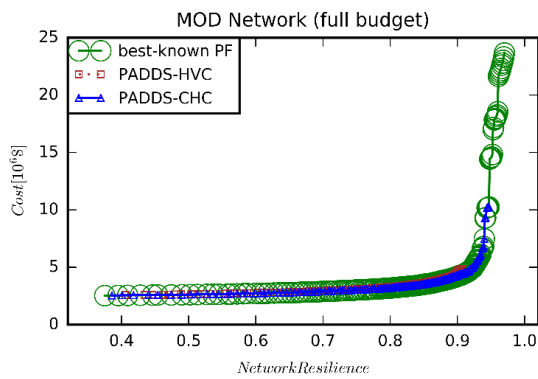
(i)



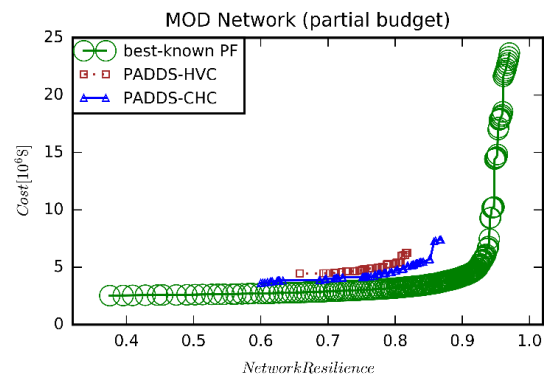
(i*)



(j)

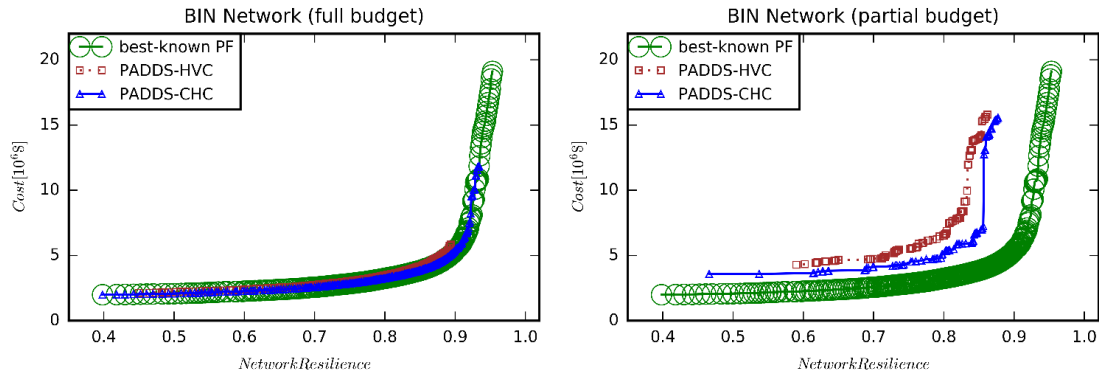


(j*)



(k*)

(k)



(I)

(I*)

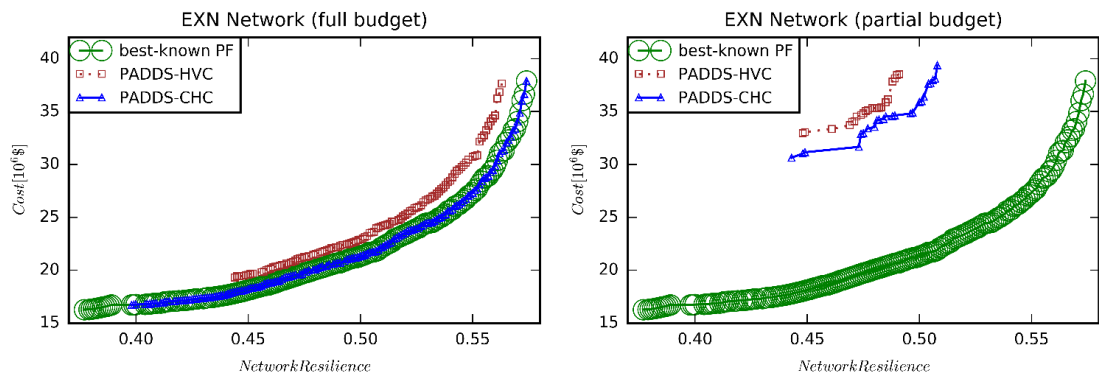


Figure 6-4 compares the PADDs results at both budgets in terms of the empirical cumulative distribution functions (CDFs) of 1-NHV, where NHV metrics are computed according to Deb (2001). NHV values were calculated for all optimization trials taking into account their corresponding best-known PFs as reference fronts. The 1-NHV (the less the better) was used to make CDF graphs easier to read and facilitate visual comparison of quality metrics. The empirical CDFs show the probability of equal or better 1-NHV value at each level of the 1-NHV performance metric. For example, CDF graph of PADDs-HVC partial budget for network BLA in Figure 6-4(e) shows the probability of 1-NHV to be less or equal to 0.05 in all 30 runs, is 0.42. The same probability, with PADDs-CHC partial budget is found to be 0.85.

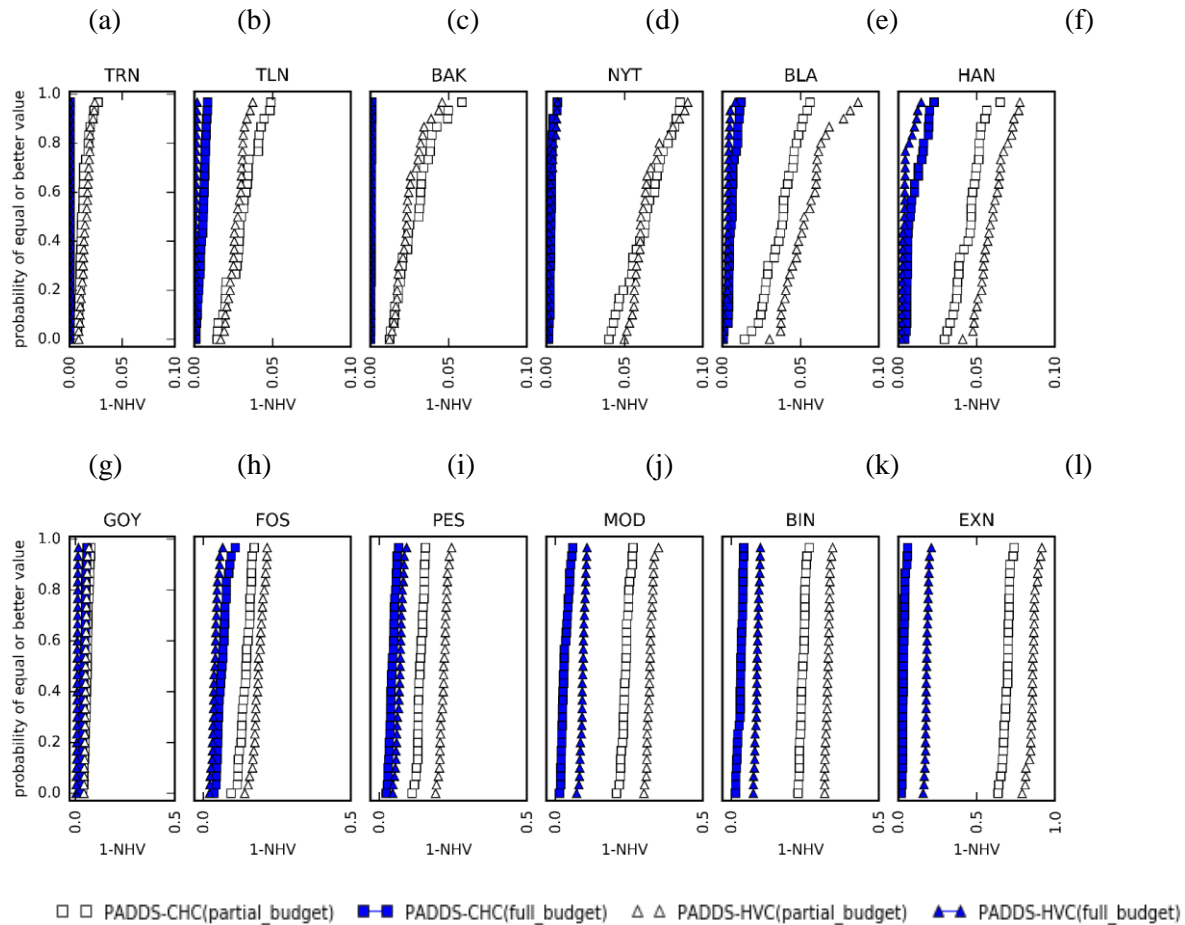


Figure 6-4 Empirical cumulative distribution functions (CDFs) of normalized hypervolume (NHV) metric applied to full budget (see Table 6-1) and partial budget (1/100th the number of solution evaluations as the corresponding full budget). A value of 1-NHV=0 is best.

Results for first six networks in Figure 6-4 (first row of panels, each with the 1-NHV axis ranging from 0 to 0.1) show minimal or small differences in NHV of approximately 0.01 at most for PADDs-CHC and PADDs-HVC at the same budget. Panels (e) and (f) show that despite the small difference, at the limited budget the PADDs-CHC results stochastically dominate the PADDs-HVC results (for any desired level of 1-NHV, PADDs-CHC always has an equal or higher probability of achieving that desired level compared to PADDs-HVC). These low budget algorithmic performance differences (Figure 6-4(e) and (f)) are not apparent when looking at the approximate aggregate PFs in Figure 6-3(e*) and Figure 6-4(f*). For full budget results in the top panel of Figure 6-4, there are even smaller differences between the algorithms. Despite these small differences, the full budget PADDs-HVC results stochastically dominate PADDs-CHC results in three cases (panels (b), (e) and (f)).

Results for last six networks in Figure 6-4 (second row of panels, each with the 1-NHV axis ranging from 0 to 0.5 except for panel (l), which ranges from 0 to 1), show more dramatic differences between the algorithms. For example, at the full budget, PADDs-CHC stochastically dominates PADDs-HVC in four cases (panels (i) through (l)) with differences in NHV of approximately 0.05-0.10 for three of these networks (MOD, BIN, EXN). At partial budgets, the results are even more different with PADDs-CHC stochastically dominating PADDs-HVC in five networks (FOS, PES, MOD, BIN, EXN) with differences in the NHV of closer to 0.10.

Overall, Figure 6-4 results suggests that with full budgets on the nine smallest problems (panels (a) through (i)), PADDs-HVC and PADDs-CHC tend to have very small performance differences in NHV with PADDs-HVC having perhaps a very slight edge over PADDs-CHC. However, PADDs-CHC is clearly preferred over PADDs-HVC at the full budget on the three largest networks (panels (j), (k) and (l)). PADDs-CHC is clearly preferred over PADDs-HVC at the limited budget as the algorithms produce similar quality NHVs in five cases but PADDs-CHC stochastically dominates PADDs-HVC in seven cases. This observation is consistent with the conclusion by Asadzadeh et al. (2014) where they observe that the improvement in PADDs performance with the CHC selection metric is most apparent when the computational budget is fairly limited.

6.4.4 Effective Archive Size Comparison

To better understand the dynamic nature of the effective archive size (EAS) in the PADDs implementations, results of a randomly selected partial budget optimization trial of the BIN network are evaluated closely in Figure 6-5. The selection probability of archived solutions after three arbitrarily selected number of iterations of the runs were extracted and plotted in Figure 6-5(a) where the x-axis is an arbitrary solution number assigned to the solutions in the PADDs archive. Results show that in all three sampled iterations, CHC assigned significant values of selection probabilities to only few of archived solutions; whereas, a relatively big portion of solutions had significant values of selection probabilities by HVC.

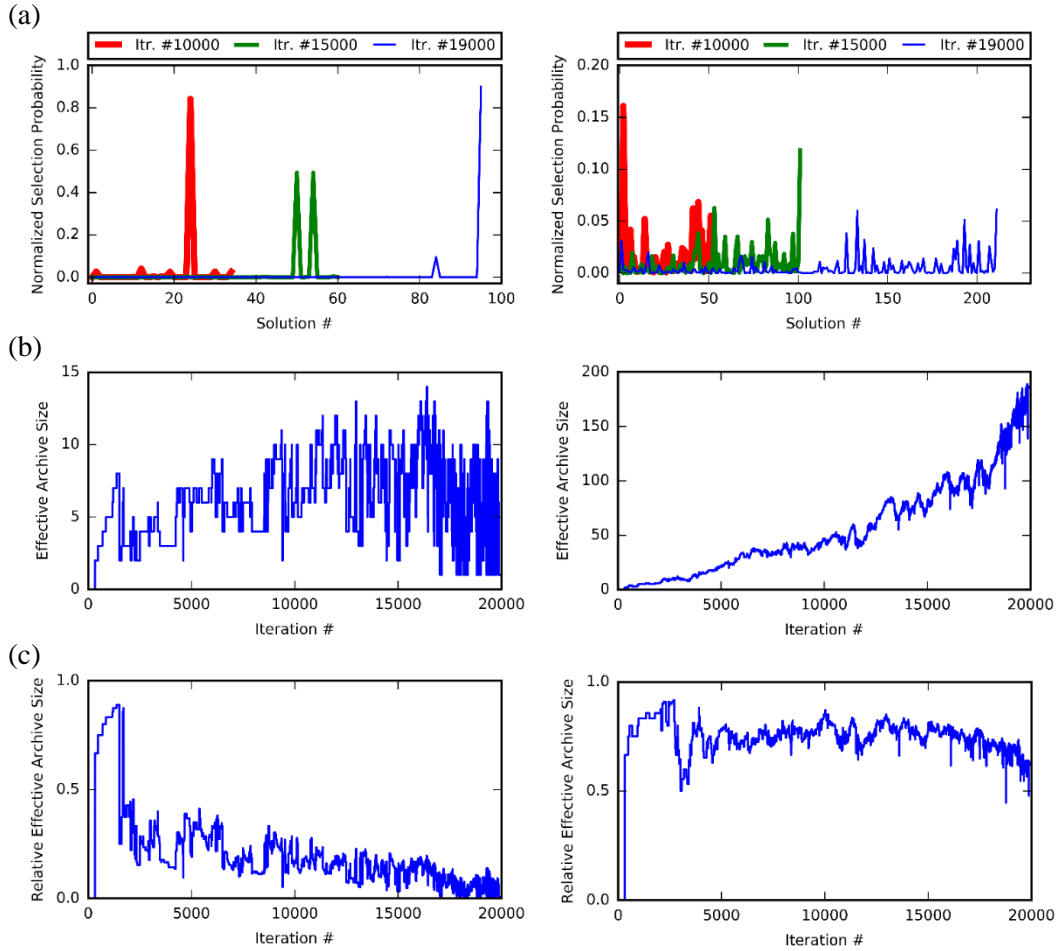


Figure 6-5 Selection probabilities, effective archive size, and relative effective archive size comparison for CHC (left column) and HVC (right column), obtained from partial budget optimization results for BIN network problem

EAS values were recorded for each iteration in the selected 20,000 NSE partial budget PADDs-CHC and PADDs-HVC optimization trial for the BIN network (Figure 6-5(b)). EAS of PADDs-CHC is stable around 5-10 solutions while the EAS of PADDs-HVC is growing steadily and reaches nearly 200 solutions. The PADDs-CHC results reflect the CHC strategy to assign a zero selection probability to non-convex solutions. It is impossible that HVC assigns selection probability of zero to any solutions in a nondominated archive of PADDs.

Figure 6-5(c) shows that the relative EAS values of archived solutions generated by PADDs-CHC are decreasing through iterations and generally have a smaller value compared to results from PADDs-HVC. This means that for a PADDs-CHC trial, the total archive size can increase while the EAS during the whole search process is limited in size and relatively stable.

To fully compare the PADDs EAS values across all problems, the PADDs archives for the full and partial budget optimization trials were recorded every 50 algorithm iterations and post-processed to generate the EAS values reported in Table 6-3. Every recorded archive snapshot was processed to compute the EAS. Then, for a given optimization trial, the maximum EAS across all the archive snapshots was computed. Finally, the maximum EAS values are averaged across the 30 optimization trials and these averages of the maximum EAS values are presented in Table 6-3. Overall, the CHC average maximum EAS values are much smaller than the HVC average maximum EAS values for both budgets (CHC EAS is 20% and 9% the size of the HVC EAS for limited and full budgets, respectively). The full budget CHC EAS value for all networks range from 16 to 73 (with a median of 31). For the largest benchmark network (EXT) the average maximum CHC EAS for the full budget is only 24 solutions yet PADDs-CHC produced the highest quality approximate PF of any of the seven algorithms (see Figure 6-2(l) and Table 6-2).

Table 6-3 Average of the maximum Effective Archive Size (EAS) throughout each of the 30 PADDs-CHC and PADDs-HVC optimization trials.

Network	Partial Budget		Full Budget	
	HVC	CHC	HVC	CHC
TRN	54	14	89	16
TLN	41	14	73	18
BAK	48	11	98	16
NYT	114	18	479	32
BLA	110	20	741	43
HAN	87	17	411	29
GOY	113	16	311	32
FOS	129	16	567	21
PES	84	15	1441	73
MOD	78	14	789	47
BIN	142	15	1452	43
EXN	32	10	493	24

Overall, compared with six other algorithms, PADDs-CHC identifies the highest percentage of the best known PF solutions in seven (TRN, TLN, BAK, NYT, MOD, BIN, EXE) of the 12 benchmark problems despite having maximum average EAS values ranging from only 16 to 47 in Table 6-3. To be clear, these results show that PADDs-CHC is generating candidate solutions by sampling from (and then randomly perturbing) a set of 16 to 47 solutions. In other words, for PADDs-CHC a sufficient level of solution diversity is maintained by using only 16 to 47 nondominated solutions. While the EAS values for the

algorithms in Wang et al. (2015) are not available for direct comparison, it is informative to note that Wang et al. (2015) report that for the three largest problems (MOD, BIN, EXN), population sizes of 400 and 800 produced the best results for AMALGAM, NSGA-II and epsilon MOEA. Furthermore, their BORG and epsilon NSGA-II implementation allowed for a maximum population size of 10,000 solutions. As such, these five MOEAs generated new candidate solutions (in the next generation) by first sampling for parent solutions out of a pool of 400 to 10,000 solutions. Presumably, Wang et al. (2015) used these large population sizes to maintain adequate solution diversity in the MOEAs they applied.

6.5 Conclusion

The twelve benchmark biobjective WDS design problems from Wang et al. (2015) were solved again here using PADDs with CHC as the selection metric (PADDs-CHC) and PADDs with HVC as the selection metric (PADDs-HVC). PADDs algorithms identified new nondominated solutions for all benchmark problems, excluding the first three problems, for which the true PFs are known from Wang et al. (2015). Consequently, the previously best-known PFs were augmented with these new PADDs solutions in order to produce an updated set of best-known PFs.

Compared with the results of the five MOEAs (AMALGAM, Borg, NSGA-II, epsilon-MOEA, and epsilon-NSGA-II) from Wang et al. (2015), PADDs-CHC and/or PADDs-HVC equals or outperforms all of these algorithms in terms in 11 of 12 benchmark problems in terms of the percentage of best-known PF solutions contributed by each algorithm. These contribution percentage differences are highest in the largest problems (biggest solution space). For example, in the four largest networks, the raw differences in these contribution percentages (computed as best PADDs – best MOEA) are 33%, 19%, 76% and 12% for the PES, MOD, BIN and EXN network problems, respectively. PADDs results are achieved under the recommended default algorithm parameter setting for the single algorithm parameter in PADDs (perturbation size parameter = 0.2). PADDs should therefore be considered a leading state-of-the-art MOO algorithm for WDS design.

Given the predominantly convex nature of the best-known PFs from Wang et al. (2015), the 12 benchmark problems were utilized in the first comprehensive comparison between the HVC and CHC selection metrics in PADDs on WDS design optimization problems. CHC was originally designed by Asadzadeh et al. (2014) for convex problems specifically and our results here confirm the efficacy of CHC on these benchmark WDS problems. PADDs-CHC completely outperforms PADDs-HVC in the three largest network problems with the largest differences on the limited budget. When computational budgets are limited to only 6,000 to 20,000 solution evaluations ($1/100^{\text{th}}$ of the full budget solution evaluations),

PADDS-CHC is clearly preferred over PADDS-HVC in terms of the NHV performance metric as the algorithms produce very similar quality results in five problems but PADDS-CHC NHV results stochastically dominate PADDS-HVC NHV results in seven problems. Even in the problems where PADDS-HVC contributed significantly more solutions to the best-known PF than PADDS-CHC (see results for BLA, HAN, GOY and PES in

Table 6-2), PADDS-CHC outperformed all five MOEAs from Wang et al. (2015) in three problems and outperformed four of five of these MOEAs in the other problem.

The success of PADDS-CHC on these problems is achieved with the algorithm searching from a surprisingly small effective archive size (EAS). The full budget EAS of PADDS-CHC grows to an average maximum value of between 16 and 73 (with a median of 31) across the 12 benchmarks. For the largest benchmark network (EXN) the average maximum EAS for the full budget is only 24 solutions for PADDS-CHC yet PADDS-CHC produced the highest quality approximate PF of any of the seven algorithms. In contrast, the PADDS-HVC average maximum EAS values are an order of magnitude larger. PADDS-CHC success is achieved despite maintaining solution diversity using only 16 to 73 solutions. While the PADDS-CHC nondominated archive is generally larger than the aforementioned CHC EAS values, the nondominated solutions that do not define the convex hull of the nondominated points (i.e., solutions on the non-convex portions of the PF) are all assigned a selection probability of zero and hence do not function to guide the search in any way.

Chapter 7

Sensor Placement

7.1 Summary

This chapter presents a step-by-step demonstration of the application of a proposed sensor placement methodology on two (one medium and one large size) distribution network models, taken from the literature. The optimization is accomplished by application of PADDs-CHC which was explained, configured, and verified in the previous chapter. The objective functions under consideration are minimizing the network-level false positive and false negative ratios. To reduce the decision space and thus computational burden of the optimization search, three criteria (practicality, proximity, and justifiability) are introduced in this chapter so as to reduce the number of candidate sensor locations considered as decision variables in the PADDs-CHC algorithm. Sets of non-dominated sensor fleet configurations are obtained as the results of the optimization. Finally, the variation of objective functions with respect to the number of sensors are investigated.

7.2 Introduction

Chapter 5 identified options for determining reasonable detection test parameters (values of single sensor significance level, number of nights to collect in the sample and the times each night samples are taken). Given such parameters are fixed, the next step in sensor network design requires optimum placement of the sensors in the network. A stochastic multi-objective optimization framework is introduced to optimally place a fleet of pressure sensors to minimize both false positives and false negatives simultaneously. The sensor placement optimization problem is then solved to obtain an approximation of the Pareto-front of optimal sensor fleet locations.

Numerous studies used single objective optimization methods to optimally place sensors in networks for the best leak diagnosis performance. Three main streams of research in the field are (Pérez et al. 2009; Pérez et al. 2011) and (Casillas et al. 2013b; Casillas, Garza-Castañón, PuigVargas-Martinez 2015; Casillas et al. 2015; Ponce et al. 2014) and (B. Farley et al. 2008; B. Farley et al. 2012). Bonada et al. (2014) reviewed studies that explicitly used hydraulic model-based diagnosis approaches. Their work presents a detailed study on the structure of the objective functions used in sensor placement optimization problems in the literature and they recommended consideration of more than one objective to optimally

place sensors for leak diagnosis purposes. Bonada et al. (2014) warn that the main disadvantage of a multiobjective framework would be the additional computational burden.

Although not totally absent in the literature, very few multiobjective algorithms have been applied to sensor placement in the context of leak diagnosis. Preis et al. (2011) used NSGA-II to optimize placement of hydraulic and water quality sensors conjunctively. Objectives in their work are maximizing contaminant event sensor detection likelihood and sensor hydraulic sensitivity to variations in nodal demands. Their bigger case study consists of one constant head source, two pumping stations, two elevated storage tanks, 170 pipes, and 129 nodes.

These objective functions are, ideally, to be minimized by the optimum set of decision variables (solution). A solution is represented as a vector of binary variables each corresponding to a candidate node; 1 and 0 refer to placing a sensor or not placing a sensor on that node, respectively.

Each node in the network is a candidate for placing a sensor on. The search space will be of the size of 2^M , where M is the number of nodes in a network, which can quickly grow into a vast search space in any real-world network. Therefore, instead of enumeration of all possible solutions, stochastic multiobjective optimization techniques need to be used to solve the problem. These methods are gradient-free and instead rely on information obtained only from the evaluation of the objective functions. This creates a computational burden that needs to be addressed accordingly. This is a crucial consideration in order to make the implementation of the proposed methodology in the real-world applications practically achievable. The time required to perform a single evaluation of objective functions effectively dominates the minimal computational time spent on other parts of the optimization process. Therefore, a solver needs to be able to approach to the true Pareto-front of the problem in as few iterations as possible so that the operation is conducted in a reasonable time length.

In the case of Net3 network, every evaluation of objective functions, which calculates false positive and false negative ratios for a candidate sensor fleet, takes around 2 seconds¹. The only way to be able to solve the optimization problem despite the slow evaluation time of the objective function and large decision space is to develop, configure and implement the most efficient multiobjective solver. The study in Chapter 6 showed that PADDs-CHC is a promising choice among other solvers. In this chapter, this algorithm is employed to solve the sensor placement optimization problems for the two case studies.

¹ Processor: Intel Core i7 running at 5.0 GHz

7.3 Sensor Placement Optimization Problem

Eq. (7-1) shows the formulation of the multiobjective optimization problem of sensor placement.

$$\begin{aligned} \text{Minimize: } \mathbf{F}(\mathbf{sf}) &= [\varphi_{\mathbf{sf}}(\Delta T, S, \alpha, \mathbf{sf}, \mathbf{X}), \omega_{\mathbf{sf}}(\Delta T, S, \alpha, \mathbf{sf}, \mathbf{X})] \\ \text{subject to: } \mathbf{sf} &\subseteq \mathbf{M}'' \end{aligned} \quad (7-1)$$

where \mathbf{F} is the vector of objective functions, α is the level of significance, \mathbf{X} is the prearranged detection experiment results database, \mathbf{sf} is the sensor fleet, and \mathbf{M}'' is a reduced subset of all network nodes (\mathbf{M}) where installing a node adheres to below regulations.

- Practicality
- Proximity
- Justifiability

Candidate locations for installing a sensor are limited to \mathbf{M}'' which is a subset of network nodes \mathbf{M} , in order to incorporate three main considerations which are explained below.

7.3.1 Practicality

There are nodes in every network that, for whatever technical reason or field condition, it might be impossible to install sensors on them. For practical considerations, these nodes are excluded from the list of candidates.

7.3.2 Proximity

Nodes that are right beside storage units (i.e., tanks and reservoirs) are not suitable locations for pressure sensors because they are influenced largely (often only) by the hydraulic head imposed by the tank or reservoir. Therefore, their pressure is influenced neither by demand fluctuations nor by leaks. These nodes are removed from the options for sensor placement.

By implementing the practicality and proximity considerations, \mathbf{M}' , as a subset of \mathbf{M} is obtained.

7.3.3 Justifiability

A metric is defined to identify the degree to which a node, as a candidate location for a sensor, is unfitting for a pressure sensor. This metric is then used to remove a certain number of nodes that rank the

highest (worst) from \mathbf{M}' and thus produce \mathbf{M}'' . The proposed metric is termed as the dominance order and is noted by θ . Let us define the domination per below. It is said that node A dominates node B if:

$$\begin{aligned} \varphi (\Delta T, S, \alpha, \mathbf{sf} = [A], \mathbf{X}) &< \varphi (\Delta T, S, \alpha, \mathbf{sf} = [B], \mathbf{X}) \\ &\text{and} \\ \frac{\sum_{j \in \mathbf{M}'} \omega (\Delta T, S, \alpha, \mathbf{sf} = [A], \mathbf{X}(\mathbf{m} = [j]))}{\text{size of } \mathbf{M}'} &< \frac{\sum_{j \in \mathbf{M}'} \omega (\Delta T, S, \alpha, \mathbf{sf} = [B], \mathbf{X}(\mathbf{m} = [j]))}{\text{size of } \mathbf{M}'} \end{aligned} \quad (7-2)$$

Based on the above definition, $\theta(i)$, is defined as the number of nodes in \mathbf{M}' that dominate node i . When node A dominates node B , it means a sensor installed on node A , in comparison with B , has a smaller (better) false positive and average false negative values in response to leaks on each and every node in \mathbf{M}' . This implies that node A is a better choice compared to node B under conditions of experiment \mathbf{X} because both false positive and false negative ratios in average improve in response to leaks in every node in \mathbf{M}' .

If node A has a high domination order (θ), it means that under the condition of the arranged detection experiment results database, there are many other nodes in the network that produce more preferable false positive and false negative ratios (in average) to node A , given the same leak size.

\mathbf{M}'' is obtained by removing a certain number of nodes from \mathbf{M}' with the worst domination order ranks.

7.4 Case Study Net3

As the last step of the test design, the sensor placement problem is solved as an optimization problem (Eq. (7-3)) using PADDs-CHC.

$$\begin{aligned} \text{Minimize: } F(\mathbf{sf}) &= [\varphi_{sf} (\Delta T, S, \alpha, \mathbf{sf}, \mathbf{X1}), \omega_{sf}^{m=M} (\Delta T, S, \alpha, \mathbf{sf}, \mathbf{X1})] \\ &\text{subject to: } \mathbf{sf} \subseteq \mathbf{M}'' \end{aligned} \quad (7-3)$$

Where $\Delta T = 1, S = 9$, and $M = [1: 91]$. The problem will be solved separately for two level of significances $\alpha = 0.01$, and $\alpha = 0.1$. \mathbf{M}'' is obtained from \mathbf{M} in the following.

7.4.1 Practicality and Proximity

Nodes 1 to 8 in Net3 are right beside reservoirs and tanks. There is no available knowledge about practical obligations/considerations for this network. Therefore:

$$M' = [9: 91] \tag{7-4}$$

7.4.2 Justifiability

Domination order was calculated for the detection experiment results database **X1** while considering $\Delta T = 1, S = 9$ (from the previous section) under $\alpha = 0.01$ and $\alpha = 0.1$. Figure 7-1 shows the average false positive and false negative ratios for all the nodes in M' under $\alpha = 0.01$. Domination order for each node is then obtained by enumerating the dominating nodes. Nodes with $\theta = 0$ are highlighted with triangle markers in the plot. These are nodes that are not dominated by any other node in M' . Other nodes have domination orders larger than zero meaning that they are, at least, dominated by one other node. In the worse case, there are nodes with $\theta = 71$.

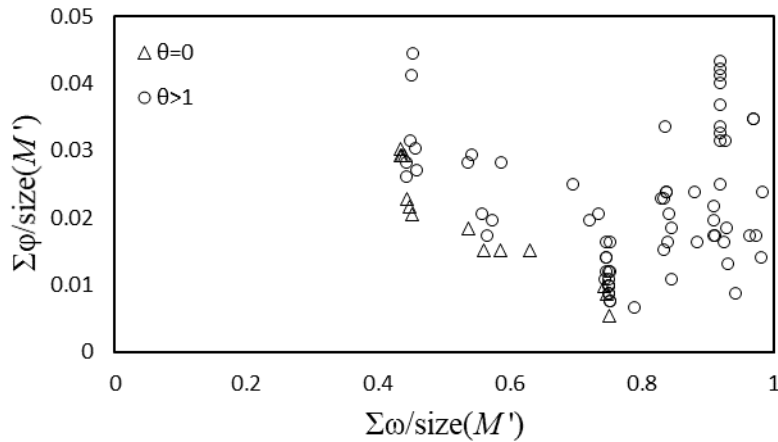


Figure 7-1. Average false positive and false negative ratios for all the nodes (Net3)

For the case of $\alpha = 0.01$, all the nodes with domination order larger than zero are discarded from candidate locations of sensor placement which leaves it the below 14 nodes:

$$M'' = 45, 46, 47, 48, 49, 50, 55, 57, 66, 68, 69, 73, 74, 85 \tag{7-5}$$

For the case of $\alpha = 0.1$, similar evaluations were performed. To keep the consistency with the $\alpha = 0.01$ case, 14 nodes with the lowest (best) domination order were selected in this case as well. Those nodes, for which θ is at most 3, are listed below:

$$M'' = 43, 45, 46, 47, 60, 68, 44, 48, 78, 57, 72, 76, 82, 27 \tag{7-6}$$

M'' is the list of nodes that are used as candidate sensor locations in the sensor placement optimization procedure.

7.4.3 Optimization Results

Following the best optimization practice obtained from Chapter 6, PADDs was configured with selection metric CHC and set up to solve the sensor placement problem. A budget of 4000 evaluations of objective functions was used. The optimization process took about 6 days of serial computing time in total. Results for $\alpha = 0.01$ and $\alpha = 0.1$ are presented in Table 7-1 and Table 7-2, respectively. Final Pareto-fronts are shown in Figure 7-2.

Table 7-1. Best-found Pareto front for sensor placement optimization problem of Net3 with $\alpha = 0.01$ (Net3)

Sol #	Nodes														ω	φ	# of Sensors
	45	46	47	48	49	50	55	57	66	68	69	73	74	85			
1	1	1	1	1	0	0	1	0	0	0	0	0	1	1	0.27	0.12	7
2	1	0	1	1	0	0	1	0	0	0	0	0	0	1	0.27	0.10	5
3	1	1	1	0	0	0	1	0	0	0	0	0	0	1	0.27	0.09	5
4	0	0	1	1	1	0	1	0	0	0	0	0	0	1	0.27	0.08	5
5	1	0	1	0	0	0	1	0	0	0	0	0	0	1	0.28	0.08	4
6	0	0	1	0	1	0	1	0	0	0	0	0	0	1	0.28	0.07	4
7	1	0	1	0	0	1	0	0	0	0	0	0	0	1	0.28	0.06	4
8	0	0	1	0	0	0	1	0	0	0	0	0	0	1	0.28	0.06	3
9	0	0	1	0	0	1	0	0	0	0	0	0	0	1	0.29	0.05	3
10	0	0	1	0	1	0	0	0	0	0	0	0	0	1	0.29	0.05	3
11	0	0	1	0	0	0	0	0	1	0	0	0	0	1	0.31	0.04	3
12	0	0	1	0	0	0	0	0	0	0	0	0	0	1	0.31	0.04	2
13	0	0	0	0	1	0	0	0	0	0	0	0	0	1	0.43	0.03	2
14	0	0	1	0	0	0	0	0	1	0	0	0	0	0	0.47	0.03	2
15	0	1	0	0	0	0	0	0	0	0	0	0	0	0	0.47	0.03	1
16	0	0	1	0	0	0	0	0	0	0	0	0	0	0	0.47	0.02	1
17	0	0	0	0	1	0	0	0	0	0	0	0	0	0	0.58	0.02	1
18	0	0	0	0	0	0	0	0	1	0	0	0	0	0	0.75	0.01	1
19	0	0	0	0	0	0	0	0	0	0	0	0	0	0	1.00	0.00	0

Table 7-2. Best-found Pareto front for sensor placement optimization problem of Net3 with $\alpha = 0.1$ (Net3)

Sol #	Nodes														ω	φ	# of Sensors
	43	45	46	47	60	68	44	48	78	57	72	76	82	27			
1	1	1	1	1	0	0	1	0	0	0	0	0	1	1	0.26	0.53	6
2	1	0	1	1	0	0	1	0	0	0	0	0	0	1	0.26	0.50	6
3	1	1	1	0	0	0	1	0	0	0	0	0	0	1	0.26	0.50	5
4	0	0	1	1	1	0	1	0	0	0	0	0	0	1	0.26	0.47	5
5	1	0	1	0	0	0	1	0	0	0	0	0	0	1	0.27	0.46	4
6	0	0	1	0	1	0	1	0	0	0	0	0	0	1	0.27	0.44	4
7	1	0	1	0	0	1	0	0	0	0	0	0	0	1	0.27	0.40	4
8	0	0	1	0	0	0	1	0	0	0	0	0	0	1	0.27	0.39	3
9	0	0	1	0	0	1	0	0	0	0	0	0	0	1	0.28	0.38	3
10	0	0	1	0	1	0	0	0	0	0	0	0	0	1	0.28	0.38	3
11	0	0	1	0	0	0	0	0	1	0	0	0	0	1	0.29	0.36	3
12	0	0	1	0	0	0	0	0	0	0	0	0	0	1	0.34	0.29	2
13	0	0	0	0	1	0	0	0	0	0	0	0	0	1	0.34	0.26	3
14	0	0	1	0	0	0	0	0	1	0	0	0	0	0	0.34	0.25	2
15	0	1	0	0	0	0	0	0	0	0	0	0	0	0	0.35	0.24	2
16	0	0	1	0	0	0	0	0	0	0	0	0	0	0	0.35	0.23	2
17	0	0	0	0	1	0	0	0	0	0	0	0	0	0	0.41	0.22	2
18	0	0	0	0	0	0	0	0	1	0	0	0	0	0	0.41	0.16	1
19	0	0	0	0	0	0	0	0	0	0	0	0	0	0	0.49	0.12	1
20	0	0	0	0	0	1	0	0	0	0	0	0	0	0	0.75	0.12	1
21	0	0	0	0	0	0	0	0	0	0	0	0	0	0	1.00	0.00	0

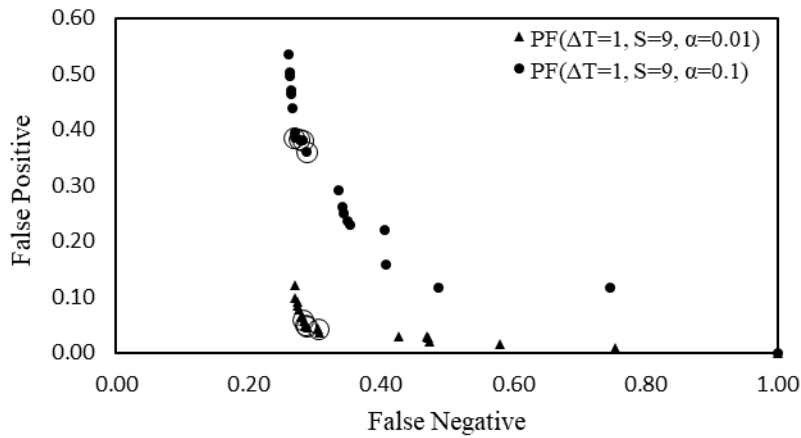


Figure 7-2. Best-found Pareto fronts for sensor placement optimization problem of Net3

Figure 7-2 shows Pareto fronts found using $\Delta T = 1, S = 9, \alpha = 0.01$ and $\Delta T = 1, S = 9, \alpha = 0.1$ denoted simply as $PF(\Delta T = 1, S = 9, \alpha = 0.01)$ and $PF(\Delta T = 1, S = 9, \alpha = 0.1)$ respectively henceforth.

It can be seen from Figure 7-2 that both $PF(\Delta T = 1, S = 9, \alpha = 0.01)$ and $PF(\Delta T = 1, S = 9, \alpha = 0.1)$ present more or less convex trade-offs between false positive and false negative ratios. In both cases, it can be seen that as the false negative decreases from its maximum value of 1.0, the false positive increases from 0.0 gradually and later exponentially terminating when the minimum value of false negative is reached. The minimum false negative values in both $PF(\Delta T = 1, S = 9, \alpha = 0.01)$ and $PF(\Delta T = 1, S = 9, \alpha = 0.1)$ are around the same magnitude; both of which correspond to sensor configurations with 7 and 6 sensors, respectively.

Compared to $PF(\Delta T = 1, S = 9, \alpha = 0.01)$, $PF(\Delta T = 1, S = 9, \alpha = 0.1)$ covers a wider range in the $\varphi - \omega$ space. However, solutions in $PF(\Delta T = 1, S = 9, \alpha = 0.01)$ dominate the majority of $PF(\Delta T = 1, S = 9, \alpha = 0.1)$ solutions and produce a much larger normalized hypervolume (see Chapter 6). This suggests, should the level of significance count as a decision parameter, smaller values of α are more promising. This is because dominating sensor placement designs would be generated with having $\alpha = 0.01$ rather than $\alpha = 0.1$.

Results from Table 7-1 and Table 7-2 show that both $PF(\Delta T = 1, S = 9, \alpha = 0.1)$ and $PF(\Delta T = 1, S = 9, \alpha = 0.01)$ share a mutual design solution which is having no sensor at all. This solution, although it is not a practically acceptable answer to the problem, serves as a verification for PADDs-CHC showing that the algorithm, in both cases, has probed at least one of the extreme ends of the search space (i.e., sensors everywhere and no sensor at all). Corresponding objective function values of the no-sensor solution shows a false positive ratio of zero and false negative equal to one. This matches with the logical inference that in absence of any sensor, all actual leaks will be missed ($\omega = 1$) and no sudo-leak scenario is mistaken as a leak scenario ($\varphi = 0$).

Variation of a false negative in response to increment in the number of sensors is plotted in Figure 7-3.

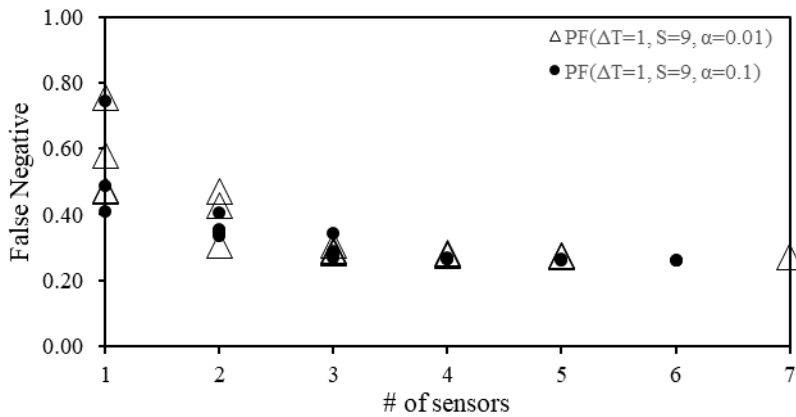


Figure 7-3. False negative variation with the number of sensors in Net3

A notable negative correlation between the number of sensors and false negative exists for solutions in both $PF(\Delta T = 1, S = 9, \alpha = 0.01)$ and $PF(\Delta T = 1, S = 9, \alpha = 0.1)$. This observation logically makes sense because the more sensors in the network, a lower (better) false negative is expected. This observation is particularly interesting because it shows that by having minimized the false negative ratio (as one of the objective functions), number of sensors, which is a proxy of the design cost, is being implicitly minimized as well. This means that the proposed two-objective optimization framework in fact implicitly is considering a proxy of cost, eliminating the need for a third objective to represent cost.

Should a decision maker pick a solution from each of $PF(\Delta T = 1, S = 9, \alpha = 0.01)$ or $PF(\Delta T = 1, S = 9, \alpha = 0.1)$ as for the final design of the sensor fleet, Figure 7-3 can be of great use. It can be seen that false negative shows a significant decrease (improvement) by adding the 1st, 2nd, and 3rd sensors; however, it does not show a perhaps “worthy” decrease by adding the 4th sensor, in both $PF(\Delta T = 1, S = 9, \alpha = 0.1)$ and $PF(\Delta T = 1, S = 9, \alpha = 0.01)$. Therefore, for this specific network, design solutions that correspond to three sensors are preferable to the others. These solutions are circled with black color on both $PF(\Delta T = 1, S = 9, \alpha = 0.1)$ and $PF(\Delta T = 1, S = 9, \alpha = 0.01)$ in Figure 7-3. However, choosing a solution among the Pareto front is a completely subjective decision and a decision maker’s judgment will be based on greater interpretation based on field facts and other practical consideration.

7.5 Case Study C-Town

Similar to the case of Net3, the sensor placement problem is solved as an optimization problem (Eq. (7-7)) using PADDs-CHC.

$$\begin{aligned} \text{Minimize: } F(sf) &= [\varphi_{sf}(\Delta T, S, \alpha, sf, X2), \omega_{sf}^{m=M}(\Delta T, S, \alpha, sf, X2)] \\ \text{subject to: } sf &\subseteq M'' \end{aligned} \tag{7-7}$$

Where $\Delta T = 1, S = 9, M = [1: 91]$ and $\alpha = 0.01$.

7.5.1 Practicality and Proximity

Due to the computational limitations and also to keep the consistency with Net3 case-study, only 91 (out of 388) nodes of C-Town were considered for calculation of false positive and false negative ratios and eventually sensor placement. These 91 nodes are randomly chosen and are made sure to adhere to the proximity criterion (not to be adjacent to a storage element). No information regarding the practical consideration in sensor placement in this network is available.

7.5.2 Justifiability

Domination order was calculated for the experiment **X2** while considering $\Delta T = 1, S = 9$ and $\alpha = 0.01$. A total of 13 nodes (out of 91) with domination orders less than 2 were selected:

$$M'' = 8, 9, 30, 45, 46, 64, 71, 72, 79, 66, 76, 78, 81 \tag{7-8}$$

7.5.3 Optimization Results

PADDs was implemented to solve the sensor placement problem. Based on the best optimization practice from Chapter 6, CHC was employed as the selection metric for the optimization algorithm. A budget of 1000 evaluation of objective functions, during around one day, was used. First, only the case of $\alpha = 0.01$ was considered in this trial. The final Pareto-front is described in Table 7-3 and plotted in Figure 7-4.

Table 7-3. Best-found Pareto front solutions for sensor placement optimization problem of C-Town network based on $\Delta T = 1, S = 9, \alpha = 0.01$.

Solution #	Nodes													ω	φ	# of Sensors
	8	9	30	45	46	64	71	72	79	66	76	78	81			
1	1	1	1	1	1	1	1	1	1	1	1	1	1	0.001	1.000	13
2	0	0	1	1	1	1	0	1	1	0	1	1	1	0.004	0.985	9
3	0	1	1	0	0	1	0	0	1	0	0	1	0	0.007	0.977	5
4	0	1	1	0	0	1	0	0	1	0	0	0	0	0.021	0.970	4
5	0	0	1	0	0	1	0	0	1	0	0	0	0	0.021	0.955	3
6	0	0	0	0	0	1	0	0	1	0	0	1	0	0.034	0.947	3
7	0	0	0	0	0	0	0	0	1	0	0	1	0	0.069	0.932	2
8	0	0	0	0	1	0	0	0	0	0	0	0	0	0.779	0.737	1
9	0	0	0	0	0	0	0	0	0	0	0	0	0	1.000	0.000	0

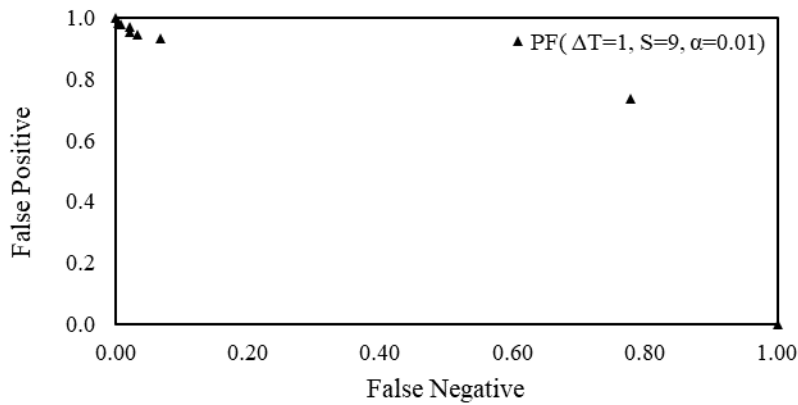


Figure 7-4. Best-found Pareto fronts in objective space for sensor placement optimization problem of C-Town with $\Delta T = 1, S = 9, \alpha = 0.01$

Figure 7-4 shows that the Pareto front found using $\Delta T = 1, S = 9$, and $\alpha = 0.01$, denoted simply as $PF(\Delta T = 1, S = 9, \alpha = 0.01)$ henceforth, for C-Town is concentrated on the left-top corner. All the solutions on the front have a high false positive and most of them have a small (desirable) false negative values. Once again, the no-sensor solution was obtained by PADDs-CHC. Unlike the case of Net3, the other extreme solution which is sensors everywhere, is among the final non-dominated set of solutions. This solution, which was a dominated solution in Net3, has a very small false negative and presents a false positive of 1.0. Meaning by having sensors on all the 91 nodes, almost all the leak scenarios are detected but also all the no-leak scenarios are asserted as leak scenarios.

Variation of false negative with respect to the number of sensors is plotted in Figure 7-5 for the Pareto front solutions $PF(\Delta T = 1, S = 9, \alpha = 0.01)$ from Figure 7-4. Similar to the case of Net3, increasing the number of sensors improves the false negative. It can be seen from Figure 7-5 that the largest drop (improvement) in the false negative ratio is achieved by adding the second sensor. Adding the third sensor does not make a significant improvement. Therefore, while regarding the fact that all solutions on the Pareto-front are non-dominated and thus not essentially better or worse, should a decision maker aims to pick a solution emphasizing the false negative and cost (number of sensors) then the sensor configuration with 2 sensors would be the most justifiable choice. This solution is number 7 in Table 7-3 and suggests placing two sensors on nodes 72 and 76. Note, however, that sensor fleets with an extremely high false positive ratio like $PF(\Delta T = 1, S = 9, \alpha = 0.01)$ (e.g., almost every no-leak scenario is classified as a leak) would be expected to have an exceedingly small false negative ratio as shown in Figure 7-5.

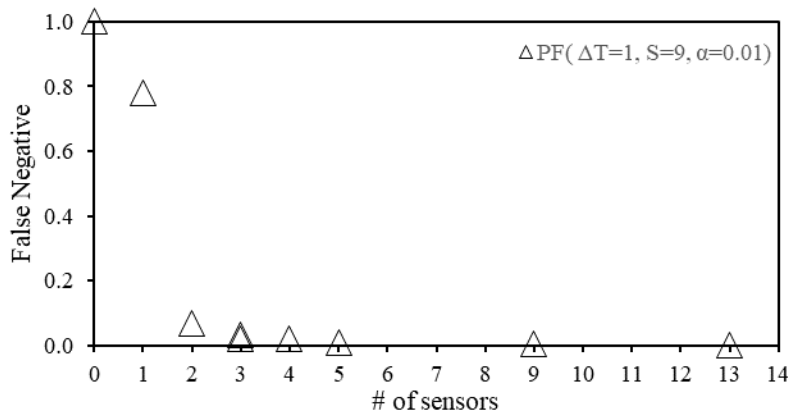


Figure 7-5. False negative variation with the number of sensors in C-Town with $\Delta T = 1, S = 9, \alpha = 0.01$

The high false positive values of $PF(\Delta T = 1, S = 9, \alpha = 0.01)$ are undesirable; therefore, other schedules were examined in the hope of reaching to smaller false positives. An alternative method for choosing ΔT and S was introduced in 5.7.7 which suggests consideration of the $(\Delta T, S)$ pair that yields the most desirable combined system level false positive and false negative. From Figure 5-17, the pair $(\Delta T = 3, S = 5)$ matches this criterion. Next, the sensor placement optimization problem is solved once again for $\Delta T = 3, S = 5$; all other setting are identical to the previous optimization run. Results of this run are presented in Table 7-4 and Figure 7-6. To explore even further, a next trial with $\Delta T = 3, S = 9$ was as well run results of which are presented in Table 7-5 and Figure 7-6.

Table 7-4. Best-found Pareto front for sensor placement optimization problem of C-Town network based on

$$\Delta T = 3, S = 5, \alpha = 0.01$$

Solution #	Nodes														ω	φ	# of Sensors
	8	9	30	45	46	64	71	72	79	66	76	78	81				
1	1	1	1	1	1	1	1	1	1	1	1	1	1	1	0.34	0.43	13
2	1	1	1	1	0	0	1	1	0	1	1	1	1	1	0.34	0.39	10
3	1	1	1	0	0	0	1	1	1	1	1	1	1	1	0.34	0.38	10
4	1	1	1	0	0	0	1	1	0	1	1	1	1	1	0.34	0.36	9
5	1	1	1	0	0	0	1	0	0	1	1	1	1	1	0.35	0.35	8
6	1	1	0	1	0	0	1	1	1	1	1	1	1	1	0.35	0.32	10
7	1	1	0	1	0	0	1	1	0	1	1	1	1	1	0.35	0.30	9
8	1	1	0	0	0	0	1	1	1	1	1	1	1	1	0.35	0.29	9
9	1	1	0	0	0	0	1	1	0	1	1	1	1	1	0.35	0.27	8
10	1	1	0	0	0	0	1	0	0	1	1	1	1	1	0.36	0.25	7
11	1	1	0	0	0	0	1	0	0	1	1	1	0	0	0.37	0.25	6
12	1	1	0	0	0	0	0	0	0	1	1	1	1	1	0.38	0.24	6
13	1	1	0	0	0	0	0	0	0	1	1	1	0	0	0.40	0.23	5
14	0	1	0	0	0	0	1	1	0	1	1	1	1	1	0.40	0.22	7
15	0	1	0	0	0	0	1	0	0	1	1	1	1	1	0.41	0.21	6
16	0	1	0	0	0	0	1	0	0	1	1	1	0	0	0.42	0.20	5
17	0	1	0	1	0	0	1	0	0	0	1	1	0	0	0.42	0.19	5
18	0	1	0	0	0	0	1	0	0	1	1	0	1	0	0.44	0.18	5
19	0	1	0	0	0	0	1	1	0	1	0	1	0	0	0.46	0.18	5
20	0	1	0	0	0	1	1	0	0	0	0	1	0	0	0.46	0.17	4
21	0	1	0	0	0	1	0	1	1	0	0	1	1	1	0.47	0.16	6
22	0	1	0	1	0	0	0	1	0	0	0	1	1	1	0.48	0.15	5
23	0	1	0	0	0	1	0	1	0	0	0	1	1	1	0.48	0.14	5
24	0	1	0	1	0	0	0	0	0	0	0	1	1	1	0.48	0.13	4
25	0	1	0	0	0	1	0	0	0	0	0	1	1	1	0.49	0.12	4
26	0	1	0	0	0	1	0	0	1	0	0	1	0	0	0.51	0.12	4
27	0	1	0	0	0	1	0	1	0	0	0	1	0	0	0.51	0.11	4
28	0	1	0	0	0	1	0	0	0	0	0	1	0	0	0.52	0.09	3
29	0	1	0	0	0	0	0	0	0	0	0	1	1	1	0.59	0.08	3
30	0	1	0	1	0	0	0	0	0	0	0	0	0	0	0.62	0.07	2
31	0	1	0	0	0	0	0	0	0	0	0	1	0	0	0.64	0.05	2
32	0	1	0	0	0	0	0	1	0	0	0	0	0	0	0.77	0.02	2
33	0	1	0	0	0	0	0	0	0	0	0	0	0	0	0.78	0.00	1

Table 7-5. Best-found Pareto front for sensor placement optimization problem of C-Town network based on $\Delta T = 3, S = 9, \alpha = 0.01$

Solution #	Nodes														ω	φ	# of Sensors
	8	9	30	45	46	64	71	72	79	66	76	78	81				
1	1	0	1	1	0	0	1	1	1	1	1	1	1	0.07	0.82	10	
2	1	0	1	1	0	1	1	0	1	1	1	1	1	0.07	0.81	10	
3	1	0	1	0	0	0	1	1	1	1	1	1	1	0.08	0.80	9	
4	1	0	1	0	0	1	1	0	1	1	1	1	1	0.08	0.79	9	
5	1	0	1	1	0	1	1	0	1	1	1	1	0	0.08	0.78	9	
6	1	0	1	1	0	1	1	0	0	1	1	1	0	0.08	0.78	8	
7	1	0	1	0	0	1	1	0	1	1	1	1	0	0.08	0.75	8	
8	1	0	1	0	0	1	1	0	0	1	1	1	0	0.09	0.74	7	
9	1	0	1	0	0	0	1	0	1	1	1	0	0	0.09	0.73	6	
10	1	0	0	0	0	1	1	0	1	0	1	1	0	0.11	0.70	6	
11	1	0	0	0	0	1	1	0	0	0	1	1	0	0.11	0.69	5	
12	1	0	0	0	0	1	1	0	1	0	0	1	0	0.12	0.68	5	
13	1	0	0	0	0	0	1	0	1	1	0	0	0	0.13	0.68	4	
14	1	0	0	0	0	1	0	0	1	1	1	1	0	0.14	0.66	6	
15	1	0	0	0	0	1	0	0	0	1	1	1	0	0.15	0.65	5	
16	1	0	0	0	0	1	0	0	1	0	1	1	0	0.15	0.64	5	
17	1	0	0	0	0	1	0	0	0	0	1	1	0	0.16	0.62	4	
18	1	0	0	0	0	1	0	0	1	1	0	1	0	0.16	0.60	5	
19	1	0	0	0	0	0	0	0	1	1	0	1	0	0.16	0.59	4	
20	1	0	0	0	0	1	0	0	1	0	0	1	0	0.17	0.57	4	
21	1	0	0	0	0	1	0	0	0	0	0	1	0	0.20	0.55	3	
22	1	0	0	0	0	0	0	0	1	0	0	0	0	0.28	0.50	2	
23	0	0	0	0	0	1	0	0	0	0	0	1	0	0.33	0.49	2	
24	1	0	0	0	1	0	0	0	0	0	0	0	0	0.41	0.48	2	
25	1	1	0	0	0	0	0	0	0	0	0	0	0	0.41	0.47	2	
26	0	0	0	0	0	0	0	0	1	0	0	0	0	0.44	0.40	1	
27	0	0	0	0	0	0	0	0	0	0	0	1	0	0.46	0.39	1	
28	0	1	0	0	0	0	0	1	0	0	0	0	0	0.77	0.38	2	
29	0	0	0	0	1	0	0	0	0	0	0	0	0	0.78	0.22	1	
30	0	1	0	0	0	0	0	0	0	0	0	0	0	0.78	0.17	1	
31	0	0	0	0	0	0	0	0	0	0	0	0	0	1.00	0.00	0	
32	1	0	1	1	0	0	1	1	1	1	1	1	1	0.07	0.82	10	

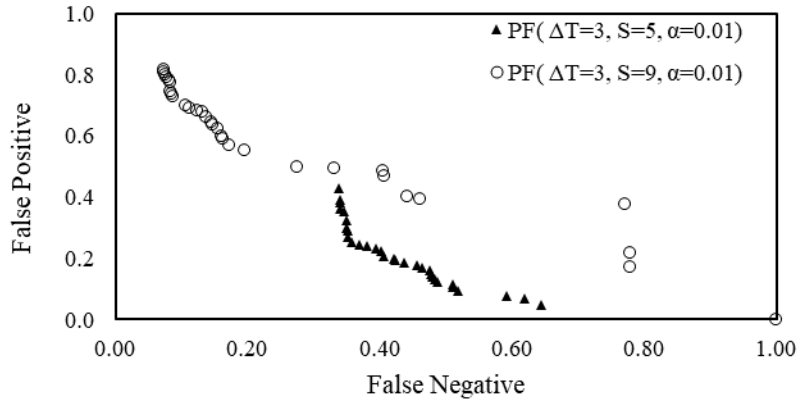


Figure 7-6. Best-found Pareto fronts for sensor placement optimization problem of C-Town with $\Delta T = 3, S = 5, \alpha = 0.01$ and $\Delta T = 3, S = 9, \alpha = 0.01$

The Pareto front using $\Delta T = 3, S = 5, \alpha = 0.01$ for C-Town (Figure 7-6), similar to Net3, has a more or less convex shape and shows the trade-off between false negative and false positive ratios. This front's position in the $\omega - \varphi$ space is more or less similar to the Pareto front using $\Delta T = 1, S = 9$, and $\alpha = 0.01$ of Net3. False negative values of solutions in this front are significantly smaller than the front with $\Delta T = 1, S = 9$, and $\alpha = 0.01$ of C-Town (Figure 7-4).

Solutions in $PF(\Delta T = 3, S = 9, \alpha = 0.01)$ have higher false positive ratios compared to $PF(\Delta T = 3, S = 5, \alpha = 0.01)$. It can be inferred, from Figure 7-6, that by increasing S from 5 to 9, the crowded part of the obtained Pareto-front shifts to the area of high false positive and small false negative. In fact, $PF(\Delta T = 3, S = 9, \alpha = 0.01)$ looks more similar to $PF(\Delta T = 1, S = 9, \alpha = 0.01)$ rather to $PF(\Delta T = 3, S = 5, \alpha = 0.01)$. This suggests a positive correlation between the lengths of sampling time (S) and the system level false positives in C-Town.

The similarity between $PF(\Delta T = 3, S = 9, \alpha = 0.01)$ and $PF(\Delta T = 1, S = 9, \alpha = 0.01)$ is again noted in the variation of their false negatives with the number of sensors in Figure 7-7 and Figure 7-5, respectively. In both cases, false negative improves abruptly by adding the second sensor which is unlike the benign decreasing trend for $PF(\Delta T = 3, S = 5, \alpha = 0.01)$.

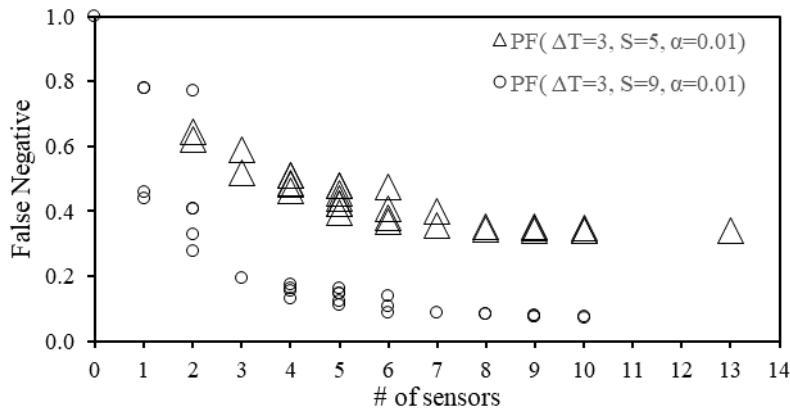


Figure 7-7. False negative variation with the number of sensors in C-Town with $\Delta T = 3, S = 5, \alpha = 0.01$ and $\Delta T = 3, S = 9, \alpha = 0.01$

To explore the influence of α on the Pareto-front of solutions, another optimization run was performed using $\Delta T = 3, S = 5, \alpha = 0.005$ where the computational budget and other optimization parameters were identical to the previous runs for C-Town. Results of this run are shown in Table 7-6 and Figure 7-8 below. It can be seen from Figure 7-6 and Figure 7-8 that this new Pareto front, $PF(\Delta T = 3, S = 5, \alpha = 0.005)$,

is very similar to $PF(\Delta T = 3, S = 5, \alpha = 0.01)$. Reducing α from 0.01 to 0.005 did not make much difference except creating two new non-dominated solutions with very small false positive values of 0.0 and 0.02. This confirms the fact that in order to obtain design solutions with smaller system level false positive, smaller α needs to be employed.

Table 7-6. Best-found Pareto front for sensor placement optimization problem of C-Town network based on $\Delta T = 3, S = 5, \alpha = 0.005$

Solution #	Nodes														ω	ϕ	# of Sensors
	8	9	30	45	46	64	71	72	79	66	76	78	81				
1	1	1	1	1	1	1	1	1	1	1	1	1	1	1	0.34	0.43	13
2	1	1	1	1	0	1	1	1	0	1	1	1	1	1	0.34	0.42	11
3	1	0	1	0	1	1	1	1	1	1	1	1	1	1	0.34	0.41	11
4	1	0	1	0	1	1	1	1	0	1	1	1	1	1	0.34	0.40	10
5	1	0	0	1	1	1	1	1	0	1	1	1	1	1	0.35	0.34	10
6	1	1	0	1	1	0	1	1	1	0	1	1	1	1	0.35	0.31	10
7	1	0	0	1	1	0	1	1	0	0	1	1	1	1	0.35	0.28	8
8	1	0	0	1	1	0	1	0	0	0	1	1	1	1	0.36	0.27	7
9	1	1	0	1	0	0	1	0	0	0	1	1	0	0	0.37	0.25	6
10	0	1	0	1	0	0	1	0	0	1	1	1	1	1	0.40	0.24	7
11	1	1	0	1	0	0	1	0	0	0	1	0	0	0	0.40	0.23	5
12	0	1	0	1	0	0	1	0	0	0	1	1	1	1	0.41	0.21	6
13	0	1	0	1	0	0	1	0	0	0	1	1	0	0	0.42	0.19	5
14	0	1	0	1	0	0	1	0	0	0	1	0	1	1	0.44	0.18	5
15	0	1	0	0	0	1	1	0	0	0	0	1	0	0	0.46	0.17	4
16	0	1	0	1	0	0	1	0	0	0	0	1	0	0	0.47	0.16	4
17	0	1	0	0	0	1	0	1	0	0	0	1	1	1	0.48	0.14	5
18	0	1	0	0	0	1	0	0	0	0	0	1	1	1	0.49	0.12	4
19	0	1	0	0	0	1	0	0	1	0	0	1	0	0	0.51	0.12	4
20	0	1	0	0	0	1	0	1	0	0	0	1	0	0	0.51	0.11	4
21	0	1	0	0	0	1	0	0	0	0	0	1	0	0	0.52	0.09	3
22	0	1	0	0	0	1	0	0	0	0	0	0	0	0	0.61	0.08	2
23	0	1	0	0	0	0	0	1	0	0	0	1	0	0	0.64	0.06	3
24	0	1	0	0	0	0	0	0	0	0	0	1	0	0	0.64	0.05	2
25	0	1	0	0	0	0	0	1	0	0	0	0	0	0	0.77	0.02	2
26	0	1	0	0	0	0	0	0	0	0	0	0	0	0	0.78	0.00	1

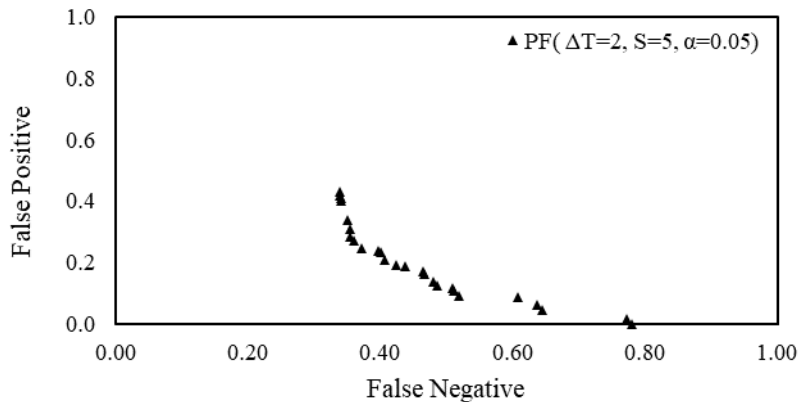


Figure 7-8. False negative variation with the number of sensors in C-Town with $\Delta T = 3, S = 5, \alpha = 0.005$

7.6 Conclusion

The sensor placement problem, as the second step of the detection test design, was solved as a multi-objective optimization problem for two networks from the literature. PADDs-CHC was utilized to obtain Pareto-fronts of sensor placement solutions in a reasonable time. The Pareto-fronts were found to hold a more or less convex shape which confirms the convexity assumption which justifies the application of CHC selection metric.

A strategy, termed as justifiability, was presented by which the decision space can be reduced prior to the formal optimization. This strategy is flexible in the sense that it can be used to choose a desired number of most justifiable network nodes as candidate locations for pressure sensors. Depending on the available computational budget, a certain number of sensor nodes, and thus the corresponding search space can be decided.

Results for Net3 are good quality as sensor fleets were identified that have a false negative rate of less than 0.30 and a simultaneous false positive rate of 0.10 or less. First trial results for the C-town, under the maximum sample number settings, are not good quality as sensor fleets identified have excessively high false positive rates (0.8 or higher). There are a few potential causes for the poor quality result. One could be that the assumed detection test parameter settings used for Net3 are not appropriate for C-town. It was shown that the results improved significantly by changing the detection test parameter settings to the ones suggested by the alternative design method suggested in 5.7.7. This proves that different networks need to be separately investigated for their optimum detection test parameter settings.

Chapter 8

Summary, Conclusions, and Recommendation for Future Work

8.1 Summary and Conclusion

Among the large number of studies focused on monitoring pressure measurements to detect leakages, far too little attention has been paid to the uncertain aspects of the problem. Application of MFD in leak detection setting seems promising yet one cannot ignore, or even simplify too much, the vast uncertainties in water distribution networks. The aleatory uncertainty in the nodal demands is the most important uncertainty aspect in this context because MFD relies on pressure fluctuations which are influenced similarly by leaks as by the uncertain nodal demands. This concern was explored in Chapter 3 where it was shown that for a leak size around the ones mentioned in MFD literature, the magnitude of nodal pressure drops in absence of the leak and yet the presence of demand noise (uncertainty in demand) can easily exceed the size of pressure drops only due to the leak. This, in turn, results in high false positive ratios and thus the waste of machine/human resources successively assigned to investigate, localize, and repair non-existing leakages.

To address the issue, Chapter 4 proposed a novel comparison framework which was used to perform exploratory analysis on differences of the pressure signals under leak and demand noise. An exhaustive search over all conceivable configurations of nodal demand values is unattainable due to the number of demand nodes in a WDS. Generating realizations of nodal demands across the network by sampling from their probability distributions is a more tractable approach. A key piece of such a sampling tactic was that even though individual nodal demands are uncertain, fortunately, there is knowledge available that helps create more realistic demand realizations. For example, the sum of all nodal demands for each realization has to match the actual observed total system demand, which is available from the municipalities' database. All previous deterministic MFD studies ignore this information when computing expected pressure responses (and instead utilize assumed nominal total demand).

It was shown that for a certain size of leak and larger, it is possible to distinguish between the observations resulted by a leak and those coming from the no-leak condition while considering significant uncertainty in the nodal demand. This achievement, which was proven to be out of reach by using deterministic implementation of MFD, is only possible by performing the comparison under the particular detailed process determined by the suggested comparison framework.

Based on the success of the comparison framework in distinguishing leak effects from the demand noise, a novel stochastic application of MFD in the field of WDS leak detection was introduced in Chapter 5. The method is established on the pressure analysis tool offered in Chapter 4 and is presented in the form of a statistical hypothesis test.

The method was shown to be able to handle the nodal demand uncertainties and detect leakages successfully in two case-studies in this chapter. The structure of the stochastic detection test is flexible and allows customized sampling schedule and level of significances. This is especially important in the actual implementation of the methodology where practical aspects and field limitations need to be adhered to. However, the influence of scheduling and level of significance on the behaviour of the detection test was studied by designing experiments and evaluating the test performance via the two quality performance metrics (i.e., false positive and false negative). Each experiment contained a set of leak and no-leak scenarios generated using Monte-Carlo methods. Leak scenarios refer to a set of hypothetical leaks of certain EDC occurring at different locations in the network. This analysis was performed extensively for the smaller case-study (Net3) for which a large set of the randomly generated leak and no-leak scenarios were used to evaluate each configuration of the detection test. It was shown for Net3, how the augmentation in sampling enhances the false negative rate and does not, in general, degrade the false positive rate.

Based on the introduced detection method and performance metrics, the sensor placement problem was solved as a multi-objective optimization issue. The candidate sensor fleet layouts were evaluated for the performance of the leak detection test when applied to a set of pre-defined leak and no-leak scenarios. Two objective functions are used to characterize the performance of a candidate sensor placement. These include the minimization of the false negative (as a proxy of regret) and false positive ratios. False negative evaluates the frequency that a sensor fleet fails to detect leaks in the network. Low values of this objective show that the proposed sensor fleet detects most of the leak scenarios successfully. However, if minimizing the false negative ratio is considered as the only objective function, then the candidate set may be vulnerable to excessive false positives produced by demand fluctuations. In order to avoid this issue, a second objective function was introduced to guide the optimization search trajectory. This objective, defined as the false positive ratio, enumerates the number of times the candidate sensor set falsely asserts the existence of a leak that does not actually exist at that time.

Even with the reduced number of network nodes, the optimization problem was proven to be cumbersome highlighting the need for a multi-objective solver that can approach to the optimum Pareto-

front with fewer calls to the objective function evaluation process. Development, configuration, and verification of PADDs-CHC in the context of benchmark design of 12 literature WDS was performed in Chapter 6. PADDs-CHC was proven to be the most efficient multi-objective solver for the convex problems and thus used to solve the sensor placement optimization problem. The convex structure of the obtained Pareto-fronts in both case-studies (Net3 and C-Town) justifies the application of CHC as the selection metric for PADDs which was established in Chapter 6.

Results of the optimization of sensor location showed that the number of sensors, as a proxy of cost, was implicitly minimized in the process of minimizing the false negative ratios. This removes the need to introduce a third objective to represent the cost of the design. Each solution on the obtained Pareto-fronts can be considered as sensor placement configuration. While the final choice is on the decision makers, by the study of variation of a false negative with respect to the number of sensors, suggestions were made to support the final decision by highlighting the maximum number of sensors by which false negatives improves significantly.

It was shown in the case of Net3 that the schedule associated with the maximum sample number (smallest interval and greatest length) improves the system level false negative and does not deteriorate the false positive. However, the same configuration resulted in poor results for C-Town emphasizing the importance of exploring multiple scheduling plans. Although more samples generally improve the false negative, nevertheless, it is important to consider more than one schedule setting and level of significance for a new network. In the case of C-Town, best sensor fleet location designs were obtained by implementing the ΔT and S that were found to produce the most desirable system level false positive and false negative (not the ΔT and S that result in the maximum number of samples).

A novel aspect of this thesis is the incorporation of false positives as a quality metric for designing the detection test and solving the sensor placement problem. MFD-based studies in the past have only focused on improving the false negative. Without having the false positive as an objective (i.e., minimizing false negative only) one would end up obtaining solutions with the maximum number of sensors. This setup ignores the trade-off between false negative and false positive. Under this setup, still, the best false negative value would be achieved yet at the cost of significantly high and unacceptable false positive ratios.

The proposed leak detection method is applicable to any WDS hydraulic model. Instructions to implement the methodology were provided in the form of the best schedule (sampling frequency and length) and optimum sensor locations. Once computational work for sensor placement is done and sensors

are installed in the field, the proposed detection hypothesis test is applicable using the observation data to construct the distributions of the plausible nodal pressure under the no-leak condition to obtain a P-value for each sensor. Final assertion for the existence of the anomaly is made based on the comparison of the P-values with the relevant level of significance.

8.2 Future Research

Following items are recommended as the next stages of this research:

- Instead of breaking the design of the detection test into two successive steps of schedule planning and sensor placement, a future study may consider all the design parameters (ΔT , S , α , and \mathbf{sf}) altogether. Under such an outline, all the four parameters will be optimized simultaneously. The challenging aspect of such a layout would be the even larger decision space which takes a lot more iterations to be properly explored by a solver.
- Consideration of more than one leak at a time is another suggestion for future work. The expectation is that when more than one leak occur in the network, the pressure deviations should become even more unlikely under the no-leak pressure distributions and thus more likely to be noted by the detection methodology.
- Further work could optimize the process of characterizing the distributions of the nodal pressures in response to uncertain demands with guided sampling. More attention to the equivalency criteria for system states can help better definition of thresholds. For example, to consider two system states as equal, tank levels should not exceed a certain threshold which is currently defined through trial and error and is constant for all the tank elements. This threshold needs to be defined independently for each tank (probably as a function of its diameter).
- Extreme variation in demands can cause EPANET2 to fail in finding a balance in the hydraulic network (and thus terminate with an error message) which results in a waste of computational resources. A caveat to the process of demand realization sampling could be to avoid generating excessively large demand noises. Work needs to be done studying a smart/guided filtering mechanism as a post-processing step for the sampling step.
- Incorporation of the historical nodal pressure of the case-studies would help verify/improve stochastically generated non-leak pressure. Once such data is available, these historical nodal

pressures could replace the stochastic sampling and hydraulic simulations described in the comparison framework (explained in Chapter 4).

- The correlation coefficient, variance, and mean of nodal demands which are used in the multivariate random sampling process would ideally be extracted for each node out of the field data. In the current study, these values had to be either mined from the network model or assumed. Follow-up research would benefit from field data to replace these assumptions.
- The proposed stochastic leak detection mechanism can potentially be used simultaneously for the purpose of model calibration.
- The performance of the leak detection method was investigated by solving two more or less branched networks. Future work can address the case of highly looped networks.
- The hydraulic solver for the proposed model-based leak diagnosis method, which is currently EPANET2 in its demand-driven mode, may be replaced with pressure-driven solvers or, once available in the future, a transient solver.

References

- Abdulshaheed, A., Mustapha, F., Ghavamian, A. (2017). "A Pressure-Based Method for Monitoring Leaks in a Pipe Distribution System: A Review." *Renewable and Sustainable Energy Reviews*, 69, 902-911.
- Abraham, E., Blokker, M., Stoianov, I. (2017). "Decreasing the Discoloration Risk of Drinking Water Distribution Systems through Optimized Topological Changes and Optimal Flow Velocity Control." *J. Water Resour. Plann. Manage.*, 144(2), 04017093.
- Alegre, H., Baptista, J. M., Cabrera Jr, E., Cubillo, F., Duarte, P., Hirner, W., Merkel, W., Parena, R. (2006). *Performance Indicators for Water Supply Services*, IWA publishing, .
- Alkassseh, J. M., Adlan, M. N., Abustan, I., Aziz, H. A., Hanif, A. B. M. (2013). "Applying Minimum Night Flow to Estimate Water Loss using Statistical Modeling: A Case Study in Kinta Valley, Malaysia." *Water Resour. Manage.*, 27(5), 1439-1455.
- Alperovits, E., and Shamir, U. (1977). "Design of Optimal Water Distribution Systems." *Water Resour. Res.*, 13(6), 885-900.
- Aral, M. M., Guan, J., Maslia, M. L. (2008). "A multi-objective optimization algorithm for sensor placement in water distribution systems." *Proc., World Environmental and Water Resources Congress 2008: Ahupua'A*, , 1-11.
- Asadzadeh, M., and Tolson, B. A. (2009). "A new multi-objective algorithm, pareto archived DDS." *Proc., Proceedings of the 11th Annual Conference Companion on Genetic and Evolutionary Computation Conference: Late Breaking Papers*, ACM, Montreal, QC, Canada. ACM, New York, NY, USA., 1963-1966.
- Asadzadeh, M., and Tolson, B. (2012). "Hybrid Pareto Archived Dynamically Dimensioned Search for Multi-Objective Combinatorial Optimization: Application to Water Distribution Network Design." *J. Hydroinformatics*, 14(1), 192-205.
- Asadzadeh, M., Tolson, B. A., Burn, D. H. (2014). "A New Selection Metric for Multiobjective Hydrologic Model Calibration." *Water Resour. Res.*, 50(9), 7082-7099.
- Asadzadeh, M., and Tolson, B. (2013). "Pareto Archived Dynamically Dimensioned Search with Hypervolume-Based Selection for Multi-Objective Optimization." *Engineering Optimization*, 45(12), 1489-1509.
- Ayala-Cabrera, D., Herrera, M., Izquierdo, J., Ocana-Levario, S. J., Pérez-García, R. (2013). "GPR-Based Water Leak Models in Water Distribution Systems." *Sensors*, 13(12), 15912-15936.

- Barber, C. B., Dobkin, D. P., Huhdanpaa, H. (1996). "The Quickhull Algorithm for Convex Hulls." *ACM Transactions on Mathematical Software (TOMS)*, 22(4), 469-483.
- Beck, S., Curren, M., Sims, N., Stanway, R. (2005). "Pipeline Network Features and Leak Detection by Cross-Correlation Analysis of Reflected Waves." *J. Hydraul. Eng.*, 131(8), 715-723.
- Bi, W., Dandy, G., Maier, H. (2016). "Use of Domain Knowledge to Increase the Convergence Rate of Evolutionary Algorithms for Optimizing the Cost and Resilience of Water Distribution Systems." *J. Water Resour. Plann. Manage.*, 142(9), 04016027-1-04016027-12.
- Bicik, J., Kapelan, Z., Makropoulos, C., Savić, D. A. (2011). "Pipe Burst Diagnostics using Evidence Theory." *J. Hydroinf.*, 13(4), 596-608.
- Blesa, J., Nejjari, F., Sarrate, R. (2016). "Robust Sensor Placement for Leak Location: Analysis and Design." *J. Hydroinf.*, 18(1), 136-148.
- Blokker, E., Beverloo, H., Vogelaar, A., Vreeburg, J., Van Dijk, J. (2011). "A Bottom-Up Approach of Stochastic Demand Allocation in a Hydraulic Network Model: A Sensitivity Study of Model Parameters." *J. Hydroinf.*, 13(4), 714-728.
- Blokker, E., Vreeburg, J., Van Dijk, J. (2009). "Simulating Residential Water Demand with a Stochastic End-use Model." *J. Water Resour. Plann. Manage.*, 136(1), 19-26.
- Blokker, M., Agudelo-Vera, C., Mesman, G. (2018). "Drinking water demand under stressed conditions; quantification with SIMDEUM." *Proc., WDSA/CCWI Joint Conference Proceedings*, .
- Bonada, E., Meseguer, J., Mirats-Tur, J. M. (2014). "On the structure of the objective function for A pressure sensor placement optimizing methodology based on genetic algorithms applied to model-based leakage localization in distribution water networks." 11th International Conference on Hydroinformatics.
- Boulos, P. F., Lansley, K. E., Karney, B. W. (2006). *Comprehensive Water Distribution Systems Analysis Handbook for Engineers and Planners*, American Water Works Association, .
- Bradley, J. V. (1968). "Distribution-Free Statistical Tests." *Distribution-Free Statistical Tests*, .
- Bragalli, C., D'Ambrosio, C., Lee, J., Lodi, A., Toth, P. (2008). "Water Network Design by MINLP." *Rep. no. RC24495, IBM Research, Yorktown Heights, NY*, .
- Branisavljević, N., Prodanović, D., Ivetić, M. (2009). "Uncertainty Reduction in Water Distribution Network Modelling using System Inflow Data." *Urban Water Journal*, 6(1), 69-79.
- Buchberger, S. G., and Nadimpalli, G. (2004). "Leak Estimation in Water Distribution Systems by Statistical Analysis of Flow Readings." *J. Water Resour. Plann. Manage.*, 130(4), 321-329.

- Buchberger, S. G., Carter, J., Lee, Y., Schade, T. (2003). *Random Demands, Travel Times, and Water Quality in Deadends*, AWWA Research Foundation Denver, .
- Campisano, A., and Modica, C. (2015). "Two-Step Numerical Method for Improved Calculation of Water Leakage by Water Distribution Network Solvers." *J. Water Resour. Plann. Manage.*, 142(2), 04015060.
- Carr, R. D., Greenberg, H. J., Hart, W. E., Phillips, C. A. (2004). "Addressing Modeling Uncertainties in Sensor Placement for Community Water Systems." *Critical Transitions in Water and Environmental Resources Management*, 1-10.
- Casillas, M. V., Garza-Castañón, L. E., Puig, V. (2015). "Optimal Sensor Placement for Leak Location in Water Distribution Networks using Evolutionary Algorithms." *Water*, 7(11), 6496-6515.
- Casillas, M. V., Garza-Castañón, L. E., Puig, V., Vargas-Martinez, A. (2015). "Leak Signature Space: An Original Representation for Robust Leak Location in Water Distribution Networks." *Water*, 7(3), 1129-1148.
- Casillas, M. V., Puig, V., Garza-Castanón, L. E., Rosich, A. (2013a). "Optimal Sensor Placement for Leak Location in Water Distribution Networks using Genetic Algorithms." *Sensors*, 13(11), 14984-15005.
- Casillas, M. V., Puig, V., Garza-Castanón, L. E., Rosich, A. (2013b). "Optimal Sensor Placement for Leak Location in Water Distribution Networks using Genetic Algorithms." *Sensors*, 13(11), 14984-15005.
- Chastain Jr, J. R. (2006). "Methodology for Locating Monitoring Stations to Detect Contamination in Potable Water Distribution Systems." *J Infrastruct Syst*, 12(4), 252-259.
- Chen, J., and Patton, R. J. (2012). *Robust Model-Based Fault Diagnosis for Dynamic Systems*, Springer Science & Business Media, .
- Christodoulou, S. E., Gagatsis, A., Xanthos, S., Kranioti, S., Agathokleous, A., Fragiadakis, M. (2013). "Entropy-Based Sensor Placement Optimization for Waterloss Detection in Water Distribution Networks." *Water Resour. Manage.*, 27(13), 4443-4468.
- Covas, D., Graham, N., Maksimovic, C., Kapelan, Z., Savic, D., Walters, G. (2003). *An Assessment of the Application of Inverse Transient Analysis for Leak Detection. Part II: Collection and Application of Experimental Data*, Swets & Zeitlinger Lisse, The Netherlands, .
- Covas, D., Ramos, H., De Almeida, A. B. (2005). "Standing Wave Difference Method for Leak Detection in Pipeline Systems." *J. Hydraul. Eng.*, 131(12), 1106-1116.
- Das, I. (1999). "On Characterizing the "knee" of the Pareto Curve Based on Normal-Boundary Intersection." *Struct. Opt.*, 18(2-3), 107-115.

- Deb, K., Pratap, A., Agarwal, S., Meyarivan, T. (2002). "A Fast and Elitist Multiobjective Genetic Algorithm: NSGA-II." *IEEE Transactions on Evolutionary Computation*, 6(2), 182-197.
- Deb, K., Mohan, M., Mishra, S. (2005). "Evaluating the Epsilon-Domination Based Multi-Objective Evolutionary Algorithm for a Quick Computation of Pareto-Optimal Solutions." *Evol. Comput.*, 13(4), 501-525.
- Deb, K. (2001). *Multi-Objective Optimization using Evolutionary Algorithms*, John Wiley & Sons, New York, NY, USA.
- Dorini, G., Jonkergouw, P., Kapelan, Z., Di Pierro, F., Khu, S., Savic, D. (2008). "An efficient algorithm for sensor placement in water distribution systems." *Proc., Water Distribution Systems Analysis Symposium 2006*, , 1-13.
- Eck, B., Fusco, F., Taheri, N. (2015). "Scenario generation for network optimization with uncertain demands." *Proc., World Environmental and Water Resources Congress 2015*, , 844-852.
- Farley, B., Mounce, S., Boxall, J. (2012). "Development and Field Validation of a Burst Localization Methodology." *J. Water Resour. Plann. Manage.*, 139(6), 604-613.
- Farley, B., Mounce, S., Boxall, J. (2010). "Field Testing of an Optimal Sensor Placement Methodology for Event Detection in an Urban Water Distribution Network." *Urban Water Journal*, 7(6), 345-356.
- Farley, B., Boxall, J., Mounce, S. (2008). "Optimal Locations of Pressure Meters for Burst Detection." *Water Distribution Systems Analysis 2008*, 1-11.
- Farley, M. (2007). "Finding Difficult Leaks." *Water*, 21, 1.
- Farmani, R., Savic, D. A., Walters, G. A. (2004). "Exnet" Benchmark Problem for Multi-Objective Optimization of Large Water Systems." *Modelling and Control for Participatory Planning and Managing Water Systems*, IFAC Workshop, Venice, Italy.
- Filion, Y., Adams, B., Karney, B. (2007). "Cross Correlation of Demands in Water Distribution Network Design." *J. Water Resour. Plann. Manage.*, 133(2), 137-144.
- Fujiwara, O., and Khang, D. B. (1990). "A Two-Phase Decomposition Method for Optimal Design of Looped Water Distribution Networks." *Water Resour. Res.*, 26(4), 539-549.
- Gertler, J. (1998). *Fault Detection and Diagnosis in Engineering Systems*, CRC press, .
- Gessler, J. (1985). "Pipe network optimization by enumeration." *Proc., Proc., Computer Applications for Water Resources*, ASCE, New York, 572-581.
- Gheisi, A., Forsyth, M., Naser, G. (2016). "Water Distribution Systems Reliability: A Review of Research Literature." *J. Water Resour. Plann. Manage.*, 142(11), 04016047.

- Giustolisi, O., Berardi, L., Laucelli, D., Savic, D., Walski, T., Brunone, B. (2014). "Battle of Background Leakage Assessment for Water Networks (BBLAWN) at WDSA Conference 2014." *Procedia Engineering*, 89, 4-12.
- Gong, J., Zecchin, A. C., Simpson, A. R., Lambert, M. F. (2013). "Frequency Response Diagram for Pipeline Leak Detection: Comparing the Odd and Even Harmonics." *J. Water Resour. Plann. Manage.*, 140(1), 65-74.
- Goulet, J., Coutu, S., Smith, I. F. (2013). "Model Falsification Diagnosis and Sensor Placement for Leak Detection in Pressurized Pipe Networks." *Advanced Engineering Informatics*, 27(2), 261-269.
- Gupta, R., Nair, A. G. R., Ormsbee, L. (2016). "Leakage as Pressure-Driven Demand in Design of Water Distribution Networks." *J. Water Resour. Plann. Manage.*, 142(6), 04016005.
- Hadka, D., and Reed, P. (2013). "Borg: An Auto-Adaptive Many-Objective Evolutionary Computing Framework." *Evol. Comput.*, 21(2), 231-259.
- Hagos, M., Jung, D., Lansley, K. E. (2016). "Optimal Meter Placement for Pipe Burst Detection in Water Distribution Systems." *J. Hydroinf.*, 18(4), 741-756.
- Hall, J. W. (2003). "Handling Uncertainty in the Hydroinformatic Process." *J. Hydroinf.*, 5(4), 215-232.
- Hanne, T. (1999). "On the Convergence of Multiobjective Evolutionary Algorithms." *Eur. J. Oper. Res.*, 117(3), 553-564.
- Hart, W. E., and Murray, R. (2010). "Review of Sensor Placement Strategies for Contamination Warning Systems in Drinking Water Distribution Systems." *J. Water Resour. Plann. Manage.*, 136(6), 611-619.
- Hutton, C. J., Kapelan, Z., Vamvakeridou-Lyroudia, L., Savić, D. A. (2012). "Dealing with Uncertainty in Water Distribution System Models: A Framework for Real-Time Modeling and Data Assimilation." *J. Water Resour. Plann. Manage.*, 140(2), 169-183.
- Jahanpour, M., Tolson, B. A., Mai, J. (2017). "PADDS Algorithm Assessment for Biobjective Water Distribution System Benchmark Design Problems." *J. Water Resour. Plann. Manage.*, 144(3), 04017099.
- Jung, D., and Lansley, K. (2014). "Water Distribution System Burst Detection using a Nonlinear Kalman Filter." *J. Water Resour. Plann. Manage.*, 141(5), 04014070.
- Kang, D., and Lansley, K. (2012). "Novel Approach to Detecting Pipe Bursts in Water Distribution Networks." *J. Water Resour. Plann. Manage.*, 140(1), 121-127.
- Kapelan, Z., Savic, D., Walters, G. (2004). "Incorporation of Prior Information on Parameters in Inverse Transient Analysis for Leak Detection and Roughness Calibration." *Urban Water Journal*, 1(2), 129-143.

- Kapelan, Z., Savic, D., Walters, G. (2005). "Multiobjective Design of Water Distribution Systems Under Uncertainty." *Water Resour. Res.*, 41(11).
- Kapelan, Z. S., Savic, D. A., Walters, G. A. (2003). "A Hybrid Inverse Transient Model for Leakage Detection and Roughness Calibration in Pipe Networks." *Journal of Hydraulic Research*, 41(5), 481-492.
- Khedr, A., Tolson, B., Ziemann, S. (2015). "Water Distribution System Calibration: Manual Versus Optimization-Based Approach." *Procedia Engineering*, 119, 725-733.
- Kim, J. H., Kim, T. G., Kim, J. H., Yoon, Y. N. (1994). "A Study on the Pipe Network System Design using Non-Linear Programming." *J. Korean Water Resour. Assoc.*, 27(4), 59.
- Kleiner, Y., and Rajani, B. (2001). "Comprehensive Review of Structural Deterioration of Water Mains: Statistical Models." *Urban Water*, 3(3), 131-150.
- Knowles, J. D., Corne, D. W., Fleischer, M. (2003). "Bounded archiving using the lebesgue measure." *Proc., Evolutionary Computation, 2003. CEC'03. the 2003 Congress On, IEEE*, , 2490-2497.
- Kollat, J. B., and Reed, P. M. (2006). "Comparing State-of-the-Art Evolutionary Multi-Objective Algorithms for Long-Term Groundwater Monitoring Design." *Adv. Water Resour.*, 29(6), 792-807.
- Krause, A., and Guestrin, C. (2009). "Robust sensor placement for detecting adversarial contaminations in water distribution systems." *Proc., World Environmental and Water Resources Congress 2009: Great Rivers*, , 1-10.
- Lambert, A. (2002). "International Report: Water Losses Management and Techniques." *Water Science and Technology: Water Supply*, 2(4), 1-20.
- Lansley, K. (2011). "Uncertainty in Water Distribution Network Modeling." *Journal of Contemporary Water Research and Education*, 103(1), 5.
- LeChevallier, M. W., Gullick, R. W., Karim, M. R., Friedman, M., Funk, J. E. (2003). "The Potential for Health Risks from Intrusion of Contaminants into the Distribution System from Pressure Transients." *Journal of Water and Health*, 1(1), 3-14.
- Lee, S., and Lee, S. (2001). "Genetic Algorithms for Optimal Augmentation of Water Distribution Networks." *Journal of Korea Water Resources Association*, 34(5), 567-575.
- Lee, S. J., Lee, G., Suh, J. C., Lee, J. M. (2015). "Online Burst Detection and Location of Water Distribution Systems and its Practical Applications." *J. Water Resour. Plann. Manage.*, 142(1), 04015033.
- Li, R., Huang, H., Xin, K., Tao, T. (2015). "A Review of Methods for Burst/Leakage Detection and Location in Water Distribution Systems." *Water Science and Technology: Water Supply*, 15(3), 429-441.

- Liemberger, R., and Farley, M. (2004). "Developing a nonrevenue water reduction strategy part 1: Investigating and assessing water losses." *Proc., Paper to IWA Congress*, Citeseer, .
- Liggett, J. A., and Chen, L. (1994). "Inverse Transient Analysis in Pipe Networks." *J. Hydraul. Eng.*, 120(8), 934-955.
- Mahmoud, H. A., Savić, D., Kapelan, Z. (2017). "New Pressure-Driven Approach for Modeling Water Distribution Networks." *J. Water Resour. Plann. Manage.*, 143(8), 04017031.
- Mainali, G., Dineva, S., Nordlund, E. (2015). "Experimental Study on Debonding of Shotcrete with Acoustic Emission during Freezing and Thawing Cycle." *Cold Reg. Sci. Technol.*, 111, 1-12.
- Marchi, A., Salomons, E., Ostfeld, A., Kapelan, Z., Simpson, A., Zecchin, A., Maier, H., Wu, Z., Elsayed, S., Song, Y., Walski, T., Stokes, C., Wu, W., Dandy, G., Alvisi, S., Creaco, E., Franchini, M., Saldarriaga, J., Páez, D., Hernández, D., Bohórquez, J., Bent, R., Coffrin, C., Judi, D., McPherson, T., van Hentenryck, P., Matos, J., Monteiro, A., Matias, N., Yoo, D., Lee, H., Kim, J., Iglesias-Rey, P., Martínez-Solano, F., Mora-Meliá, D., Ribelles-Aguilar, J., Guidolin, M., Fu, G., Reed, P., Wang, Q., Liu, H., McClymont, K., Johns, M., Keedwell, E., Kandiah, V., Jasper, M., Drake, K., Shafiee, E., Barandouzi, M., Berglund, A., Brill, D., Mahinthakumar, G., Ranjithan, R., Zechman, E., Morley, M., Tricarico, C., de Marinis, G., Tolson, B., Khedr, A., Asadzadeh, M. (2014). "Battle of the Water Networks II." *J. Water Resour. Plann. Manage.*, 140(7), 04014009.
- Marques, G., Lund, J., Howitt, R. (2010). "Modeling Conjunctive use Operations and Farm Decisions with Two-Stage Stochastic Quadratic Programming." *J Water Res Pl*, 136(3), 386-394.
- Meseguer, J., Mirats-Tur, J. M., Cembrano, G., Puig, V. (2015). "Model-Based Monitoring Techniques for Leakage Localization in Distribution Water Networks." *Procedia Engineering*, 119, 1399-1408.
- Millán-Roures, L., Epifanio, I., Martínez, V. (2018). "Detection of Anomalies in Water Networks by Functional Data Analysis." *Mathematical Problems in Engineering*, 2018.
- Moosavian, N., and Lence, B. (2016). "Nondominated Sorting Differential Evolution Algorithms for Multiobjective Optimization of Water Distribution Systems." *J. Water Resour. Plann. Manage.*, , 04016082.
- Mounce, S., Boxall, J., Machell, J. (2009). "Development and Verification of an Online Artificial Intelligence System for Detection of Bursts and Other Abnormal Flows." *J. Water Resour. Plann. Manage.*, 136(3), 309-318.
- Mutikanga, H. E., Sharma, S. K., Vairavamoorthy, K. (2012). "Methods and Tools for Managing Losses in Water Distribution Systems." *J. Water Resour. Plann. Manage.*, 139(2), 166-174.
- Nasirian, A., Faghfour Maghrebi, M., Yazdani, S. (2013). "Leakage Detection in Water Distribution Network Based on a New Heuristic Genetic Algorithm Model." *Journal of Water Resource and Protection*, 5.

Nilsson, K. A., Buchberger, S. G., Clark, R. M. (2005). "Simulating Exposures to Deliberate Intrusions into Water Distribution Systems." *J. Water Resour. Plann. Manage.*, 131(3), 228-236.

Nixon, W., Ghidaoui, M. S., Kolyshkin, A. A. (2006). "Range of Validity of the Transient Damping Leakage Detection Method." *J. Hydraul. Eng.*, 132(9), 944-957.

Ostfeld, A., Salomons, E., Ormsbee, L., Uber, J. G., Bros, C. M., Kalungi, P., Burd, R., Zazula-Coetzee, B., Belrain, T., Kang, D. (2011). "Battle of the Water Calibration Networks." *J. Water Resour. Plann. Manage.*, 138(5), 523-532.

Ostfeld, A., Uber, J. G., Salomons, E., Berry, J. W., Hart, W. E., Phillips, C. A., Watson, J., Dorini, G., Jonkergouw, P., Kapelan, Z. (2008). "The Battle of the Water Sensor Networks (BWSN): A Design Challenge for Engineers and Algorithms." *J. Water Resour. Plann. Manage.*, 134(6), 556-568.

Paez, D., Suribabu, C., Fillion, Y. (2018). "Method for Extended Period Simulation of Water Distribution Networks with Pressure Driven Demands." *Water Resour. Manage.*, 32(8), 2837-2846.

Pérez, R., Puig, V., Pascual, J., Peralta, A., Landeros, E., Jordanas, L. (2009). "Pressure Sensor Distribution for Leak Detection in Barcelona Water Distribution Network." *Water Science and Technology: Water Supply*, 9(6), 715-721.

Pérez, R., Puig, V., Pascual, J., Quevedo, J., Landeros, E., Peralta, A. (2011). "Methodology for Leakage Isolation using Pressure Sensitivity Analysis in Water Distribution Networks." *Control Eng. Pract.*, 19(10), 1157-1167.

Pérez, R., Sanz, G., Cugueró, M., Blesa, J., Cugueró, J. (2015). "Parameter Uncertainty Modelling in Water Distribution Network Models." *Procedia Engineering*, 119, 583-592.

Ponce, M. V. C., Castañón, L. E. G., Cayuela, V. P. (2014). "Model-Based Leak Detection and Location in Water Distribution Networks Considering an Extended-Horizon Analysis of Pressure Sensitivities." *J. Hydroinf.*, 16(3), 649-670.

Prasad, T., and Park, N. (2004). "Multiobjective Genetic Algorithms for Design of Water Distribution Networks." *J. Water Resour. Plann. Manage.*, 130(1), 73-82.

Preis, A., Whittle, A., Ostfeld, A. (2011). "Multi-Objective Optimization for Conjunctive Placement of Hydraulic and Water Quality Sensors in Water Distribution Systems." *Water Science and Technology: Water Supply*, 11(2), 166-171.

Prodon, A., DeNegre, S., Liebling, T. M. (2010). "Locating Leak Detecting Sensors in a Water Distribution Network by Solving Prize-Collecting Steiner Arborescence Problems." *Math. Program.*, 124(1), 119-141.

Pudar, R. S., and Liggett, J. A. (1992). "Leaks in Pipe Networks." *J. Hydraul. Eng.*, 118(7), 1031-1046.

- Puust, R., Kapelan, Z., Savic, D., Koppel, T. (2010). "A Review of Methods for Leakage Management in Pipe Networks." *Urban Water Journal*, 7(1), 25-45.
- Qi, Z., Zheng, F., Guo, D., Maier, H. R., Zhang, T., Yu, T., Shao, Y. (2018). "Better Understanding of the Capacity of Pressure Sensor Systems to Detect Pipe Burst within Water Distribution Networks." *J. Water Resour. Plann. Manage.*, 144(7), 04018035.
- Reca, J., and Martínez, J. (2006). "Genetic Algorithms for the Design of Looped Irrigation Water Distribution Networks." *Water Resour. Res.*, 42(5), W05416.
- Romano, M., Woodward, K., Kapelan, Z. (2017). "Statistical Process Control Based System for Approximate Location of Pipe Bursts and Leaks in Water Distribution Systems." *Procedia Engineering*, 186, 236-243.
- Rossman, L. A. (2000). "Epanet 2 Users Manual, Us Environmental Protection Agency." *Water Supply and Water Resources Division, National Risk Management Research Laboratory, Cincinnati, OH*, 45268.
- Sanz, G., Pérez, R., Kapelan, Z., Savic, D. (2015). "Leak Detection and Localization through Demand Components Calibration." *J. Water Resour. Plann. Manage.*, 142(2), 04015057.
- Sarrate, R., Blesa, J., Nejjari, F., Quevedo, J. (2014). "Sensor Placement for Leak Detection and Location in Water Distribution Networks." *Water Science and Technology: Water Supply*, 14(5), 795-803.
- Schaake, J. C., and Lai, F. H. (1969). *Linear Programming and Dynamic Programming Application to Water Distribution Network Design*, M.I.T. Hydrodynamics Laboratory, Cambridge, Mass.
- Sherali, H. D., Subramanian, S., Loganathan, G. (2001). "Effective Relaxations and Partitioning Schemes for Solving Water Distribution Network Design Problems to Global Optimality." *J. Global Optimiz.*, 19(1), 1-26.
- Steffelbauer, D., Neumayer, M., Günther, M., Fuchs-Hanusch, D. (2014). "Sensor Placement and Leakage Localization Considering Demand Uncertainties." *Procedia Engineering*, 89, 1160-1167.
- Stoianov, I., Nachman, L., Madden, S., Tokmouline, T. (2007). "PIPENET: A wireless sensor network for pipeline monitoring." *Proc., 2007 6th International Symposium on Information Processing in Sensor Networks*, , 264-273.
- Taghvaei, M., Beck, S., Staszewski, W. (2006). "Leak Detection in Pipelines using Cepstrum Analysis." *Measurement Science and Technology*, 17(2), 367.
- Todini, E., and Pilati, S. (1988). "A gradient algorithm for the analysis of pipe networks." *Proc., Computer Applications in Water Supply: Vol. I---Systems Analysis and Simulation*, Research Studies Press Ltd., , 1-20.

- Tolson, B. A., Khedr, A., Asadzadeh, M. (2012). "The battle of the water networks (BWN-II): PADDs based solution approach." *Proc., Proceedings of the WDSA Conference*, Adelaide, Australia.
- Tolson, B. A., Asadzadeh, M., Maier, H. R., Zecchin, A. (2009). "Hybrid Discrete Dynamically Dimensioned Search (HD-DDS) Algorithm for Water Distribution System Design Optimization." *Water Resour. Res.*, 45(12), W12416.
- Tolson, B. A., and Shoemaker, C. A. (2007). "Dynamically Dimensioned Search Algorithm for Computationally Efficient Watershed Model Calibration." *Water Resour. Res.*, 43(1), W01413.
- Vrugt, J. A., and Robinson, B. A. (2007). "Improved Evolutionary Optimization from Genetically Adaptive Multimethod Search." *Proceedings of the National Academy of Sciences*, 104(3), 708-711.
- Walpole, R. E., and Myers, R. H. (1985). *Probability and Statistics for Engineering and Scientists*, Macmillan, .
- Walski, T. M., Chase, D. V., Savic, D. A., Grayman, W., Beckwith, S., Koelle, E. (2003). "Advanced Water Distribution Modeling and Management." .
- Wang, X., Lambert, M. F., Simpson, A. R., Liggett, J. A., V í tkovský, John P. (2002). "Leak Detection in Pipelines using the Damping of Fluid Transients." *J. Hydraul. Eng.*, 128(7), 697-711.
- Wang, Q., Guidolin, M., Savic, D., Kapelan, Z. (2015). "Two-Objective Design of Benchmark Problems of a Water Distribution System Via MOEAs: Towards the Best-Known Approximation of the True Pareto Front." *J. Water Resour. Plann. Manage.*, 141(3), 04014060.
- Watson, J., Hart, W. E., Murray, R. (2008). "Formulation and optimization of robust sensor placement problems for contaminant warning systems." *Proc., Water Distribution Systems Analysis Symposium 2006*, , 1-13.
- White, F. M. (1999). "Fluid Mechanics, WCB." *Ed McGraw-Hill Boston*, .
- Wu, Y., Liu, S., Smith, K., Wang, X. (2017). "Using Correlation between Data from Multiple Monitoring Sensors to Detect Bursts in Water Distribution Systems." *J. Water Resour. Plann. Manage.*, 144(2), 04017084.
- Wu, Z. Y., Sage, P., Turtle, D. (2009). "Pressure-Dependent Leak Detection Model and its Application to a District Water System." *J. Water Resour. Plann. Manage.*, 136(1), 116-128.
- Xu, C., and Goulter, I. C. (1998). "Probabilistic Model for Water Distribution Reliability." *J. Water Resour. Plann. Manage.*, 124(4), 218-228.
- Yazdi, J. (2016). "Decomposition Based Multi Objective Evolutionary Algorithms for Design of Large-Scale Water Distribution Networks." *Water Resour. Manage.*, 30(8), 2749-2766.
- Zechner, F. (2007). "Time for a Change." *The Underground*, .

Zhang, Q., Wu, Z. Y., Zhao, M., Qi, J., Huang, Y., Zhao, H. (2017). "Automatic Partitioning of Water Distribution Networks using Multiscale Community Detection and Multiobjective Optimization." *J. Water Resour. Plann. Manage.*, 143(9), 04017057.

Zheng, F., Zecchin, A., Maier, H., Simpson, A. (2016). "Comparison of the Searching Behavior of NSGA-II, SAMODE, and Borg MOEAs Applied to Water Distribution System Design Problems." *J. Water Resour. Plann. Manage.*, 142(7), 04016017.

Zitzler, E., Knowles, J., Thiele, L. (2008). "Quality Assessment of Pareto Set Approximations." *Multiobjective Optimization*, Springer, 373-404.

Zitzler, E., Laumanns, M., Thiele, L. (2001). "SPEA2: Improving the Strength Pareto Evolutionary Algorithm." *Eurogen*, 3242(103), 95-100.

Zitzler, E., and Thiele, L. (1998). "Multiobjective optimization using evolutionary algorithms—a comparative case study." *Proc., International Conference on Parallel Problem Solving from Nature*, Springer, Berlin Heidelberg, 292-301.

Appendix A

Pareto Archived Dynamically Dimensioned Search (PADDs)

PADDs is a single-solution based heuristic multiobjective algorithm and is the multiobjective version of DDS (Tolson and Shoemaker 2007). Interested readers are referred to Asadzadeh and Tolson (2013) for all algorithmic details of PADDs. Asadzadeh et al. (2014) provide the following summary description of the algorithm. PADDs archives all nondominated solutions found during the search, so it does not suffer from deterioration defined by Hanne (1999) to occur for a bounded size archive if in a generation some nondominated solutions are discarded from the archive and later on in the search, some worse solutions are generated and archived. Based on a selection metric to define selection probabilities, PADDs applies the roulette wheel stochastic selection scheme to select one of the archived nondominated solutions per iteration and perturbs it as DDS does. If the perturbed solution is nondominated compared to all archived solutions or if it dominates an archived solution, the archive is updated to remove dominated solutions and include this recently perturbed solution, which will then be selected with probability 1.0 for perturbation in the next iteration. Otherwise, PADDs chooses another archived solution based on the selection metric. This process of selection and perturbation is repeated until the user-specified PADDs computational budget (defined as the number of solution evaluations) is exhausted. Below, a brief description of selection probability calculation by HVC and CHC metrics is presented.

HVC was first introduced by Knowles et al. (2003) as a metric to identify and discard solutions with smallest HVC from the archive of solutions. Eq. A-1, taken from Asadzadeh and Tolson (2013), defines HVC for a nondominated solution \mathbf{x}^p in Pareto approximate set \mathbf{PS}^a (where the Pareto approximate set is simply the set of currently known nondominated solutions). HVC for \mathbf{x}^p in \mathbf{PS}^a is the Lebesgue measure (λ) or simply the volume of the partition of objective space dominated solely by \mathbf{x}^p .

$$HVC(\mathbf{x}^p \in \mathbf{PS}^a) = \lambda(\mathbf{z} \in \mathbf{Z} | \mathbf{F}(\mathbf{x}^p) \leq \mathbf{z}, \nexists \mathbf{x}^q \in \mathbf{PS}^a: \mathbf{F}(\mathbf{x}^q) \leq \mathbf{z}) \quad (\text{A-1})$$

where \mathbf{F} is the vector of minimization objectives. Eq A-1 is not used to compute HVC for extreme or endpoint solutions in the archive. Instead, in Asadzadeh and Tolson (2013), HVC for these points is assigned the value of HVC of the closest non-extreme solution in the archive.

CHC is introduced in Asadzadeh et al. (2014) as a metric designed for multiobjective problems that have largely convex PFs and is expected to perform poorly for non-convex problems. In this method, a convex hull based on the archived (nondominated) solutions is built first. The convex hull of a set of points is the

smallest convex set that contains all the given points (Barber et al. 1996). Let the volume of the convex hull built using Pareto approximate set \mathbf{PS}^a be defined by $CH(\mathbf{PS}^a)$. The selection probability of a solution \mathbf{x}^p is calculated based on its location in the convex hull. Solutions inside the convex hull and vertices located on the top facet only (facing the Nadir point when all objectives are to be minimized) get selection probability of zero while vertices on bottom facet only and those on the intersection of top and bottom facets are assigned a non-zero selection probability obtained as a function of the reduction in volume of the convex hull calculated by Eq. A-2 when solution \mathbf{x}^p is removed from \mathbf{PS}^a :

$$CHC(\mathbf{x}^p \in \mathbf{PS}^a) = CH(\mathbf{PS}^a) - CH(\mathbf{PS}^a \setminus \{\mathbf{x}^p\}) \quad (\text{A-2})$$

The term $CH(\mathbf{PS}^a \setminus \{\mathbf{x}^p\})$ is the volume of the convex hull without solution \mathbf{x}^p in the archive. The idea of the CHC approach is to place more emphasis on solutions that are located on the convex part of the Pareto front. CHC helps PADDs focus on the knee part of the Pareto front instead of extensively sampling from solutions on the extended tails of the Pareto front (Asadzadeh et al. 2014). Das (1999) introduces the concept of the knee which is essentially the point of the Pareto front with the maximum bulge. Eq A-2 is not used to compute CHC for extreme or endpoint solutions in the archive. Instead, as noted in Asadzadeh et al. (2014), CHC for these points is assigned the value of CHC of the closest non-extreme solution in the archive that is active (e.g., has a non-zero CHC value).

The selection probability for solution \mathbf{x}^p in PADDs is computed by normalizing $HVC(\mathbf{x}^p \in \mathbf{PS}^a)$ and $CHC(\mathbf{x}^p \in \mathbf{PS}^a)$ to the range of 0 to 1. Normalization in either case is accomplished by dividing each contribution metric for a specific solution by the total of the contribution metrics for all solutions in \mathbf{PS}^a .